

Andreas Ulm, BSc

# Fast manufacturing of microstructures via greyscale two-photon initiated polymerization

## **MASTER'S THESIS**

to achieve the university degree of  
Diplom-Ingenieur  
Master's degree programme: Technical Physics

submitted to

**Graz University of Technology**

## **Supervisor**

Joachim Krenn, Ao.Univ.-Prof. Mag. Dr.rer.nat.  
Institute of Physics, University of Graz

Graz, November 2020

## **AFFIDAVIT**

I declare that I have authored this thesis independently, that I have not used other than the declared sources/resources, and that I have explicitly indicated all material which has been quoted either literally or by content from the sources used. The text document uploaded to TUGRAZonline is identical to the present master's thesis.

---

Date, Signature

## Acknowledgement

I would like to thank Prof. Joachim Krenn from the University of Graz, who provided excellent support. Thank you for the mentoring, comments and improvements for my work.

I would also like to express my sincere thanks to the company Joanneum Research and all the people involved there, who made it possible to carry out this Master's thesis at the location Weiz. Special thanks go to Dr. Bernhard Lamprecht, who gave me excellent guidance, advice and support.

## Abstract

In this master's thesis, a self-built system for two photon polymerisation (TPP) is tested. For the generation of structures, we use a femtosecond laser. Due to the flexible setup, a laser diode could be aligned collinearly. So, one photon polymerisation (OPP) is conducted on the exact same setup. The light sources can be switched on independently, allowing structuring and direct comparison on one single sample.

A focus is laid on grayscale TPP for the fast manufacturing of micro-optics. The fundamental difference of this grayscale technique compared to the 3D TPP is the modulation of the exposure dose while moving the laser focus across the sample. To establish an in-sync modulation of the laser power to the stage movement, the stage controller is used to generate the power modulation signal. The necessary files for processing the trajectories on the controller, so-called PVT (Point-Velocity-Time) trajectory files, are generated by a self-written Python software. A collinearly aligned He-Ne laser, an in-line camera and a LabVIEW program help in finding the resist-substrate interface, support the levelling of the sample and enable the supervision of the polymerization process in real-time.

We investigate the polymerization behaviour with respect to different resists as well as the writing behaviour with respect to achievable resolutions in detail. Test structures are generated with various writing parameters to achieve fast fabrication and high shape fidelity. Moreover, truncated pyramid arrays are manufactured on large-scale, achieving a fabrication time of less than 12 hours for an area as large as  $1\text{ cm}^2$ .

## Kurzbeschreibung

In dieser Masterarbeit wird ein selbst-installiertes System zur Ausführung von Zwei-Photonen-Polymerisation (TPP) getestet. Ein Femtosekundenlaser wird für die Generierung von Strukturen verwendet. Durch den flexiblen Aufbau konnte eine Laserdiode kollinear justiert werden. Somit kann auf der exakt selben Anlage Ein-Photonen-Polymerisation durchgeführt werden. Die Lichtquellen werden unabhängig geschaltet, wodurch eine Strukturierung und ein Vergleich auf ein und derselben Probe möglich sind.

Es wird insbesondere Graustufen-Zwei-Photonen-Polymerisation zur schnellen Herstellung von Mikrooptiken untersucht. Der grundlegende Unterschied dieser Graustufen-Technik im Vergleich zur 3D-TPP ist die Modulation der Belichtungsdosis während der Ausführung der Bewegungstrajektorie. Um eine synchrone Modulation der Laserleistung bezogen auf die Bewegung zu erreichen, wird das Signal zur Modulation der Laserleistung vom Stage-Controller berechnet und ausgesendet. Die dazu notwendigen Dateien, die sogenannte PVT-Trajektorien beschreiben, werden mit Hilfe eines selbst erstellten Python-Programms generiert. Ein kollinear justierter He-Ne Laser, eine In-line-Kamera und ein LabVIEW-Programm ermöglichen das Finden der Photolack-Substrat-Grenzfläche, unterstützen das Einebnen der Probe und erlauben das Über-

wachen des Polymerisationsprozesses in Echtzeit.

Das Schreibverhalten wird in Bezug auf erreichbare Auflösung sowie unterschiedliche Photolack-Polymerisationsverhalten detailliert untersucht. Teststrukturen werden mit verschiedensten Schreibparameter generiert, um eine schnelle Herstellung und hohe Formgenauigkeit zu erreichen. Pyramidenstümpfe werden großflächig geschrieben. Eine Herstellungszeit von unter 12 Stunden für eine Fläche von  $1\text{ cm}^2$  wird erreicht.

## Abbreviations

| Abbr. | Definition                                   |
|-------|--|
| Bmp   | Bitmap picture file                          |
| LMS   | Laser machining software                     |
| OPP   | one photon initiated polymerization          |
| PVT   | Point-Velocity-Time (Trajectory file format) |
| Stl   | Stereolithography CAD geometry file          |
| TPP   | two photon initiated polymerization          |

Table 1: Abbreviations

## Contents

|   |           |
|---|-----------|
| <b>Abstract</b>   | <b>I</b>  |
| <b>Kurzbeschreibung</b>   | <b>I</b>  |
| <b>Abbreviations</b>  | <b>II</b> |
| <b>1 Introduction</b>   | <b>1</b>  |
| <b>2 Fundamentals</b>   | <b>2</b>  |
| 2.1 Two photon absorption and polymerization . . . . .          | 2         |
| 2.1.1 Nonlinear absorption . . . . .                            | 2         |
| 2.1.2 Photoresists . . . . .                                    | 3         |
| 2.2 Focusing light . . . . .                                    | 5         |
| 2.2.1 Objective lenses with low numerical aperture . . . . .    | 6         |
| 2.2.2 Objective lenses with high numerical aperture . . . . .   | 7         |
| 2.2.3 Aspect ratio . . . . .                                    | 11        |
| 2.3 Conventional 3D TPP . . . . .                               | 11        |
| 2.4 Grayscale TPP . . . . .                                     | 12        |
| 2.5 Comparison to grayscale one photon lithography . . . . .    | 13        |
| 2.5.1 Non-linear resist response and proximity effect . . . . . | 14        |
| 2.6 Fast two photon polymerization . . . . .                    | 16        |
| 2.6.1 Common speeds of TPP . . . . .                            | 16        |
| 2.6.2 Physical parameters for fast TPP . . . . .                | 17        |
| 2.6.3 Engineering parameters for fast TPP . . . . .             | 18        |
| <b>3 Method</b>   | <b>20</b> |
| 3.1 General setup . . . . .                                     | 20        |
| 3.2 Femtosecond laser . . . . .                                 | 20        |
| 3.3 Objective lenses . . . . .                                  | 21        |
| 3.4 Stage . . . . .   | 22        |
| 3.5 Online monitoring of the production process . . . . .       | 22        |
| 3.6 Writing strategies . . . . .                                | 22        |
| 3.6.1 Writing with xy-axis group . . . . .                      | 23        |
| 3.6.2 Writing with xyzpv-axis group . . . . .                   | 23        |
| 3.7 Resists and placing the sample . . . . .                    | 27        |
| 3.7.1 OrmoComp . . . . .  | 27        |
| 3.7.2 Negative resist - drop procedure . . . . .                | 29        |
| 3.7.3 Negative resist - spin coating . . . . .                  | 29        |
| 3.7.4 Negative resists - development . . . . .                  | 30        |
| 3.7.5 Positive resists - spin coating . . . . .                 | 30        |
| 3.7.6 Positive resists - development . . . . .                  | 31        |
| 3.8 Characterization of the samples . . . . .                   | 31        |
| 3.8.1 Keyence Laser-Scanning Microscope . . . . .               | 31        |
| 3.8.2 Scanning electron microscopy . . . . .                    | 33        |

---

|          |  |           |
|----------|--|-----------|
| 3.9      | One photon polymerization . . . . .                  | 33        |
| 3.10     | Freerun distance . . . . .                           | 34        |
| 3.11     | Stability tests . . . . .                            | 35        |
| 3.12     | Test structures . . . . .                            | 36        |
| <b>4</b> | <b>Results</b>                                       | <b>37</b> |
| 4.1      | Stability tests . . . . .                            | 37        |
| 4.2      | Variation of the focus offset . . . . .              | 42        |
| 4.3      | Test structures . . . . .                            | 45        |
| 4.3.1    | Plateaus - Non-linear resist response . . . . .      | 45        |
| 4.3.2    | Staircase and chessboard pattern . . . . .           | 47        |
| 4.3.3    | Pyramids - Manufacturing time . . . . .              | 51        |
| <b>5</b> | <b>Conclusion</b>                                    | <b>56</b> |
| <b>6</b> | <b>Outlook</b>                                       | <b>57</b> |
| <b>7</b> | <b>Appendix</b>                                      | <b>58</b> |
| 7.1      | XPS-D Controller Manual - PVT Trajectories . . . . . | 58        |
| 7.2      | Python software - Manual . . . . .                   | 65        |
|          | <b>References</b>                                    | <b>97</b> |
|          | <b>List of Tables</b>                                | <b>98</b> |
|          | <b>List of Figures</b>                               | <b>99</b> |

# 1 Introduction

3D printing is a growing sector of economy. There are various versions of 3D printers on the market. However, most printers have a feature size of  $50\ \mu\text{m}$  or larger. Two photon polymerization (TPP) on the other hand, enables 3D fabrication with resolutions about the tenth of the used wavelength, e.g.  $80\ \text{nm}$  for a  $800\ \text{nm}$ -laser [22, 23]. This is a big advantage compared to other optical methods where the wavelength is the smallest possible resolution limit.

Introduced in 1997 [14] by Maruo et al., TPP has gained attention rapidly. The manufacturing strategy allows various applications ranging from photonic crystals [20] to issue engineering [6]. Furthermore, a very important field of application is optics. With TPP, micro-optical components can be manufactured for integration in novel mobile devices or in future technologies related to data and signal processing [19].

TPP as a maskless lithography method creates arbitrary structures by solidifying voxels along a trajectory travelled by the laser focus [8]. Mostly however, layers are written one by one. This leads to long manufacturing times for the conventional approach of TPP. An alternative to this approach is grayscale TPP where 2D and relief micro-parts like micro-lenses or freeform micro-optics can be printed fast [19]. This variation of the high-precision microfabrication technique works with fast and accurate modulation of the exposure dose. Usually, the velocity is fixed throughout the writing range and the power of the laser is modified because the electronic signal controlling the power can react faster than the stage which needs to satisfy mechanical laws. High speeds are preferable and structures have been written with a linear velocity as high as  $80\ \text{mm/s}$  [23].

The full design freedom is enlarged by the availability of various positive-tone and negative-tone photoresists. While positive resists are solid and become soluble by exposure to light, negative resists are liquid and become solid. The thickness of the resist layer on top of the substrate can be controlled by spin coating on a wide range. E.g. the negative OrmoComp allows thicknesses from  $20\ \mu\text{m}$  down to a few hundred nanometers [18].

In this master's thesis, TPP is conducted in positive and negative resists, emphasizing the advantages and disadvantages of the 3D printing strategy. Furthermore, TPP is compared with one photon polymerization (OPP). Due to the very flexible setup, the light sources used can be switched independently, allowing to write OPP and TPP structures on a single sample. The details of the setup are explained in section 3. In section 4, the results of OPP and TPP are compared and possible parameter ranges are found.

In order to establish the fast grayscale TPP manufacturing process, a self-written Python program is used. The manual of the program is included in section 7.2.



## 2 Fundamentals

This chapter contains information about two photon initiated polymerization (two photon polymerization, TPP). The absorption itself and the following polymerization are explained, especially cross-linking of negative resists. The focusing through an objective lens with the resulting volume element (voxel) is discussed. Finally, the motivation and strategies for fast TPP are elaborated. Information for the chapters 2.1, 2.2 and 2.6 are mainly based on the book of Baldacchini [1].

### 2.1 Two photon absorption and polymerization

This section discusses two photon absorption with the underlying principles. The chemical reaction taking place in negative photo resists is explained in detail.

#### 2.1.1 Nonlinear absorption

When light is absorbed by matter, the energy of the light usually fits to an energy difference between an occupied and an unoccupied state within the material. This is the process of linear absorption. But, a material may also absorb light when the energies of two (or more) photons collectively match the energy gap between two states. This is called two (many) photon absorption. In order of making this process possible, enough photons have to be around the same place in space at the same time, i.e. high intensities are necessary.

In a typical two photon absorption process, there is no resonant state absorbing individual photons. Rather, the first photon causes a transition to a virtual state. The virtual state is a combination of non-equilibrium states of the molecule. The lifetime of the virtual state is very short because the states involved are far off resonance. For the transition probability to be non-neglectable, the second transition must occur within roughly  $\Delta t = 1 \text{ fs}$  of the initial transition. Thus, the light intensity needs to be high enough. To measure the effect in an experiment, a laser is necessary to provide the high intensity needed.

The response of the medium to an applied field, called polarization  $\mathbf{P}$ , can be written:

$$\mathbf{P} = \epsilon_0 * (\chi^{(1)} \mathbf{E} + \chi^{(2)} \mathbf{E} \mathbf{E} + \chi^{(3)} \mathbf{E} \mathbf{E} \mathbf{E} + \dots). \quad (1)$$

Here,  $\mathbf{E}$  is the magnitude of the optical field and  $\epsilon_0$  is the permittivity of free space.  $\chi^{(n)}$  is the  $n^{\text{th}}$ -order susceptibility, with  $\chi^{(1)}$  being the linear susceptibility.  $\chi^{(n)}$  is a tensor of  $n^{\text{th}}$  order, e.g.  $\chi^{(3)}$  has 27 components.

At low intensities, the material responds linearly to the applied optical field. The contributions of the  $\chi^{n \geq 2}$  are neglectable. The higher terms become important as the intensity increases.

The process of absorbing two photons depends on the square of the intensity. In general, an n-photon absorption process can involve the addition of photons of n different frequencies. However, the majority of multi-photon fabrication processes use photons of a single frequency, emitted by a single laser.

### 2.1.2 Photoresists

The material aspect is an important one within the topic of two-photon polymerization. Some materials react to light by rendering the local exposed environment insoluble. A material whose solubility decreases on exposure to light is known as a negative-tone photoresist (negative resist). Positive-tone photoresists (positive resists) are usually solid, exposure to light increases the solubility locally.

#### Negative resists

Negative resists have a lot of applications, e.g. in photolithography and in coating. Many of these materials can be adapted to serve in two photon fabrication. An important subcategory of negative resists are materials that consist of organic monomers that can be cross-linked by exposure to light. To make the cross-linking happen, radicals are needed. In two-photon polymerization, the light generates free radicals by splitting the photoinitiator. This photoactive substance is extremely relevant and influences the process of polymerization. Usually, the resist contains around 1 % photoinitiator. Most traditional radical photoinitiators are aromatic ketones. Benzophenone is shown in Figure 1.a as an example. Photoexcitation is followed by intersystem crossing in the Norrish Type I photoinitiator, creating a triplet diradical. (Figure 1.b) After that, homolytic bond cleavage creates two reactive free radicals. The chain reaction starts. In Norrish Type II photoinitiators, hydrogen of a second molecule creates the reactive radical which begins the chain reaction. (Figure 1.c)

There exist several factors which affect the efficiency of two-photon initiated polymerization:

- Linear and two-photon cross-section of the initiator:  
The larger the two-photon absorption cross-section, the more efficient is the initiation. In the focal region, the intensity is high enough for the two-photon absorption to take place. However, the linear absorption cross-section should be low. Mostly, thicker resist films are used in fabrication methods. To avoid intensity loss in other parts of the material than the focus, a radical photoinitiator needs a small linear absorption cross-sections. This parameter set, light can propagate through the material with minimal loss.
- Quantum efficiency for the creation of radicals:  
Ideally, every excitation of the photoinitiator leads to radical generation. Since development requires non-Norrish mechanisms like electron transfer, the yield is reduced.
- Initiation velocity of the photoinitiator:  
The chemical process needs finite time, the degree of reactivity differs from one photoinitiator to another.

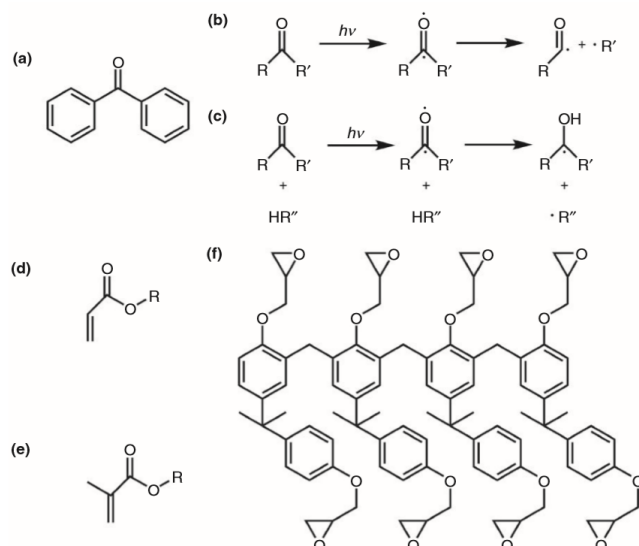


Figure 1: Structure of a benzophenone, a photoinitiator (a); Mechanism for radical generation Norrish Type I (b) and Norrish Type II (c) with a coinitiator  $HR''$ , chemical structure of acrylate (d), methacrylate (e) and an SU-8 oligomer (f). Reprinted from [1].

Two common types for two-photon radical polymerization are either acrylates (Figure 1.d) or methacrylates (Figure 1.e). Both types are stable on their own. However, they react fast with radicals and become cross-linked, i.e. they are polyfunctional. This process converts a negative photoresist, which is a viscous liquid, into a hard, insoluble polymer. Different types of acrylic and methacrylic monomers are used. Properties such as solvent compatibility, shrinkage and so on, can be tuned for the specific use case. Generally, the advantage of acrylates is the higher reactivity, leading to lower intensities needed.

Once polymerization starts, radical monomers react with other monomers. Theoretically, the radical oligomers produced grow until the entire material becomes cross-linked. However, two processes slow down the propagation and reduce the influence radius of a produced radical:

- **Quenching** takes place when a radical reacts with an oxygen molecule, a radical inhibitor or a similar weakly reactive molecule present in the resist.
- **Termination** occurs by combination of two radicals. They form a bond, losing the reactivity.

In addition to intensity and exposure time, these two mechanisms determine the size of the voxel created. Ideally, the influence radius is kept small around the laser beam spot. A good photoresist for two photon polymerization satisfies this condition.

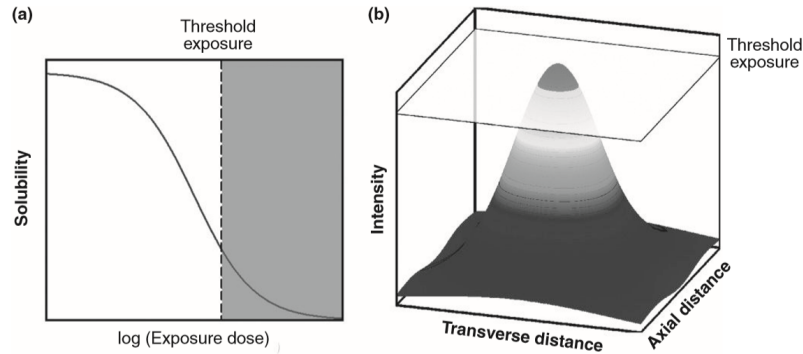


Figure 2: Exposure curve - solubility of the resist as a function as the exposure dose (a): The gray region on the right indicates insolubility, sketch for the threshold dose for insolubility in a lateral intensity profile (b): Feature sizes of the tenth of the wavelength used are possible. Reprinted from [1].

The exposure curve is an important tool for controlling the process of two photon polymerization. It shows the solubility as a function of exposure dose. The exposure curve for a negative-tone photoresist is highly nonlinear and can be seen in Figure 2.a. This chemical non-linearity is of great importance. It implies that there is an exposure threshold below which the photoresist will remain soluble. In conventional two photon polymerization processes, the laser beam intensity is slightly above the threshold for insolubility. So, the voxels created are small. A laser beam's Gaussian profile is shown in Figure 2.b. The voxels can be tiny, a fraction of the wavelength of light used. Using a photoresist with a steep exposure curve and an objective with high numerical aperture, one can create voxels with a transverse dimension of  $d = 80 \text{ nm}$  using light with a wavelength  $\lambda = 800 \text{ nm}$ . [23]

## 2.2 Focusing light

This chapter discusses the principle of the creation of a voxel. The polymerization of a TPP process will only happen at high enough doses. Considering a laser beam as the only light source, the polymerization will only happen where the laser exposes the resist long enough. By focusing the beam through an objective lens, the polymerization will only happen around the focal spot. The focusing characteristics of the lens is therefore important. A mathematical treatment for describing objective lenses is shown below. Finally, an empirical function for the voxel's aspect ratio is stated, depending on material parameters and the numerical aperture of the objective lens.

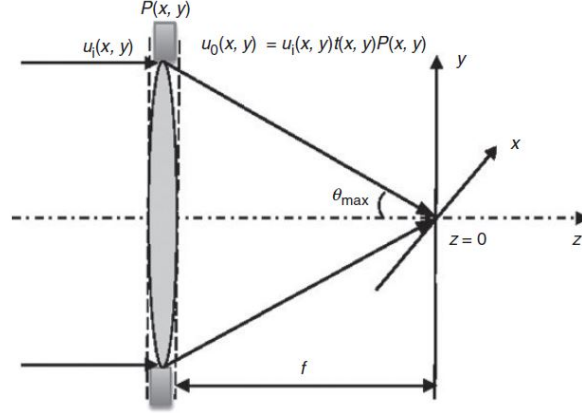


Figure 3: Sketch of a low-NA objective lens with indicated focal field calculation and used coordinates. Reprinted from [1].

### 2.2.1 Objective lenses with low numerical aperture

An objective lens focuses light. The propagating wave can be modelled from the interference of the optical fields created at different pupil plane's locations. If the numerical aperture (NA) of a objective lens is low, it can be considered as a thin lens. Then, the adaption of the incident field is a pure phase modulation. The highest angle between two propagating waves through the lens relates to the highest spatial frequency fringes. The angle from the rim of the objective lens with respect to the optical axis is denoted by  $\Theta_{max}$ . It determines the resolution of the objective (see Figure 3). The NA is defined as  $NA = n \sin(\Theta_{max})$ , where  $n$  is refractive index in the image space. The NA is a measure of the spatial resolution power of an objective lens.

Assuming uniform illumination, the optical field near the focal plane can be described by applying Fresnel propagation

$$u(x, y, z) \sim \int_{area} u_0 P(x', y') t(x - x', y - y') dx' dy'. \quad (2)$$

Here  $u_0$  is the incident field,  $t$  the transmission function and  $P$  the pupil function. The transmission function  $t(x, y)$  of the lens is given by

$$t(x, y) = e^{i \frac{k}{2f} (x^2 + y^2)} \quad (3)$$

where  $f$  is the focal length and  $k$  is the wave vector on the object side.

The pupil function  $P$  for a circular lens with radius  $a$  is

$$P(x, y) = \begin{cases} 1 & \text{for } \sqrt{x^2 + y^2} \leq a \\ 0 & \text{otherwise.} \end{cases} \quad (4)$$

One can introduce normalized radial and axial coordinates by:

$$\nu = \frac{2\pi}{\lambda} r \sin(\Theta_{max}) = k_0 r (NA) \quad (5)$$

$$u = \frac{2\pi}{\lambda} z \frac{a^2}{f^2} = k_0 \frac{z}{n} (NA)^2 \quad (6)$$

With these equations,  $\nu$  is the scaled lateral dimension ( $r$ ) and  $u$  is the scaled axial dimension ( $z$ ).  $k_0$  is the wave vector of the incident plane wave with wavelength  $\lambda$ . An important observation is the quadratic dependence of  $u$  on the NA, whereas  $\nu$  changes linearly with NA. Looking at equations (5) and (6), it is easy to see, that a higher NA leads to a smaller spot size.

The optical field simplifies to a one dimensional integral by using equations (3) - (6):

$$u(\nu, u) = 2iN e^{-ikf} u_0 e^{i\frac{\nu^2}{4N}} \int_0^1 e^{iur'^2/2} J_0(\nu r') r' dr' \quad (7)$$

Here  $N = \frac{\pi a^2}{\lambda f}$  is the Fresnel number,  $r'$  the normalized radial distance and  $J_0$  the zeroth-order Bessel function. One can interpret three parts of the formula. The first factors are a prefactor describing the influence of the light wavelength and the focal length of the lens. The last factor in front of the integral  $e^{i\frac{\nu^2}{4N}}$  is the phase modulation relating to the phase shift of wavelets on different pupil plane points due to their lateral distance to the origin. Finally,  $J_0(\nu \cdot r')$  describes the intensity modulation of the light along the optical axis, caused by the overlapping virtual point sources created on the lens. This formula needs to be studied in higher detail to see the voxel's behavior. Calculated with this formula, the voxel dimensions for a NA of 0.1 are shown in Figure 4. The first minima of the field for the lateral distribution (Figure 4 (a) and (c)) differ by  $\sim 12$  wavelengths, on the other hand, the first minimums enclose  $\sim 400$  wavelengths in the axial direction (Figure 4 (b) and (d)). The dimensions of a voxel differ by an order of magnitude.

High-NA lenses are needed to achieve a high spacial resolution. Since the Fresnel propagation was applied, the focal field is here calculated from the transmitted field of a planar reference surface right after the lens. The approach inherits an increasing error for higher NA lenses since these lenses cannot be considered as thin lenses. Therefore, an extension of the theory is necessary.

### 2.2.2 Objective lenses with high numerical aperture

To express the optical field correctly for the high-NA case, Debye diffraction theory uses a spherical reference plane. A lens converts a incident planar wave into a spherical wave converging towards the geometrical focal point. The incident optical field  $u_i(x, y)$  can, therefore, be mapped onto a spherical reference wavefront  $u_0(\Theta, \Psi)$ . This wavefront is located after the lens and can be used to calculate the focal field. This procedure is shown in Figure 5.

With an integration over the solid angle  $\Omega$ , the focal field follows, (Debye integral formula):

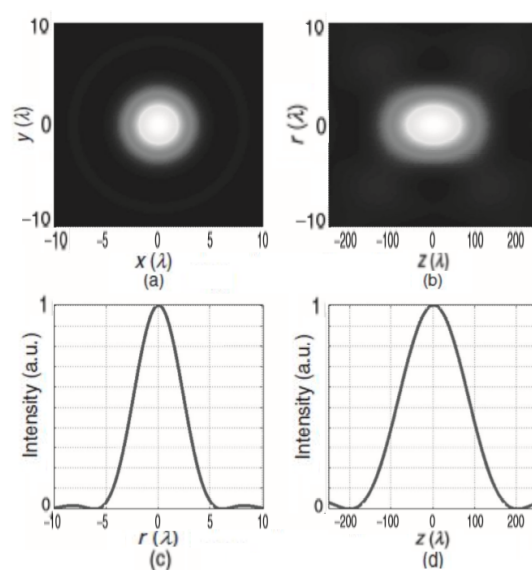


Figure 4: Elongated focal spot for an objective lens with  $NA = 0.1$ . The focal field distributions in the focal plane (a) and normal to the focal plane (b) have different orders of magnitude in length. The horizontal line scans for the figures a and b show the lateral (c) and axial (d) field distributions, respectively. Reprinted from [1].

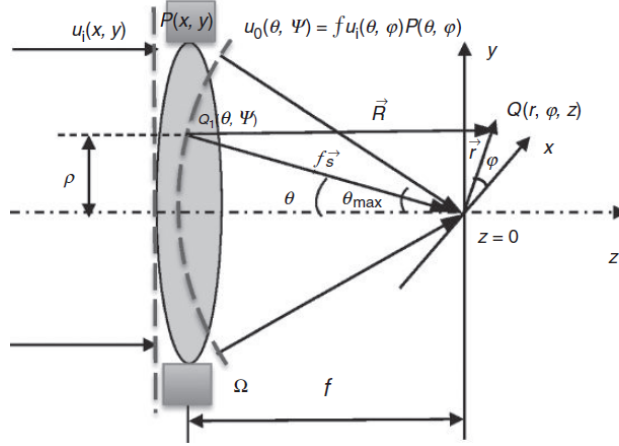


Figure 5: Sketch of the focal field calculation for a high-NA objective lens with the focal length  $f$ . The incident wave  $u_i$  is mapped onto a spherical reference plane (dashed arched line,  $u_0(\Theta, \Psi)$ ).  $Q_1(\Theta, \Psi)$  is a point on this reference plane and  $Q(r, \phi, z)$  is an observation point within the focal volume. Reprinted from [1].

$$u(\vec{r}) = u(r, \phi, z) = \frac{i}{\lambda} \int_{\Omega} u_0(\Theta, \Psi) e^{ik\vec{s}\vec{r}} d\Omega. \quad (8)$$

$r$ ,  $\phi$  and  $z$  are the cylindrical coordinates in the image space. A point on the reference wavefront is addressed by the coordinates  $\Theta$  and  $\Psi$ , the vector originating in this point and leading to the image plane origin is given by  $\vec{s}$ . The integration over the solid angle  $\Omega$  includes the whole reference plane. The formula assumes spherical wavelets originating from points of the reference plane which are, as a collective, equivalent to the incident wave. In contrast to this, the Huygens–Fresnel principle used for the low-NA case for planar lenses assumes plane wavelets. The illumination field at the pupil, where  $\Theta$  and  $\Psi$  are the spherical coordinates, relates to the field on the reference sphere (radius  $f$ ):

$$u_0(Q_1) = u_0 f u(Q_1) P(Q_1) = u_0 f u(\Theta, \Psi) P(\Theta, \Psi). \quad (9)$$

A sine condition lens has the pupil function

$$P(\Theta) = \begin{cases} \sqrt{\cos(\Theta)} & \text{for } \Theta \leq \Theta_{max} \\ 0 & \text{otherwise.} \end{cases} \quad (10)$$

The expression for the surface element becomes  $d\Omega = \sin(\Theta) d\Theta d\Psi$ . Including this, equation (9) becomes equation (11) by expressing the scalar product  $\vec{s}\vec{r}$  in terms of  $\Theta$  and  $\Psi$  and assuming rotational symmetry.



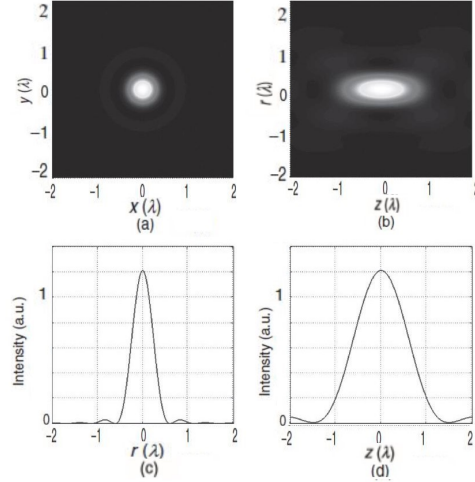


Figure 6: Focal spot for an objective lens with  $NA = 0.95$ , The length scales of the focal field distributions in the focal plane (a) and normal to the focal plane (b) differ in a factor of  $\sim 2$ . The horizontal line scans for the figures a and b show the lateral (c) and axial (d) field distributions, respectively. Reprinted from [1].

$$u(r, z) = \frac{2i\pi u_0 f}{\lambda} \int_0^{\Theta_{max}} u(\Theta) J_0(kr \sin(\Theta)) e^{ikz \cos(\Theta)} \sin(\Theta) d\Theta \quad (11)$$

The result formula (11) includes some similar elements as equation (7) for the low-NA case, for example the Bessel function  $J_0$ . However, the treatment is a little bit harder because of the appearance of the angular functions. Numerical treatment can be used to analyse aberrations, phase modulations and so on.

One example of the focal field calculated with equation (11) is shown in Figure 6. In this example, the illumination is assumed to be uniform. The NA of the objective lens is chosen with 0.95. The spot dimensions can be seen. The first minima of the field for the lateral distribution differ by  $\sim 0.6$  wavelengths, on the other hand, the first minima in the axial direction enclose  $\sim 1.4$  wavelengths.

Compared with the  $NA = 0.1$  case shown in Figure 4, clearly the spot size is significantly reduced as expected. In both cases, the lateral dimension is lower than the axial dimension but the aspect ratio for the high-NA aperture's spot is very different. A further empirical discussion can be found in the next section.

### 2.2.3 Aspect ratio

One important aspect of the voxel tuning is the aspect ratio. It can be extracted from the normalized coordinates from equations (5) and (6). For a specific setup, the axial resolution  $res_{axial}$  and the lateral resolution  $res_{lat}$  are given by

$$res_{axial} = \frac{k_2 \lambda}{NA^2}, \quad res_{lat} = \frac{k_1 \lambda}{NA} \quad (12)$$

with the empirical constants  $k_1$  and  $k_2$  [20]. The constants are added to account for various effects like material anisotropy and system parameters, influencing the spot's dimensions.

The aspect ratio  $ar$  with chosen constants  $k_1 = 0.6$  (between 0.5 and 1,  $\sim \frac{1}{n}$  with the refractive index  $n$ ),  $k_2 = 2.3$  (material property relating to the longitudinal resolution) follows by:

$$ar = \frac{res_{axial}}{res_{lat}} = \frac{k_2}{k_1} \frac{1}{NA} \approx \frac{3.83}{NA}. \quad (13)$$

For high-NA oil-immersion objectives with  $NA = 1.4$ , an aspect ratio of  $ar = \sim 3$  is possible. A x10-objective lens with  $NA = 0.1$  will create voxels with an aspect ratio close to 40. This is in agreement with the aspect ratios seen in Figure 4 ( $ar = \sim 33$ ) and Figure 6 ( $ar = \sim 2.3$ ).

These results show that a high-NA objective lens is necessary to use the two-photon polymerization technique for manufacturing 3D structures with best resolution. Objective lenses with low-NA lead to elongated spots and very different resolution limits in the axial and lateral directions.

## 2.3 Conventional 3D TPP

The principle of TPP is simple, a laser beam is focused into a resist which reacts when the intensity is high enough that TPA takes place at a non-negligible rate. The modified resist then forms a structure. The remaining unmodified resist is washed away by a developer, in case of a negative-tone photoresist. One can produce micro structures like the spiral in Figure 7 which was formed by moving the laser focus along the spiral trajectory.

A large variety of trajectories is possible, but one has to make sure that the created structures stick together and onto the substrate. Loose structures inside the resist and without connection to the substrate will start to float around randomly. Therefore, 3D printing often works in layers. When conducting conventional 3D lithography, a CAD model is sliced and hatched. Slicing means splitting the model in discrete layers. Each layer is afterwards printed, starting either on the top or at the bottom. Hatching is necessary since TPP is a serial process. Only lines, not areas, can be written. In lithography, hatching means writing combinations of point or line patterns which should be stable enough to fulfill the same function as the whole solid area would.

Several strategies can be applied to create a layer. One way is to raster it in a meander form. Whenever the focus is moving over a position where a

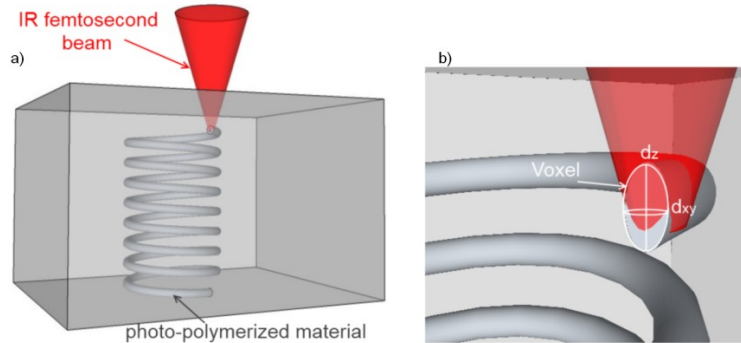


Figure 7: Sketch of a TPP process. The laser focus is moved through the resist and creates a spiral. Reprinted from [8].

pixel inside the negative resist should be solidified, the laser is switched on. Otherwise, the laser is switched off. Another option is to create trajectories of arbitrary form, moving along curved lines which should be written. This is especially time saving since it is sometimes sufficient to write the contour. In the latter, the structure might be exposed to UV light after development creating a solid structure by solidifying the liquid resist inside the hull. However, stability of the structure and shape fidelity must be assured.

In conventional TPP the laser is driven at constant power and lines are written with constant velocity. This is done to ensure a uniform voxel throughout the writing process. The resolution of the process is related to this voxel.

## 2.4 Grayscale TPP

It is possible to change the dose of exposure continuously while scanning over a sample. This might be done by different velocities or the change of other parameters. However, the output power of the laser is mostly used as this parameter while the velocity is kept constant. This is done because the electronic signal controlling the laser power can react faster than the stage response which needs to satisfy mechanical laws.

In grayscale TPP, a common strategy is to write a single layer. The sample is scanned similar to approach of the conventional TPP where the trajectory is of meander form. While line by line is scanned, the power is changed in-sync with the movement, altering the voxel's size continuously. This procedure creates a relief, so-called 2.5D, structure on the surface of the resist. The restriction to 2.5D structures is usually not a problem for freeform microoptics or relief structures which is an important field of application of TPP. With having only one layer to be scanned, the time needed to write a structure is very low compared to conventional TPP.

As mentioned, the basic principle of this lithography method is the tuning the voxel size by the laser power. Now, we will discuss this dependence which

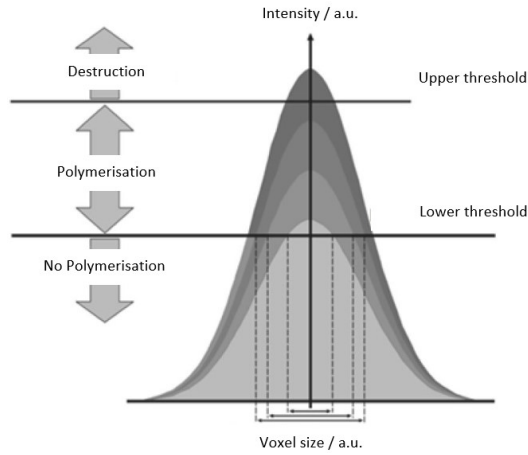


Figure 8: Process window of TPP. The voxel's dimension scales with the laser intensity between the lower and upper threshold of polymerization. Adapted from [10].

is illustrated in Figure 8. The resist will react to the laser in three different ways. At low intensities nothing will happen. Exceeding a certain threshold, the polymerisation will start, generating the smallest possible voxel. This is called the lower threshold of polymerization. At too high intensities, the resist will evaporate immediately, creating bubbles in a liquid resist or causing a tiny explosion in a solid resist. This is called the upper threshold of polymerization. Between the lower and the upper threshold, the voxel's dimension is proportional to the laser intensity. The dependence is non-linear which is discussed in section 2.5.1.

In conventional 3D TPP, only one intensity will be used. One will choose an intensity which is slightly above the lower threshold to manufacture an object with maximal resolution.

## 2.5 Comparison to grayscale one photon lithography

One photon polymerization (OPP) uses usually blue or near UV light. The beam is guided to the sample with the resist which is exposed. The conventional approach is to write into a positive spincoated resist. Due to the absorption in the resist, the dosage decreases exponentially for increasing depth. A small dosage is sufficient for the chemical reaction to take place in upper regions in the material. For higher incident light intensities, the dosage will also cause depolymerization in lower levels in the material. This fundamental relation between penetration depth and dosage leads to the possibility to control the height of the structure by tuning the intensity of the light source. This is similar to the height control for TPP where the voxel size can be tuned by the laser power (see last section). However, the fundamental difference is that no structure can be created inside

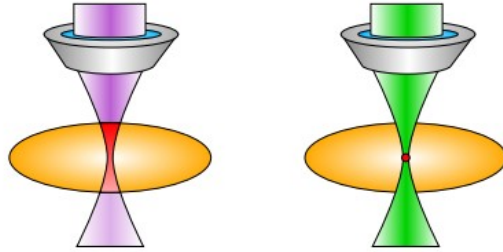


Figure 9: The volume modified by OPP is shown on the left-hand side. The whole beam reacts with the resist. In TPP (right-hand side), the polymerization only takes place in the focus where the intensity is high enough. Figure modified from [21].

a volume like shown in Figure 7. This approach only works for grayscale lithography, since the polymerisation will take place at very low intensities. I.e. the whole light beam, not only the focus, exposes the resist. The light will always be absorbed starting from the upper side of the material. In Figure 9 one can see a beam exposing a resist in OPP and TPP which emphasizes the different reaction volumes. In Figure 10 the behaviour of the penetration depth depending on the intensity can be seen. Higher intensities lead to bigger penetration depths. To a certain extend, the resolution is influenced by the intensity and the offset of the focal spot from the air-resist surface. Another important factor for the resolution is, of course, the objective lens used.

### 2.5.1 Non-linear resist response and proximity effect

One want to make sure that constant depth increments can be reached by varying the exposure dose accordingly. It turns out to be not trivial since the resist does not react linearly. This is due to the resist's optical and chemical properties. Figure 11a shows the resist response for a linear dose variation. One can observe that the resist will not create the desired structure but react non-linear. The exposure dose as a function of the resulting depth can be measured. The manufacturing process can adapted in order to take account for this effect. It is done by modifying the design or altering the intensity output levels corresponding to the height values measured. The correction of the non-linear behaviour by adapting the light distribution with its resulting linear depth variation can be seen in Figure 11b.

Furthermore, the proximity effect can cause deviations from the desired structure. One voxel may be effected by the additional dosage when nearby voxels are exposed. I.e. while exposing a specific region, other regions are exposed as well due to a fading but non-zero intensity. To reduce this effects, a similar approach can be done like the one for the non-linearity compensation. For a given exposure, the result is inspected. The deviations from the target structure are

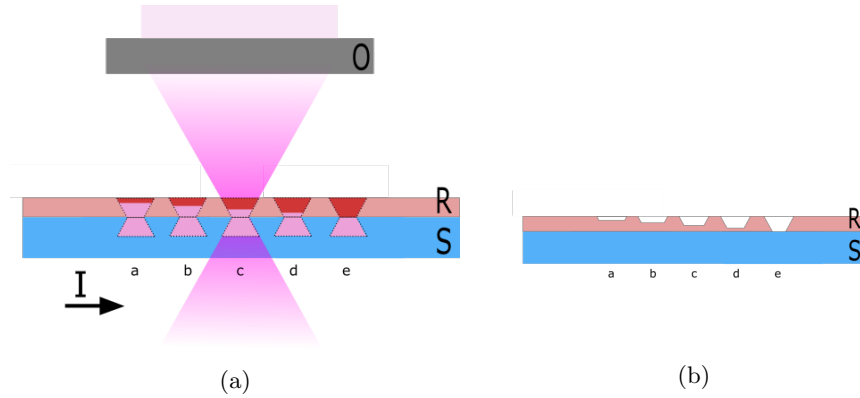


Figure 10: Resist manipulation by OPP. A sketch of the exposure of the resist (a) is shown. The light is focused through an objective lens O onto the sample consisting of the substrate S with the spincoated resists R. The depth of the structures is proportional to the light intensity (both increasing from left to right). The manipulated resist is indicated in deep red. The left-hand side shows the structure after developing (b).

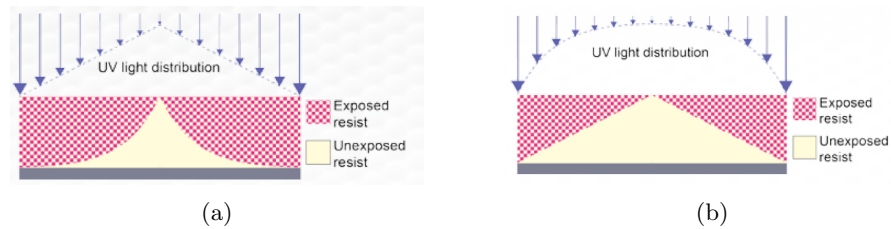


Figure 11: When applying a linear dose variation, the resulting structure will behave non-linear (a). By correcting the dosage distribution, one can achieve linear depth variations (b). Adapted from [7].

measured and a new optimized design is created. Iteratively, the exposure is redone with the new design and under consideration of the previously used scaling. This process can be repeated until the deviations from the target topography are as small as the order of magnitude of the TPP inherent uncertainty.

## 2.6 Fast two photon polymerization

A drawback of 3D printing in general, including TPP, is the long manufacturing time. The serial nature of the process sets a high limit for the duration. Additionally, the time necessary to write a structure has other contributions than the total amount of pixels. Writing with a constant voxel size means to maintain constant velocity during writing. To reach constant velocity at the beginning of a line, the trajectory has to be modified in order to include acceleration paths. Moreover, a constant velocity path might be inserted before each line written to minimize oscillations of the system. The acceleration paths and additional constant velocity paths might take more time than writing the structure itself but might be necessary to reach a good quality. In conventional 3D TPP where layer by layer has to be written, the time needed increases with the height.

Nonetheless, the speed and the total distance of the trajectory written are crucial parameters determining the duration. But, the two parameters cannot be chosen arbitrarily. Parameter constrain the speed, like the voxel overlap, voxel size or the acceleration behaviour of the movable components. Speeds of common setups for TPP are discussed below. Some physical and engineering factors which can be enhanced to make TPP faster are mentioned.

### 2.6.1 Common speeds of TPP

The scanning speed used by different research groups who have published about TPP varies. This is due to the different, often homemade setups. The setups differ in many ways like the laser, the optical components or the resin used. Here one of the leaders in commercializing TPP, the Nanoscribe GmbH, will be taken as an example. Nanoscribe uses a fiber laser with a wavelength of  $\lambda = 780 \text{ nm}$ . The fast galvo scanning mirrors allow writing speeds of  $v_{scan,galvo} = 10 \text{ mm/s}$  when using a high-NA objective lens. Since the focus gets more blurred if the laser beam is focused through the objective lens with an higher angle, the scanning range is limited to about  $140 \times 140 \mu\text{m}^2$ . The slower piezo stage has a velocity up to  $v_{scan,stage} = 100 \mu\text{m/s}$  and has a range of  $300 \times 300 \times 300 \mu\text{m}^3$  along the x-, y-, and z-axis. Since there is an underlying xy-stage capable of  $10 \times 10 \text{ cm}^2$  motion, parts made in galvo or piezo mode can be stitched together to produce a centimeter scale structure [1].

Malinauskas et al. [13] has published an equation that approximates the time required to fabricate a structure:

$$t = \frac{xyzF}{Rv} \quad (14)$$

Here, t is time needed for fabrication, F is the fill factor (between 0 and 1), R is the product of the desired lateral times the axial resolution and v is the scan

velocity.  $x$ ,  $y$  and  $z$  are the linear dimensions of the structure written. More suitable for comparison with TPP, we can also interpret the formula so that  $R$  is only the lateral dimension. Then,  $z$  is the number of layers.

For this thesis, the area of  $1\text{ cm}^2$  should be reached. The resolution is responsible for the feature size possible. Here, it should be fixed at a value of  $1\text{ }\mu\text{m}$ , and smaller feature sizes might be necessary. For 100 layers ( $z = 100$ ) and  $F$  close to 1, one would need a scanning speed of:

$$v = \frac{x y z F}{R t} = \frac{10\text{ mm} \cdot 10\text{ mm} \cdot 100}{0.001\text{ mm} \cdot 86400\text{ s}} \approx 115.7\text{ mm/s} \quad (15)$$

to finish this layer within one day. This is around 4 orders of magnitude higher than the experiments done by Malinauskas who worked with a scanning speed of  $v_{scan} = 1\text{ mm/min}$  [13]. It exceeds the galvo speed of the Nanoscribe system by a factor of 10. In addition to that, more than 5000 stitching procedures would be necessary.

It is clear that a  $1\text{ cm}^2$  structure cannot be produced with this TPP parameters. Attempts to make it faster are the strategies mentioned in the next chapters.

### 2.6.2 Physical parameters for fast TPP

There are several physical attempts to increase the output by e.g. writing with multiple beams. Replications of the structures can also be done.

- Multiple static beams:  
Faster fabrication with TPP can be done with a holographic pattern of several coherent laser beams. One single laser beam is modulated by a mask, creating more beams. Since the beams are created from a single laser beam, good temporal and spatial stability of the coherence is ensured. Kirkpatrick et. al. demonstrated large area patterning using holographic TPP [9]. They used a diffraction grating pattern which was first written in a photoresist. The laser beam was split into two beams that were overlapped in the sample plane with an angle of  $20^\circ$ . For temporal overlap, a photonic crystal was used.
- Multiple dynamic beams:  
To generate several foci of a single beam, a spatial light modulator adapts the intensity and phase of light passing. Such a modulator consists of liquid crystal pixels or deformable micro-mirrors. A hologram pattern can be sent from a computer to the spatial light modulator, the beam is then modified accordingly. Several voxels of different sizes and at different location can be written simultaneously. With this powerful approach, the sample can be scanned in a wider raster distance as usual, and therefore, significantly increases the fabrication speed. Complex structures may be produced near-simultaneously which can be an advantage. Since the time of creation is short, the internal flow of the resin is minimized and the structure will not be influenced by it.



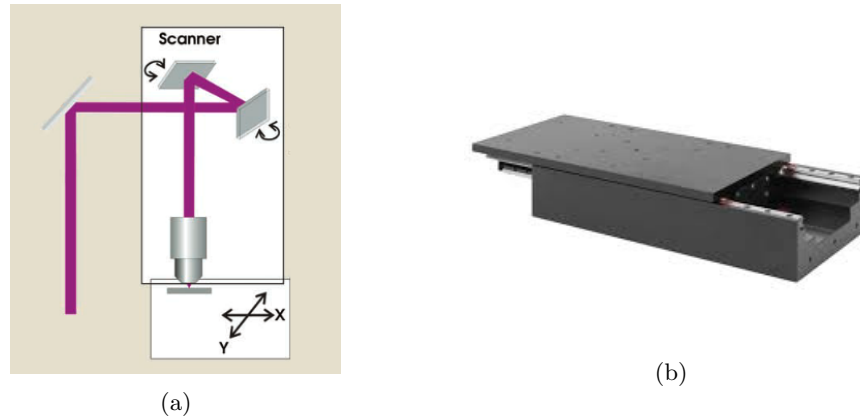


Figure 12: A mirror galvanometer scanner (a) modifies the beam direction with two movable mirrors. Sketch taken from [15]. A translation stage capable of precise in-plane movement (b). Picture taken from [4].

### 2.6.3 Engineering parameters for fast TPP

Increasing the speed of the physical movement might be an option to decrease the fabrication time. The two common motion systems, mirror galvanometer scanners and stages, are discussed with respect to their limits.

#### Mirror galvanometer scanners

A mirror galvanometer scanner, or galvo scanner for short, consists of two small mirrors mounted on motors. The mirrors are capable of guiding the laser beam through the objective lens to different points (compare Figure 12a). An engineering approach to decrease the fabrication duration would include an increase of the speed of the moving parts. This sounds easy but even a galvo scanner may need a huge force for a quick rotation because of the short acceleration and deceleration times. The linear scanning speed reached is several meters per second while maintaining a precision of 10 nm in typical TPP [28].

For controlling the motion, there are two strategies, vector positioning and raster positioning. A 2D vector is followed by the mirrors using vector positioning. A closed-loop feedback process controls the mirror position. In raster positioning, the sample is scanned in a meander form, leading to a quick movement of one axis while the other one is moving slowly. Commonly, vector scanning mode is used in TPP.

Galvo scanners are limited to 2D motion and to an area of about  $0.02 \text{ mm}^2$  with a high-NA lens. Since the angle of the objective lens' incident beam is modified in this approach, a bigger area leads to non-uniform focal spot shapes and to a bigger voxel size in other regions. To create larger 3D structures, a stage is needed to move to the next writing window attached to the one written first. This process called stitching leads to errors at the windows' boundaries.

**Translation stages**

Another possibility for performing the movement is a translation stage (compare Figure 12b). Translation stages can reach top speeds of several hundreds of mm/s. Since the stage is much heavier than the galvo scanner, the acceleration is limited to around  $5\text{ m/s}^2$ , yielding to a distance of 25 mm to reach a speed of  $500\text{ mm/s}$ . Within the 100 milliseconds of acceleration the shutter of the laser is closed. By minimizing the acceleration processes and maximizing the line length, very fast manufacturing times can be reached. The extended trajectory exceeds the boundaries of the structure due to the acceleration paths. The timing has to be precise and the shutter state has to change synchronously with the actual position of the trajectory. This critical engineering factor must be ensured by fast and accurate communication between the electronic control systems of the stage and the laser's shutter.

It is possible to speed up the manufacturing process by varying the laser power instantaneously with the speed of the stage. During acceleration one might lower the laser power accordingly to maintain a stable dosage and, furthermore, save time since the path is not only used for acceleration purposes.

In comparison to the galvo scanner, translation stages are much slower, but larger structures produced continuously. So they do not show stitching errors. Clearly, millimeter-sized structures like a microfluidic channel have much different requirements than micrometer-sized structures like a photonic crystal. The actual state of knowledge is that there is no optimally working approach for these two cases and there seems not even to be a clear cut off. A flexible TPP systems, therefore, should have both, a galvo scanner and a translation stage.

## 3 Method

This chapter describes the components, devices and strategies that were used for the work in the laboratory. This includes the laser and the optical components used for focusing. The creation and implementation of trajectories are sketched with all the software features needed. The support systems to observe the manufacturing process and to characterize the structures are mentioned.

### 3.1 General setup

Here, an overview of the installation is given. The setup is shown in Figure 13. The laser works with infrared light. An acousto-optic modulator (AOM) is used for controlling the frequency of pulses emitted, the so-called repetition rate. A second harmonic generation crystal (SHG crystal) is used to produce the green wavelength light used for TPP. The light is, then, guided to a lambda half plate and a Brewster window to control the power. After travelling through this power control, a beam expander is installed along the beam path. Via a dichromatic mirror a red He-Ne laser is collinearly aligned with the green femtosecond laser. Both beams are focused onto the sample which is fixed onto the stage. The stage is illuminated by a red LED from below. The camera observes the polymerization process. A PC and the stage controller are available to monitor and execute the trajectory as well as other process parameters. A detailed description of the parts can be found in the next chapters.

### 3.2 Femtosecond laser

In the laboratory, a Spectra-Physics Spirit laser was used to conduct the two photon polymerisation. The femtosecond laser works with the infrared wavelength  $\lambda = 1048 \text{ nm}$  and the frequency doubled  $\lambda = 524 \text{ nm}$ . The relevant parameters, such as the power output, pulse picker divider, output frequency and so on, can be set by the manufacture's program interface. However, the power output was mostly regulated by the analogue input bin of the laser which accepts a signal between  $U_{min} = 0 \text{ V}$  and  $U_{max} = 5 \text{ V}$ . The input signal sets the power output between 0 and maximum power. The maximum power for the frequency doubled laser beam were  $P_{max} = 14500 \text{ mW}$  which relates to a repetition rate of  $f = 1 \text{ MHz}$ . The pulse-enable input bin of the laser was used to achieve on and off modulation.

In order to reduce the laser intensity, a glass plate was used in reflection ( $\phi = 45^\circ$ ), leading to an attenuation to around 1%. The transmitted beam was send to a beam dump. The reflected beam was guided through a lambda half plate and after that through a Brewster window. The lambda half plate was installed on a rotatable mount. So, the power was controlled by the angle of rotation of the lambda half plate. A further reduction by two orders of magnitude was possible. An alternative option to reduce the power were gray filters with 5%, 10% and 25% transmittance.

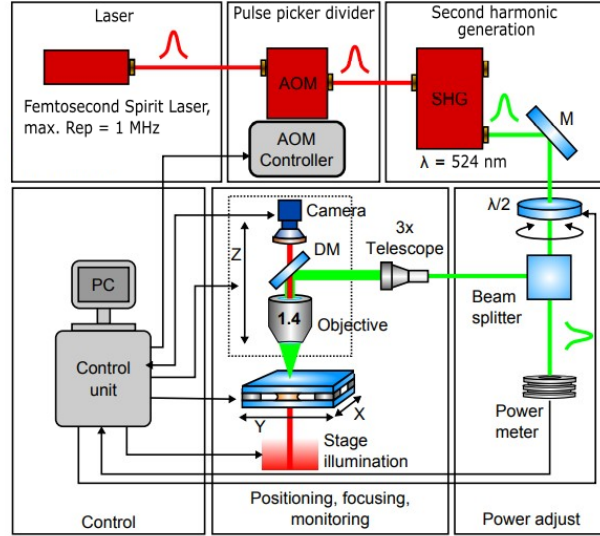


Figure 13: Setup - The laser is guided to the objective lens and focused onto the sample. The inline camera allows the observation of the writing process. Adapted from [21].

### 3.3 Objective lenses

A fixture with a beam expander was installed to widen the laser beam by a factor of three. The advantage of the beam expander is an optimal filling of the rear aperture of the objective lens leading to a narrower focus and a smaller voxel. The objective lenses used are listed in Table 2. Their numerical apertures and the expected voxel's aspect ratios are shown.

Without the beam expander, the non-uniform filling of the objective lens' rear aperture leads to an elongated spot and an effective numerical aperture which is smaller than the NA given.

| No. | Amplification | NA   | AR   | Comment       |
|-----|---------------|------|------|---------------|
| 1   | x10           | 0.25 | 15.3 |               |
| 2   | x20           | 0.5  | 7.6  |               |
| 3   | x40           | 0.75 | 5.1  |               |
| 4   | x100          | 0.8  | 4.8  |               |
| 5   | x100          | 1.4  | 2.7  | oil-immersion |

Table 2: Objective lenses used with their numerical apertures NA and expected aspect ratios AR for created voxels

### 3.4 Stage

The sample was placed on a Newport XM Linear Motor Stage. This stage was accessed by the corresponding Newport Universal XPS-D Motion Controller, or stage controller. The x and y-movement, lateral to the beam, were controlled by linear axes. In the experiments, the variation regarding the z-direction was possible by setting the distance between sample and the objective lens. The objective lens was, therefore, mounted to be movable by a z-axis spindle and a z-axis piezo element. The stage controller was extended with a laser power control output. The output was connected to the laser's "analogue in"-input. A low-pass filter was used to avoid rapid changes caused by high-frequency interference signals which were internally produced by the controller. The stage controller could be accessed by a web interface. The software used to write structures communicated with the stage controller via the .NET framework.

One important configuration is the definition of the axis groups. This is explained in section 3.6 in detail.

### 3.5 Online monitoring of the production process

The polymerization process was watched by an inline-camera. The camera used was a grayscale camera. A red LED was available as light source. It was placed to illuminate the sample from below, giving a good idea of what happens inside the volume of the sample. Filters were used to guide only red light from the light source to the photo diode array of the camera. Otherwise, the scattered light used for structuring would overexpose the camera.

A helium–neon laser (He-Ne laser) with a wavelength of  $\lambda = 632.8 \text{ nm}$  was aligned collinearly to the femtosecond laser beam. A dichroic mirror which is highly reflective for the femtosecond laser's green wavelength light and transmissive for the red light of the He-Ne laser was used to feed the He-Ne laser into the system. The He-Ne laser focal spot seen in the camera picture is used to find the air-resist or the resist-substrate interface.

### 3.6 Writing strategies

The stage controller can support up to eight axes. The power control output is seen by the controller as a virtual axis, so, five axes were used in this setup. The abbreviation for the axes are x,y and z for the corresponding movement direction; p for the z-piezo movement; and v for the power output. The connected axes now can be grouped or seen individually. An axis group is used to move the specific axes not only simultaneously but in sync. E.g. a xy-axis group moves the x and the y-axis with one command. With a multi axis group (in this case called xyzpv-axis group), all five axes are moving in sync.

The stage controller accepts only one trajectory file format for a given axis group. The structuring with the xy-axis group works with "line arc"-trajectories which allows to maintain a constant velocity while moving inside the xy plane. The structuring with xyzpv-axis group works with PVT trajectories (so-called

Point-Velocity-Time trajectory). In PVT, each individual trajectory element is defined by the relative displacement (P), the final speed (V) of each positioning and the duration for the element (T). The controller then calculates the cubic functional trajectory that passes through all defined positions at the defined times and speeds. PVT is a powerful tool for any type of trajectory with different velocities.

### 3.6.1 Writing with xy-axis group

The laser machining software LMS is a commercial software which works with an xy-axis group. A convenient interface displays the picture recorded by the camera, the chosen trajectory as well as the current stage position. However, the restriction to the xy-axis group means that one trajectory is executed with one constant power. A possibility to overcome this disadvantage is to read encoder signals from the stage controller. With the information from the encoder signals, the current position can be extracted. With a LabVIEW program, the power variation can be done externally of the LMS and during the execution of the trajectory. Due to the processing time of the program, there is a loss of an accurate sync of the different movements.

### 3.6.2 Writing with xyzpv-axis group

A LabVIEW and a python program achieved an in-sync movement by using the advantages of the multi axis group. The python program imports or creates a structure which is then converted into a PVT trajectory file. By defining the times and distances accordingly, one can make sure that the velocity is constant throughout a time interval where writing takes place. This is crucially necessary for the polymerization process because a different velocity would lead to a different exposure dose of the resist and therefore a bigger or smaller voxel.

### Generating a structure

A structure was generated by a CAD program and exported as a Stl-file. Stl-files could be imported into the Python software. A Bitmap-picture file, or Bmp-file, was created by rastering of the CAD structure. The heights were saved with the chosen grid via a Bmp-file's color values. Alternatively, any Bmp-file could be imported. One only has to specify the corresponding real width of a pixel. Figure 14 shows an example Stl-file and the Bmp-file created. Figure 15 shows the program interface for performing this transformation.

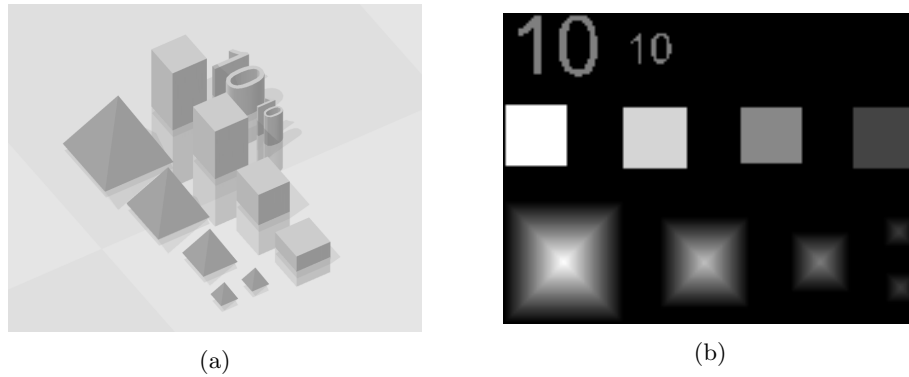


Figure 14: Imported Stl-file (a) generated with the 3D Builder and Bmp-file (b) converted with the self-made software for grayscale TPP printing.

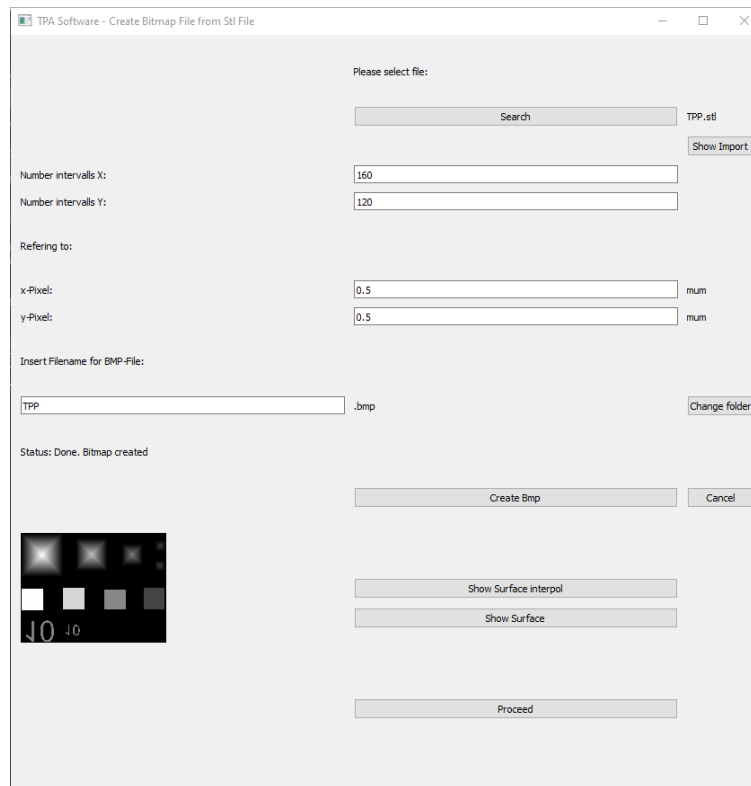


Figure 15: Python software user interface: Import of a structure's Stl-file and creation of a Bmp-file with given length and raster parameters

### Generating the PVT trajectory

Different strategies were used to write the structure. Mostly, a raster scan was used. Here, the scan accelerates to the specified velocity. One line (e.g. in x direction) of the structure is written. The stage decelerates and switches to the next line. It accelerates again to write this line and so on, in order to generate a meandering trajectory.

In the program, this means, after importing the Bmp-file, the raster scan is prepared. The acceleration and turning points have to be defined. This was done by considering the stage controller movement interpretation (for formulas see appendix 7.1). The time needed for acceleration is computed and an optimal time increment is found. The points and velocities reached after each time element were calculated. The constant velocity regions when writing the line are split accordingly to the chosen interval size. The output power signal for each interval refers to one pixel of the Bmp-file. Other parameters, like the interval duration, are determined as well. Finally, all the points can be stitched together in the right order. This process is illustrated in Algorithm 1. A short example of a PVT trajectory with only three of the five used axes can be found in Table 3. The height information encoded in the laser power output signal is here denoted as  $u$ . Figure 16 shows the resulting trajectory in a graph. The visualized xyz-plot must be interpreted in the following way. The x and y axis refer to the real physical axes while the z-coordinate is proportional to the voltage signal. The encoded velocity cannot be seen in this graph but is crucial for the writing afterwards. In Figure 17, the window for importing a Bmp-file and creating a PVT trajectory file is shown. Several structure parameters can be inserted.

With this procedure, an in-sync power modulation is established. A detailed description of the python program can be found in the guidebook in the appendix 7.2.

---

#### Algorithm 1: Construct a PVT trajectory for a given structure

---

```

Input structure defined by Bmp-file and pixel size;
Input writing parameters: speed, acceleration, ...;
Compute optimal acceleration and deceleration PVT trajectories for
given speed and intermediate line distance;
Write to file: starting acceleration PVT trajectory;
foreach Line of the picture do
    Write to file: PVT trajectory with constant velocity, the height is
    controlled by the laser power output value;
    if Not Last Line then
        | Write to file: Turning PVT trajectory
    else
        | Write to file: Final deceleration PVT trajectory
    end
end

```

---



| No. | $t/s$  | $x$       | $v_x$ | $y$      | $v_y$ | $u$  | $v_u$ |
|-----|--------|-----------|-------|----------|-------|------|-------|
| 1   | 0.0012 | 0.000008  | 0.04  | 0.000000 | 0.00  | 0.0  | 0.0   |
| 2   | 0.0012 | 0.000120  | 0.16  | 0.000000 | 0.00  | 0.0  | 0.0   |
| 3   | 0.0012 | 0.000264  | 0.28  | 0.000000 | 0.00  | 0.0  | 0.0   |
| 4   | 0.0012 | 0.000408  | 0.40  | 0.000000 | 0.00  | 0.0  | 0.0   |
| 5   | 0.0012 | 0.000552  | 0.52  | 0.000000 | 0.00  | 0.0  | 0.0   |
| 6   | 0.0012 | 0.000696  | 0.64  | 0.000000 | 0.00  | 0.0  | 0.0   |
| 7   | 0.0012 | 0.000840  | 0.76  | 0.000000 | 0.00  | 0.0  | 0.0   |
| 8   | 0.0012 | 0.000984  | 0.88  | 0.000000 | 0.00  | 0.0  | 0.0   |
| 9   | 0.0012 | 0.001128  | 1.00  | 0.000000 | 0.00  | 0.0  | 0.0   |
| 10  | 0.0050 | 0.005000  | 1.00  | 0.000000 | 0.00  | 3.0  | 0.0   |
| 11  | 0.0050 | 0.005000  | 1.00  | 0.000000 | 0.00  | 0.0  | 0.0   |
| 12  | 0.0050 | 0.005000  | 1.00  | 0.000000 | 0.00  | -3.0 | 0.0   |
| 13  | 0.0012 | 0.001128  | 0.88  | 0.000004 | 0.02  | 0.0  | 0.0   |
| 14  | 0.0012 | 0.000984  | 0.76  | 0.000060 | 0.08  | 0.0  | 0.0   |
| 15  | 0.0012 | 0.000840  | 0.64  | 0.000132 | 0.14  | 0.0  | 0.0   |
| 16  | 0.0012 | 0.000696  | 0.52  | 0.000204 | 0.20  | 0.0  | 0.0   |
| 17  | 0.0012 | 0.000552  | 0.40  | 0.000276 | 0.26  | 0.0  | 0.0   |
| 18  | 0.0012 | 0.000408  | 0.28  | 0.000348 | 0.32  | 0.0  | 0.0   |
| 19  | 0.0012 | 0.000264  | 0.16  | 0.000420 | 0.38  | 0.0  | 0.0   |
| 20  | 0.0012 | 0.000120  | 0.04  | 0.000492 | 0.44  | 0.0  | 0.0   |
| 21  | 0.0012 | 0.000008  | 0.00  | 0.000564 | 0.50  | 0.0  | 0.0   |
| 22  | 0.0012 | -0.000008 | -0.04 | 0.000564 | 0.44  | 0.0  | 0.0   |
| 23  | 0.0012 | -0.000120 | -0.16 | 0.000492 | 0.38  | 0.0  | 0.0   |
| 24  | 0.0012 | -0.000264 | -0.28 | 0.000420 | 0.32  | 0.0  | 0.0   |
| 25  | 0.0012 | -0.000408 | -0.40 | 0.000348 | 0.26  | 0.0  | 0.0   |
| 26  | 0.0012 | -0.000552 | -0.52 | 0.000276 | 0.20  | 0.0  | 0.0   |
| 27  | 0.0012 | -0.000696 | -0.64 | 0.000204 | 0.14  | 0.0  | 0.0   |
| 28  | 0.0012 | -0.000840 | -0.76 | 0.000132 | 0.08  | 0.0  | 0.0   |
| 29  | 0.0012 | -0.000984 | -0.88 | 0.000060 | 0.02  | 0.0  | 0.0   |
| 30  | 0.0012 | -0.001128 | -1.00 | 0.000004 | -0.00 | 0.0  | 0.0   |
| 31  | 0.0050 | -0.005000 | -1.00 | 0.000000 | 0.00  | 3.0  | 0.0   |
| 32  | 0.0050 | -0.005000 | -1.00 | 0.000000 | 0.00  | 0.0  | 0.0   |
| 33  | 0.0050 | -0.005000 | -1.00 | 0.000000 | 0.00  | -3.0 | 0.0   |
| 34  | 0.0012 | -0.001128 | -0.88 | 0.000000 | 0.00  | 0.0  | 0.0   |
| 35  | 0.0012 | -0.000984 | -0.76 | 0.000000 | 0.00  | 0.0  | 0.0   |
| 36  | 0.0012 | -0.000840 | -0.64 | 0.000000 | 0.00  | 0.0  | 0.0   |
| 37  | 0.0012 | -0.000696 | -0.52 | 0.000000 | 0.00  | 0.0  | 0.0   |
| 38  | 0.0012 | -0.000552 | -0.40 | 0.000000 | 0.00  | 0.0  | 0.0   |
| 39  | 0.0012 | -0.000408 | -0.28 | 0.000000 | 0.00  | 0.0  | 0.0   |
| 40  | 0.0012 | -0.000264 | -0.16 | 0.000000 | 0.00  | 0.0  | 0.0   |
| 41  | 0.0012 | -0.000120 | -0.04 | 0.000000 | 0.00  | 0.0  | 0.0   |

Table 3: An example PVT trajectory file. The intervals with the time  $t$ , their final relative positions  $x$ ,  $y$  and voltage signals  $u$  as well as the final absolute velocities  $v_x$ ,  $v_y$  and  $v_u$  are listed. The lines where structures are written have a constant velocity of  $v = 1 \text{ mm/s}$  (lines 10 - 12 and 31 - 33).

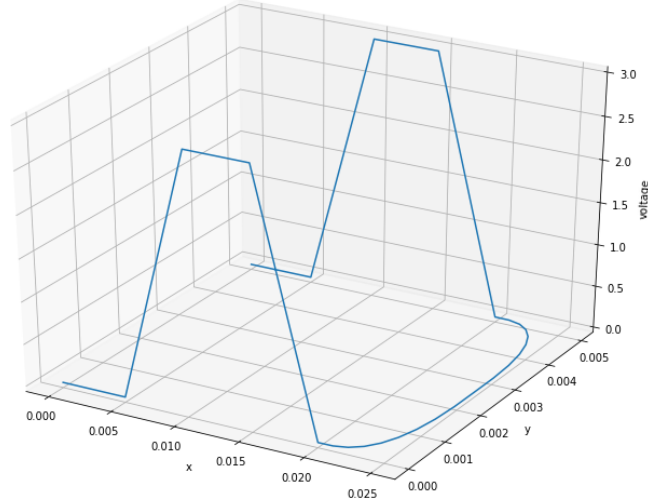


Figure 16: Visualization of the example trajectory to write a plateau consisting of two lines.

| No. | Name               | D           | Type | AGG |
|-----|--------------------|-------------|------|-----|
| 1   | OrmoComp           | OrmoDev     | n    | l   |
| 2   | IP-L780            | Isopropyl   | n    | l   |
| 3   | ma-P 1275G / 1240G | ma-D 532    | p    | s   |
| 4   | AZ 10XT            | AZ 400K 1:4 | p    | s   |

Table 4: Negative (n) and positive (p) photoresists used with their corresponding developers (D) and aggregate phases (AGG, liquid l or solid s)

### 3.7 Resists and placing the sample

The used resists are shown in Table 4. Generally, negative resists were liquid while positive resists were solid when placed onto the sample holder on top of the stage.

#### 3.7.1 OrmoComp

The most used negative-tone photoresist used was OrmoComp. OrmoComp is a UV-patternable inorganic-organic hybrid polymer for the generation of microstructures with optical applications [18]. After processing, the polymer shows transparency in the near UV and visible wavelength range as well as chemical and physical stability up to  $270^{\circ}\text{C}$ . The resist allows high resolution to sub- $50\text{ nm}$  pattern dimensions. The standard processing conditions are a temperature of about  $20^{\circ}\text{C}$  and a relative humidity of 40%. OrmoComp has to be processed under yellow light. Standard substrates are silicon, glass, or silicon

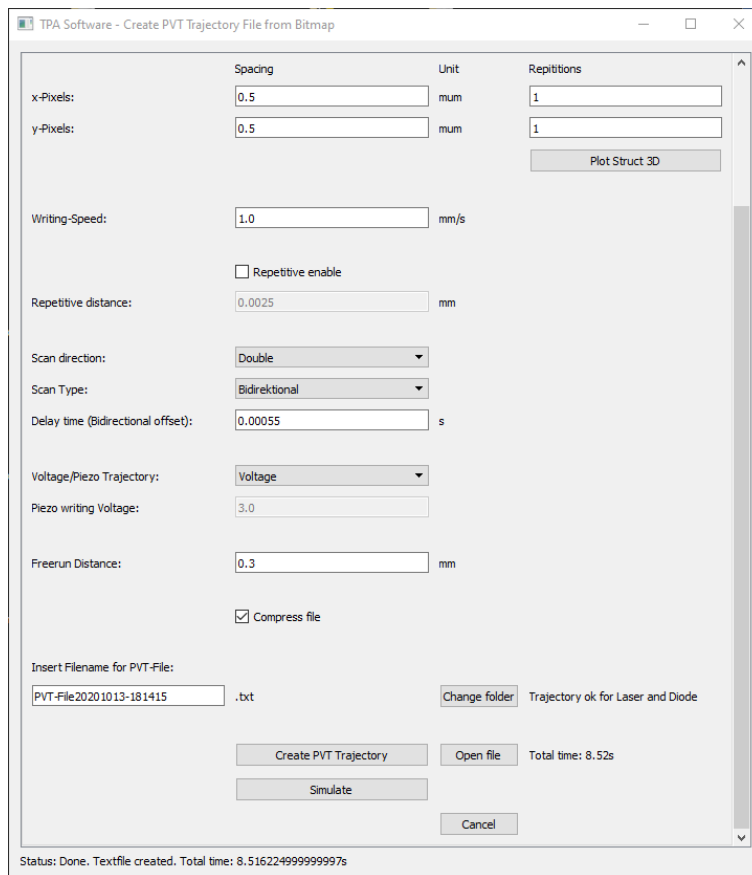


Figure 17: Python software user interface: Import of a structure's Bmp-file and creation of a PVT trajectory file with writing parameters given.

dioxide.

When **spin coating**, a film thickness of  $(20 \pm 4) \mu m$  is achieved after UV curing. To reach this thickness, the spin coating spin speed is about 3000 *rpm* and is applied for 30 *s*. A spin clean with 2-propanol and dehydration on a hotplate at 200°C for 5 *min* is recommended. However, the specific process parameters have to be chosen accordingly to the substrate and process environment.

Dilution of OrmoComp to achieve thinner film thickness can be done with OrmoThin. Specific film thickness ranges can be obtained by variation of the OrmoComp-OrmoThin mass ratio. OrmoThin is preferably applied for film thickness ranging from 20 to 0.5  $\mu m$ . For a mass ratio of 1 : 3 (OrmoComp : OrmoThin) a film thickness of  $\sim 0.5 \mu m$  is reached after UV curing.

Usually, the **exposure** is done with UV light. The material is sensitive to UV broadband, i-line (365 *nm*), or h-line exposure (405 *nm*). The substrates should be kept horizontal until the resin is cured. UV curing leads to volume shrinkage in the range of 5 – 7%. The curing at a single wavelength takes longer than exposure with broadband with the same dose. Using h-line requires longer exposure time or higher UV doses than using i-line. The resist remains still sticky after pre-bake. The exposure procedure has to be adapted to this. The exposure dose influences the resolution.

In the case of lithography, **development** is necessary. The wet-chemical development step removes uncured material. OrmoDev is a ready-for-use developer of choice. Application works best for about 20°C. Thoroughly rinsing with 2-propanol and blow-drying with nitrogen is recommended.

### 3.7.2 Negative resist - drop procedure

In this procedure, a glass substrate with a thickness 170  $\mu m$  was cleaned by acetone and by applied pressure. Afterwards, the same was done with isopropyl alcohol.

A drop of the resists was put on the glass substrate. While the total area of the glass substrate was  $2.2 \times 2.2 \text{ cm}^2$ , only the middle part with a diameter of approximately 5 *mm* was used.

The sample was placed onto the holder facing down. The sample holder had a hole, so that the sample holder is touching the sample at the boarder and does not touch the resist. The laser was focused through the glass. This can be seen in Figure 18. When using the oil-immersion x100 objective lens, the drop procedure is the setup of choice. In this case, the immersion oil is put between the objective lens and the glass substrate. No contamination of the resist by the immersion oil will take place.

### 3.7.3 Negative resist - spin coating

This sample preparation was done with a spin coater. A ratio of two parts OrmoComp and three parts OrmoThin were mixed and a few drops were placed onto a cleaned glass substrate. The spin coater applied a rotation speed of 3000 *rpm* for 30 *s*, accelerated with 1200 *rpm/s*<sup>2</sup>. After that, the substrate was

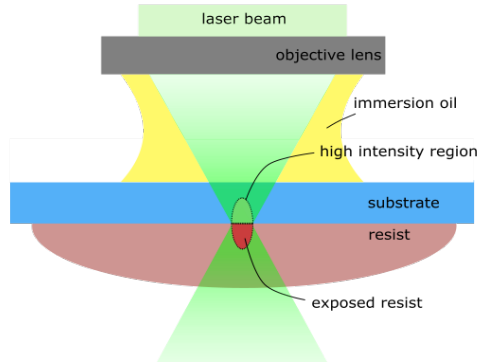


Figure 18: Drop procedure. The drop of the resist is placed on the substrate and is inserted face down.

placed on a hotplate for 2 *min* as a pre-exposure bake. The sample was processed in a timely manner, since the layer did not remain extended but started to contract within hours. A sketch after placing the sample onto the stage is shown in Figure 19. Alternatively, the sample can be inserted with the spin coated layer facing down. The spread layer had a thickness of  $(4 \pm 1) \mu\text{m}$ . However, the resist layer's thickness can be controlled in a wide range by varying the OrmoComp-OrmoThin mixture ratio as well as by varying the rotation parameters.

### 3.7.4 Negative resists - development

After the writing process, the negative resist was put into the corresponding developer for two minutes. The glass plate was placed vertically, so, the liquid resist could sink to the bottom of the container easily. Before pulling out, the container with the sample and the developer was optionally exposed to UV light to strengthen the structure. This was done, especially, for weak, small structures like voxel fields and for structures written by z-piezo scans to solidify the liquid resist inside the hull. Finally, the glass plate with the developed structure was removed from the container with the developer and rinsed by isopropyl alcohol. Finally, the sample was dried by pressured air to evaporate the remaining isopropyl from the rinse.

### 3.7.5 Positive resists - spin coating

Positive resists were spincoated on glass substrate with thickness of 1 *mm*. The total area was  $2 \times 2 \text{ cm}^2$ . The resists were processed with a rotation of 3000 *rpm* and an acceleration of 500 *rpm/s* for 30 seconds. The edge bead lead to usable area of about  $1.5 \times 1.5 \text{ cm}^2$ .

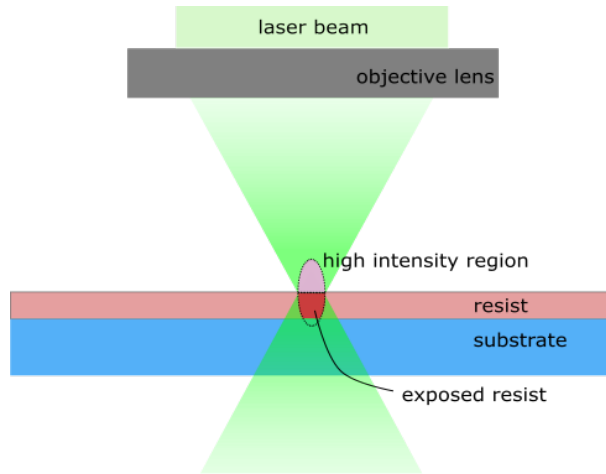


Figure 19: Spincoated sample. The resist is placed on the substrate facing up.

### 3.7.6 Positive resists - development

After the writing process, the positive resist was placed in the container with the developer. The standard development time for the resists was 75 s for ma-P 1275G, 40 s for ma-P 1240G, and 420 s for AZ 10XT. But, the depth of the structures is here tunable with the development time. So to reach deeper structures, one can increase the development time by 30 – 60 s for an increase of 1  $\mu\text{m}$  in maximum depth. After development, samples were rinsed with deionized water and dried by pressured air.

## 3.8 Characterization of the samples

### 3.8.1 Keyence Laser-Scanning Microscope

A Keyence laser scanning microscope VK-X100K [3], LSM for short, was used to examine the created structures (see Figure 20b). The LSM uses a two-way light source comprised of a laser light source and a white light source. The two light sources together provide the colors, laser intensity and height information necessary to create deep field color images, laser intensity images or height images. A very important, in this master's thesis used feature is the height measurement which is described below in detail. Additionally to the 3D reconstruction, the microscope creates significantly better contrast than a standard optical microscope because of the two light sources used. The laser confocal technology obtains images with a large depth of field. Several objective lenses are available ranging from a magnification of x5 (NA = 0.13) to x150 (NA = 0.95).

Now, the measurement procedure is described. After starting the observation application, the lens position is initialized. The sample is placed onto the



Figure 20: Pictures of the JOEL scanning electron microscope (a, SEM, Source [12]) and the Keyence laser scanning microscope (b, LSM, Source [3]).

rotatable stage. The revolver with the lenses is turned to choose the desired magnification. The x axis stage handle and y axis stage handle can be used to move the sample to a specific observation location. The angle can also be set. With the focusing handle the focus can be adjusted. With help of the observation application the sample can now be observed and measured. When measuring the height in high precision under normal circumstances, the standard x50, x100 and x150 objective lenses are suited. However, the highest magnification lens possible should be used for high-resolution height images.

### Height determination

The height is determined by a simple optical principle. In the laser confocal optics, a pinhole where the reflected light from the sample forms an image ensures that the focal position sends the maximum possible amount of light to the photoreceptor. It allows changes in the focal point to be measured and used as height information. I.e. when the focus position is reached, both, conventional optics and confocal laser optics allow all of the reflected light to enter the photoreceptor. In contrast, when out of focus the conventional optics allow all of the reflected light into the photoreceptor, confocal laser optics allow only a fraction. With a high-speed xy-scanner the image containing height information is recorded by rastering the sample for discrete positions. The focused spot light scans the image area within the field of view using the xy-scan optics. A standard division of the field of view is  $1024 \times 768$  pixels. By driving the objective lens in the z direction to repeat the scan of the image, the intensity of each pixel at every position on the z axis is obtained. Thus, the height can be measured since it is the position of the z axis where the intensity is the highest. From the height information, the shape and the roughness of the sample can be determined.

### 3.8.2 Scanning electron microscopy

We used the scanning electron microscopy JOEL JSM-IT100, SEM for short [12]. It could be controlled via a touch panel and via a computer with the corresponding software. A picture of the device is shown in Figure 20a. The specimen chamber was equipped with various detector ports such as the EDS, energy-dispersive x-ray spectrometer. In this thesis, a silicon-drift EDS detector was used. It reaches an energy resolution of  $129\text{ eV}$  or better. The SEM can select high and low vacuum type observations. However, since the structures could be easily metalized, the high vacuum mode could be used which allowed better resolution. The metalization was done by thin film deposition by vapor deposition.

After starting the equipment, the specimen chamber is vended. The metalized specimen is inserted into the specimen chamber and the evacuation is started. When the final pressure is reached, the observation starts. Images can be taken at different magnifications. In our case, the magnification was mostly in the range of  $\times 700$  and  $\times 7000$  for the structures and voxels. The microscope enables high-resolution observation, e.g. a resolution of  $4.0\text{ nm}$  at an acceleration voltage of  $20\text{ kV}$ . However, the acceleration voltage was chosen as  $10\text{ kV}$  which was more than sufficient to resolve even the smallest voxel with more than  $100\text{ nm}$  feature size. Usually pictures were made placing the specimen once perpendicular and once in an angle of  $30^\circ$  to the beam, to get a good lateral feature measure resp. to gain knowledge about the height and the shape of the structures.

### 3.9 One photon polymerization

In this section, the adaption of the system to conduct one photon polymerization (OPP) is described. For OPP, the laser diode Cobolt 06-MLD was used. It emits blue light with a wavelength  $\lambda = 405\text{ nm}$ . The power could be modulated in various ways which are described below. Before entering the objective lens, the emitted beam is guided through an lambda half plate and a Brewster window, similar to the setup of the femtosecond laser; the power can be reduced to lower levels. Furthermore, a beam expander was used here as well, to ensure total and uniform illumination of the objective lens. In the focus of the first lens of the beam expander, a pin hole with a diameter of  $d = 20\text{ }\mu\text{m}$  was installed to correct the oval profile of the beam.

The polymerization conducted with OPP cannot create structures inside a volume, since the polymerisation will also take place at very low intensities. I.e. the whole light beam, not only the focus, exposes the resist. This can also be seen in Figure 9 and 10.

In addition to the conventional approach using a positive resist, spincoated OrmoComp was processed with the diode laser as well. When the spin coated layer is facing up, only a 2D structure can be created. Here, the penetration depth has to be as thick as the layer, otherwise, the structure will not stick onto the substrate. When the spin coated layer is facing down, grayscale lithography



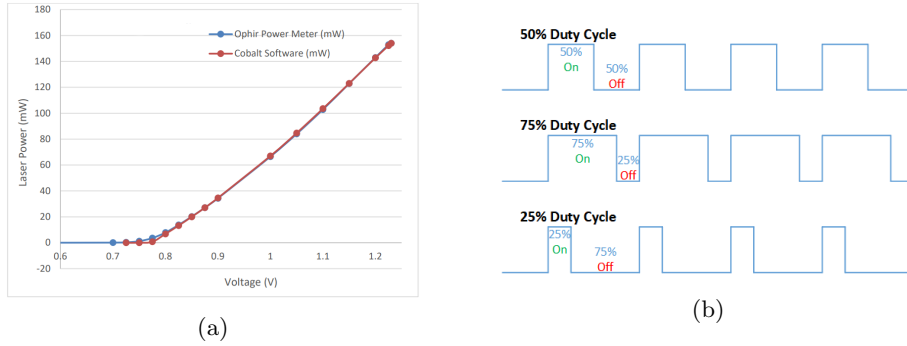


Figure 21: Controlling the output power of the laser diode. The power dependence on the analogue input voltage is shown (a). For the digital input mode, the maximum power is set via the interface and the fraction is controlled by the duty cycle signal (b, taken from [2]) generated by a microcontroller.

can be conducted, exposing resist near to the substrate first.

### OPP power control

The output power of the diode could be controlled between 0 and 150 *mW*. While it is possible to set the power via a software manually, the power could be modulated by an analogue as well as a digital signal. In addition, the laser diode allows on/off-modulation. The analogue input sets the output power directly. The input voltage ranges from 0.7 *V* to 1.2 *V* to set the power to the minimum resp. maximum power. The power-input voltage curve can be seen in Figure 21a. Due to this very limited range, the digital input mode was preferred.

The digital input signal is a on/off-signal which is  $V_{off} = 0$  *V* resp.  $V_{on} = 5$  *V*. This signal sets the duty cycle of the diode laser. The diode emits at constant power for the time the digital input is 5 *V* and is switched off totally when the input signal drops to 0 *V*. For fast modulation of this duty cycle (compare Figure 21b), a micro controller was used to process the input signal from the stage controller which is an analogue one between 0 and 3.3 *V*. The output signal is then created, transforming the height of the input signal to the "on"-time of the output signal. The controller works with an digital analogue converter with a resolution of 8 *bit* and at a sampling rate of 1 *MHz*. Since this is a very fast method compared to the movement of the stage, the dose which exposes a certain voxel can be controlled efficiently.

### 3.10 Freerun distance

The mechanical issue of stage oscillations are discussed in this section. One way to overcome large stage position error within the writing area, is by introducing a freerun distance. A linear line without output power is added in front of a writing line. Since no acceleration is applied, the control cycle of the stage

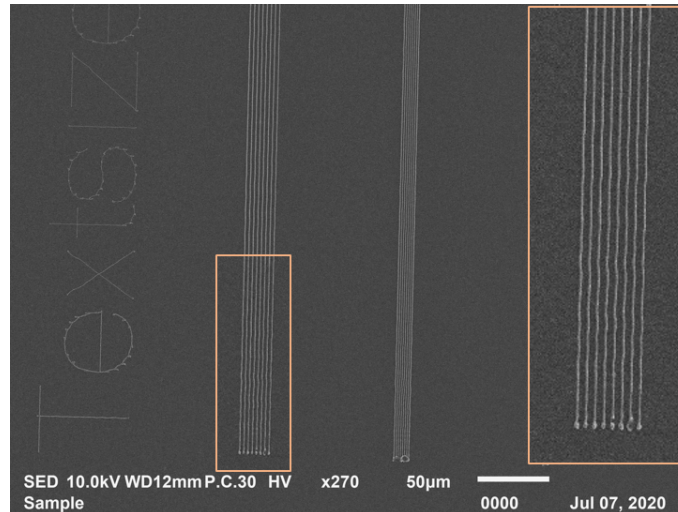


Figure 22: Lines with an intermediate distance of  $5\ \mu\text{m}$  (left and detail) and  $3\ \mu\text{m}$  (right) written with the x100 objective lens. Fluctuations to a straight line can be seen within the first  $300\ \mu\text{m}$  of the  $1\ \text{mm}$ -long lines. The scanning speed was  $v_{scan} = 1\ \text{mm/s}$ .

will reach a more accurate velocity and position. I.e. the controller is able to minimize the position error during that freerun time.

To illustrate the problem, lines without freerun distance are shown in Figure 22. One can observe fluctuations. Figure 23 shows the central part of the lines without fluctuations. The xy-scan strategy supports the stability since the y-axis only moves a little. A freerun distance of  $300\ \mu\text{m}$  per  $\text{mm/s}$  scanning speed was widely chosen.

### 3.11 Stability tests

#### TPP - Laser ablation

Since the laser power is high enough, the same set up can be used for laser ablation. Instead of the substrate with the resist, a glass plate was placed onto the stage. The upper interface of the plate was found with the help of the He-Ne laser spot and the power was adjusted to cause the glass to evaporate by exposure. The pulse picker divider was set to 1000 and the velocity to  $v = 2\ \text{mm/s}$ . So, holes with an intermediate distance of  $2\ \mu\text{m}$  were produced. The constancy of the laser power output is indicated by the uniformity of the holes.

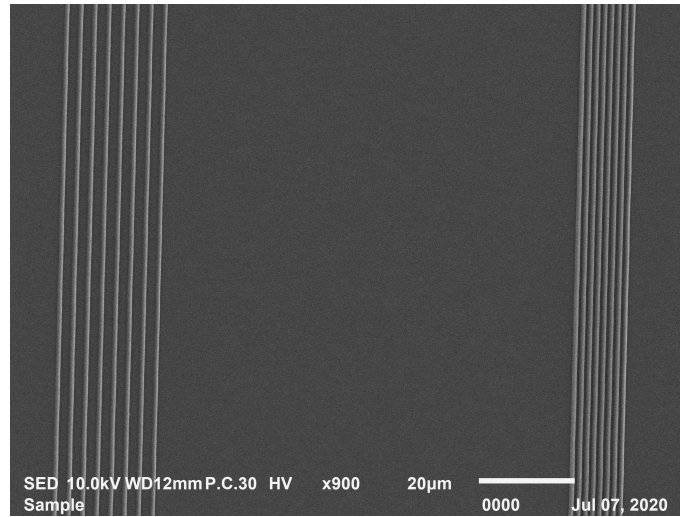


Figure 23: Lines with an intermediate distance of  $5\ \mu\text{m}$  (left) and  $3\ \mu\text{m}$  (right) written with the x100 objective. Fluctuations are not seen in the center of the  $1\ \text{mm}$ -long lines. The scanning speed was  $v_{scan} = 1\ \text{mm/s}$ .

### TPP - voxel study

Voxels were created with the x100 and the x20 objective lens. Different offsets and power inputs were examined and compared. The exposure was applied to OrmoComp by the drop procedure. The minimum voxel size can be determined which is an indicator for the spatial resolution of the process.

### OPP - bars

To control the uniform output of the laser diode, bars were written into the ma-P 1275G positive photoresist. The roughness and the visual appearance of the pattern indicate a good stability of the setup. The same was done with the femtosecond laser for comparison. The average power of the the femtosecond laser was  $750\ \mu\text{W}$ , the power of the laser diode was  $50\ \mu\text{W}$ . The speed was  $v = 1\ \text{mm/s}$  and the x20 objective lens was used.

## 3.12 Test structures

The aim of the master's thesis was the fast manufacturing of relief surfaces. Some chosen test structures show the characteristics of the writing processes. Plateaus, pyramids, staircase and chessboard patterns show the ability of the process to create constant slopes and plain surfaces. Various combinations of resists, procedures, test structure and light sources were tested and compared, e.g. plateaus written in ma-P 1240G with the diode laser, or pyramids written into drop processed OrmoComp with the femtosecond laser.

## 4 Results

In this section the written voxels, lines and structures are discussed.

### 4.1 Stability tests

#### TPP - Laser ablation

A picture of ablated holes into a glass substrate is depicted in Figure 24. The continuity of the holes can be seen in this overview. With this experiment, the chemistry taking place in a resist could be excluded from the system. The total average power was set to  $\sim 10mW$  which was much higher in this experiment than in TPP experiments. However, it is an indication that the laser emitted uniformly and had a high pulse stability.

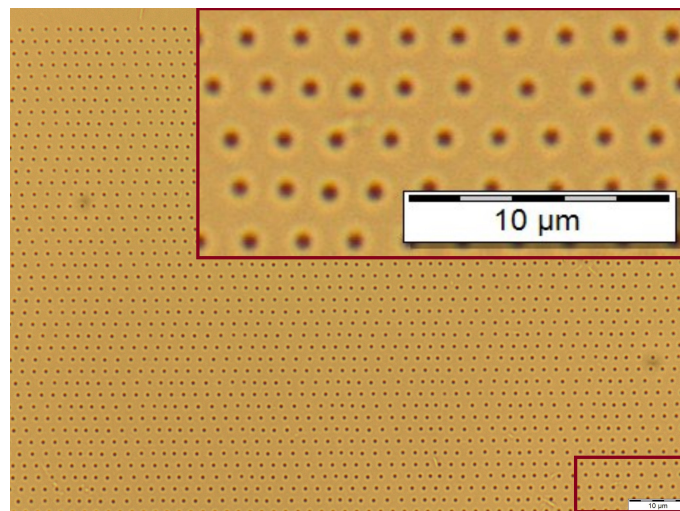


Figure 24: Ablated holes in a glass substrate written with the femtosecond laser at  $2mm/s$  with an pulse picker divider of 1000 and a repetition rate of  $1MHz$ .

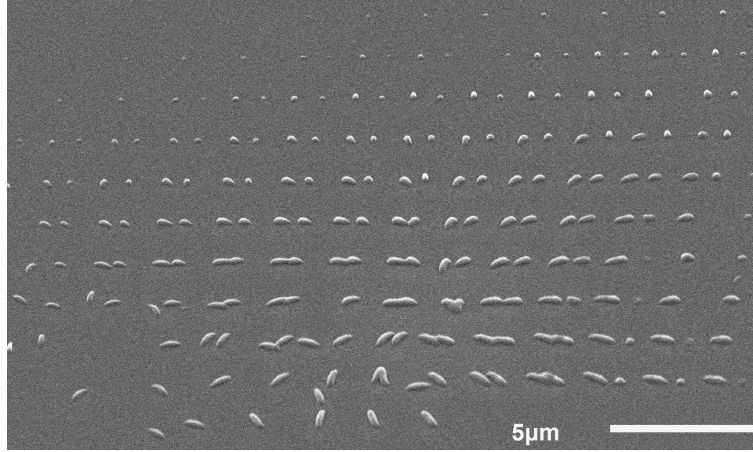


Figure 25: Voxels written with the x100 objective lens. The voxels were varied in lateral offset from top to bottom ( $\Delta z = 0.1 \mu m$  per line) and varied in power from left to right.

### TPP - Voxel study

The voxel written by the TPP technique is sensitive to the objective lens. The total dimensions as well as the aspect ratio depend on the numerical aperture of the lens chosen. A description and results are given for the x20 and the x100 objective lenses. Furthermore, the influence of the laser power is discussed in detail.

### Comparison of voxels written with x20 and x100 objective lenses

Figure 25 shows voxels written with the x100 oil-immersion objective lens into OrmoComp prepared with the drop procedure. The focus was varied in a total range of  $\Delta l_{tot} = 1 \mu m$  around the interface in steps of about  $\Delta l = 0.1 \mu m$ . Offsets into the substrate are seen at upper lines, offsets into the resist are seen in lower lines. The power was increased (left to right) by varying the input signal in the range 0 to 5 V. The maximum power was set to around  $P = 1 - 5 mW$  before the objective lens. The distances between lines were  $2 \mu m$  and the distance between the voxel within a line as well. This was achieved by setting the scanning speed to  $v_{scan} = 2 mm/s$  and the repetition rate to  $1 kHz$ .

The bottom lines in Figure 25 refer to a focus which was too deep inside the substrate. Small voxels are not shown since they are totally inside the substrate (Figure 26a situation a). The top lines, on the other hand, do not show smaller voxels because the focus was too deep inside the resist (Figure 26a situation g), the voxels created with low powers were not big enough to reach the interface. They float in the liquid resist and are washed away when developing the structures. Middle lines do show small voxels since they are half inside the substrate (Figure 26a situation d) so that good contact is assured. The diameter

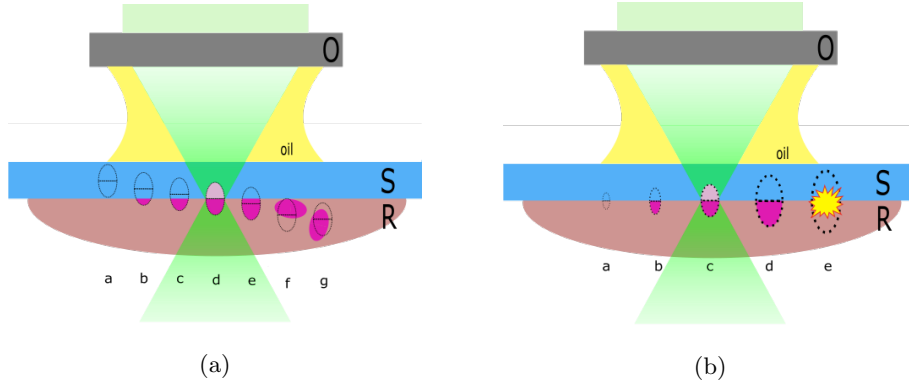


Figure 26: Behaviour of the voxel when adapting the focus offset (a) and power (b). The objective lens (O) focuses onto different planes inside the resist (R) or the substrate (S). The focus offset is lowered from a too-high offset (a, situation a-c) to a too-low offset (a, situation e-g). The power is risen from low (b, situation a) to high power (b, situation e).

| Objective lens | $d_a/\mu m$    | $d_l/\mu m$     | $ar/1$        |
|----------------|----------------|-----------------|---------------|
| x20            | $10 \pm 1$     | $1 \pm 0,1$     | $10 \pm 2$    |
| x100           | $0,5 \pm 0,05$ | $0,15 \pm 0,05$ | $3,3 \pm 1,5$ |

Table 5: Measured values of the smallest lateral  $d_l$  and axial  $d_a$  dimensions with the resulting aspect ratios  $ar$  of voxels for the different objective lenses used.

of a voxel can be examined by looking at these cases. The minimal diameter achievable can be measured by the most-left voxel in these lines. In lines with a focus inside the resist, it can happen that the voxel is attached marginally to the surface. Those voxels may lay down (Figure 26a situation f). The axial length of these voxels can be therefore measured easily.

The power increase from left to right can be seen by the growing voxel size. While at low powers (Figure 26b situation a) no voxel is created, one can tune the size easily by adapting the power (Figure 26b situation b-d). Parameter ranges of the voxels written were mainly chosen to create such cases. At too high powers, the exposed volume will immediately vaporise and bubbles inside the resist are built (Figure 26b situation e).

In comparison to the x100-voxels shown above, Figure 27b shows voxels written with the x20 objective lens at medium power. The voxels were written slightly above the interface. The intermediate voxel distance is  $1.25 \mu m$  instead of  $2 \mu m$  in the x100-case. However, one can immediately see the different aspect ratio. Table 5 shows the smallest voxel sizes measured and the derived aspect ratios. Whereas the aspect ratio of the x100-voxels are about 1 : 3 the x20-voxels have an aspect ratio of about 1 : 10. This confirms the expectations from the theoretical treatment from section 2.2.3.

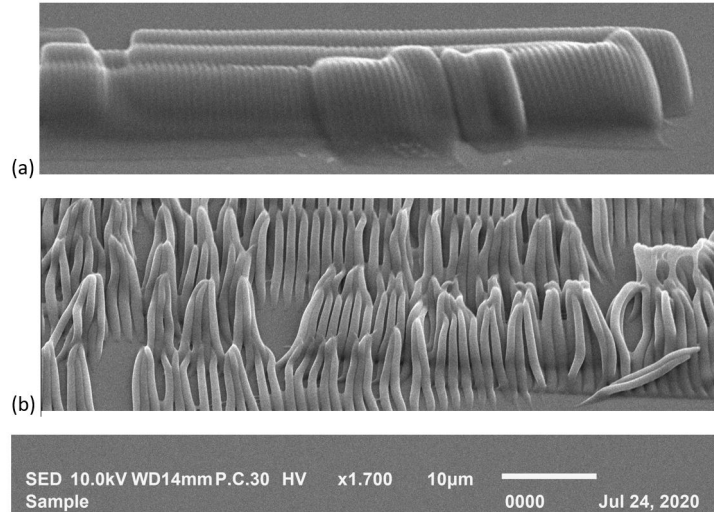


Figure 27: Voxels written with the x20 objective lens. The distance between two pulses was  $\Delta d_{(a)} = 0,7 \mu m$  and  $\Delta d_{(b)} = 1,25 \mu m$ .

### Growing lines with voxels

Figure 27 shows voxel with different intermediate distances. Where in Figure 27.b the voxels are separated, the voxels in Figure 27.a are close enough to build one enclosed volume. The ellipsoid shapes of the single voxels can still be clearly seen and it is still no perfect line. The overlap has to be chosen bigger to build a line with less fluctuation in height. A good line consists of very close lying voxels. In order to keep the dose constant, the power input has to be decreased with increasing overlap of the voxels.

The separated voxels in Figure 27.b show another interesting effect. The voxel do not remain straight like they are written. The reason are forces appearing when the developer vaporizes [16]. These forces attract voxels towards the center of longer lasting liquid drops. The relatively long voxels are not stable enough to remain in the straight position but tend to lean against each other.

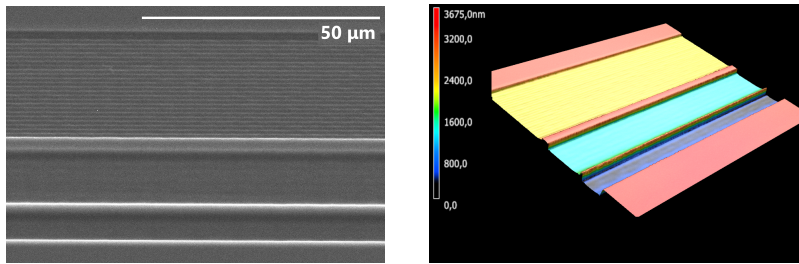


Figure 28: SEM (left) and LSM (right) picture of bars written by the laser diode. The distances between lines were  $\Delta l = 1, 0.5$  and  $0.25 \mu m$  for the upper, middle resp. the lower bar.

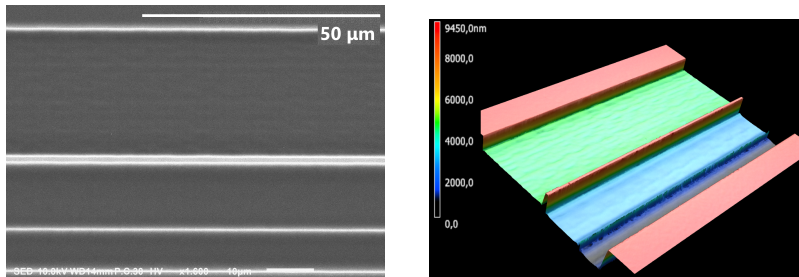


Figure 29: SEM (left) and LSM (right) picture of bars written by the femtosecond laser. The distances between lines were  $\Delta l = 1, 0.5$  and  $0.25 \mu m$  for the upper, middle resp. the lower bar.

### OPP - Bars

The diode laser was modulated by the digital signal produced by the microcontroller. The power was set to a medium value between no impact and exposure of the whole layer. Several lines were written to achieve a bar. Three bars were written by choosing the distance between two lines  $\Delta l = 1, 0.5$  and  $0.25 \mu m$ . In Figure 28, the lines can still be seen for the  $1 \mu m$ -case. The other two bars do not show any structure arising from the line nature of the polymerisation process. In comparison to the laser diode, the femtosecond laser shown in Figure 29 generates bars where also the  $0.5$  case show the line pattern. An important point to mention is the dependence of the depth from the line distance. For smaller distances, the structure gets deeper since the nearby lines overlap more. This increasing overlap, however, assures even better approximation of a plane and decreases the line nature of the structure.



## 4.2 Variation of the focus offset

Lattices were written into spincoated OrmoComp with a thickness of about  $5\ \mu\text{m}$ . The offset of the focus was adapted. Generally the focus was adjusted to be exactly at the interface between the spincoated OrmoComp and the glass substrate. The focus was risen and lowered by  $6\ \mu\text{m}$  to get a focus once near the air-resist interface and once deep inside the substrate. The experiment was conducted with the femtosecond laser as well as the laser diode. In Figure 30 the resulting lattices are shown.

Clearly, the different behaviour of OPP and TPP can be seen. The reason is the reaction volume of the technique. In Figure 31 the underlying effect is shown. First, OPP will be discussed. Moving the laser beam up, leads to a sharp structure (Figure 30a) since the focus is near the air-resist interface (Figure 31a situation a). When writing with the focus located at the resist-substrate interface, the OPP results in broader lines (Figure 31a situation c). In Figure 30e one can see a very blurred lattice due to the very low lying focus. A broad beam part is now matching with the air-resist interface (Figure 31a situation e). When using OPP, it is always written from above. The whole negative resists layer height is exposed, i.e. the resulting structures are always as high as the spincoated layer. An exception would occur at too low intensities where the structure cannot grow towards the resist-substrate interface. In this case, the structure would be washed away during developing.

Now, the laser writing behaviour can be compared to the effects mentioned in the OPP case. In Figure 30b, the TPP-structure shows a lattice with the desired height for the focus near the air-resist interface. Here it should be mentioned that the lines (direction left-write) have a waviness which is explained by the fact that the lines written first did not stick to the substrate. The lines start to float. The vertical lines were written afterwards and pin the structure onto the substrate. In Figure 31b (situation a) one can see the illustration of the process. The voxel is only slightly touching the resist-substrate interface. By exposing a point of the resist twice, which happens at the crossing of the vertical and the horizontal lines, the exposed volume gets bigger and a better adhesion is assured. By moving the focus towards lower lying z-values, the adhesion of the structure is enhanced also for single exposed points. When writing on the resist-substrate interface, the lines adhere onto the substrate perfectly while exposing the total layer thickness. A requirement is that the voxel's axial size exceeds the thickness of the layer twice. For the x20 objective lens and inside the spincoated OrmoComp layer of about  $5\ \mu\text{m}$ , this is the case (compare voxel's size from Figure 27). By lowering the focus, the TPP structure is less tall and broad (Figure 30f) since only the upper part of the voxel is located inside the resist (Figure 31b situation e). Most of the focus is located inside the glass substrate and does not have any influence to the structure. This is a totally different behaviour as in the OPP case where the structure gets bigger.

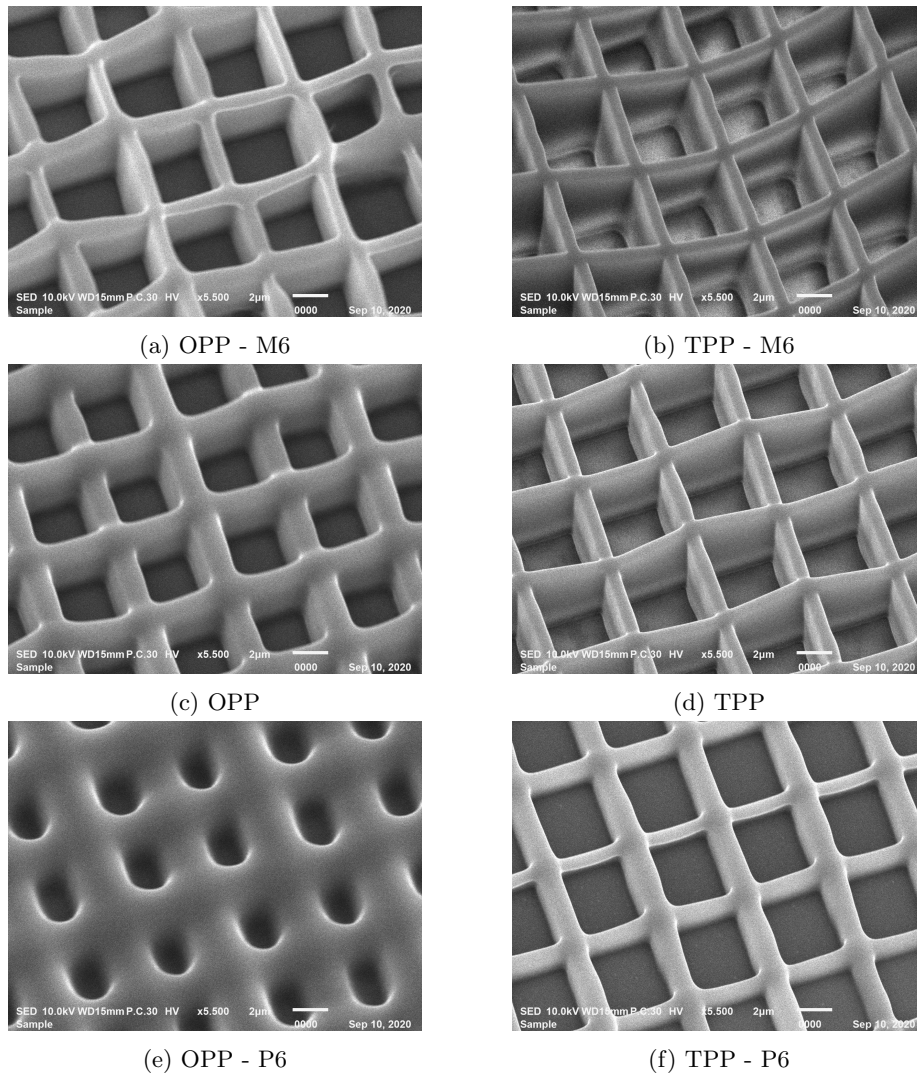


Figure 30: Lattices written with the laser diode (OPP, left column) and the femtosecond laser (TPP, right column), An offset to the glass-resist interface of  $-6\ \mu\text{m}$  (a, b),  $0\ \mu\text{m}$  (c, d) and  $+6\ \mu\text{m}$  (e, f) was chosen.

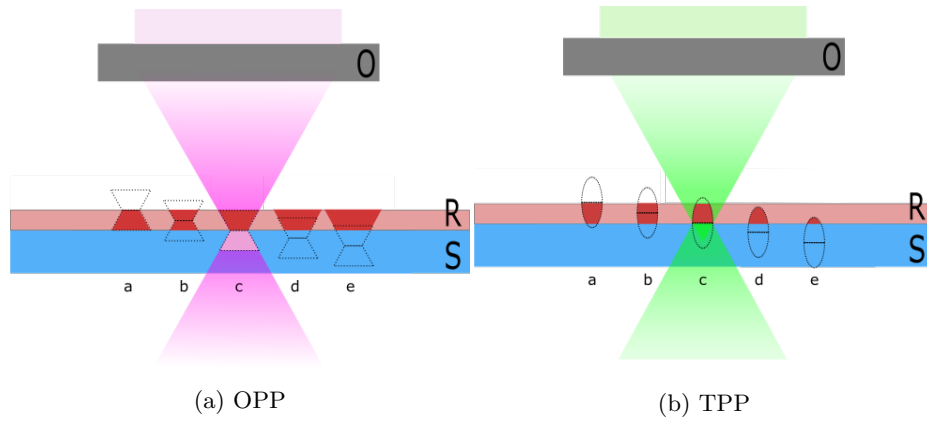


Figure 31: Exposed volume of the polymerization process shown for different focus offsets with respect to the resist-substrate interface. The objective lens (O) focuses onto different planes inside the resist (R) or the substrate (S). The femtosecond laser (TPP) writes only in the focal region, the diode laser (OPP) writes with the whole beam. The situations where the focus is too high and inside the resist are a-b the situations where the focus is too low and inside the substrate are d-e.

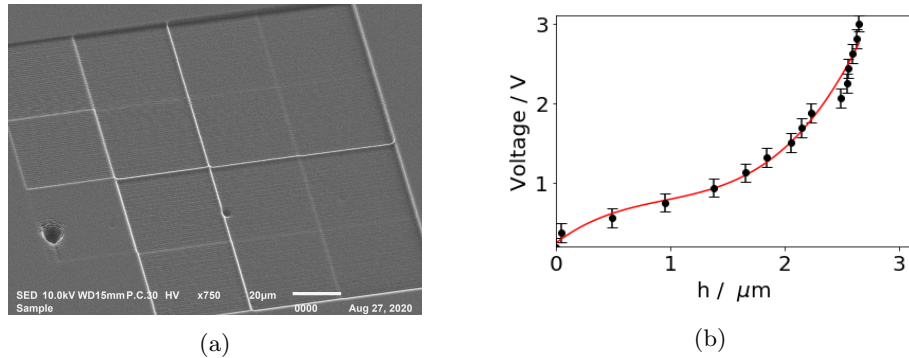


Figure 32: Plateaus written with the laser diode for different heights (a). The heights of the structures were measured. A third polynomial dependence was assumed for the dependence between the laser power (voltage) and the height (b).

### 4.3 Test structures

#### 4.3.1 Plateaus - Non-linear resist response

Plateaus of different heights were written. The power was adjusted linearly from 0 to 3 V. The ma-p 1240 G was used with an coating thickness of  $4 \mu\text{m}$ . For the positive resist the depth of the structure is strongly dependent onto the development time. Here, a low recommended time of  $t = 40 \text{ s}$  was used for the laser diode. The depth was about  $3 \mu\text{m}$ . We wanted to achieve nearly the same depth with the femtosecond laser. Since the dose cannot be increased because of the high intensity causing destruction, the development time has to be increased. It was chosen to be  $5 \text{ min}$ . Figure 32a shows the written pyramids with the diode laser. The measured data are fitted with an polynomial fit of third order. This can be seen in Figure 32b. Figure 33a shows a test pattern written within the maximal power range with the femtosecond laser. It includes a row of the desired plateaus (second line). The measured height and the fit is seen in Figure 33b.

#### Correction of input structures

The fit for the height-voltage dependence can now be used to take account for the non-linearity response of the resist. For this specific setup, the fit function is used to adapt the design. Figure 34 shows a pyramid before and after the correction. Applying this procedure, one can get a good result for a wide variety of structures. However, the proximity effect is not corrected. To reach best results for a specific structure, it needs to be written itself and tested in order to correct the influence of near pixels.

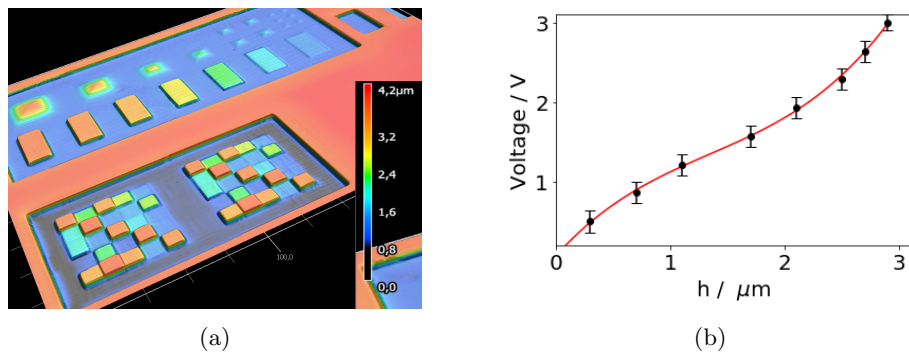


Figure 33: Test pattern including plateaus written with the femtosecond laser (a). The heights of the plateaus dependent on the power (voltage) were measured. The reverse function was fitted (b).

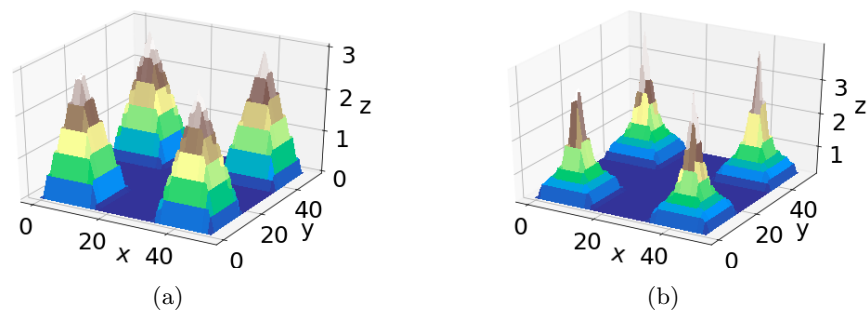


Figure 34: A test structure with pyramids (a) with a height of  $3\ \mu\text{m}$  and the corrected structure (b) scaled according to the fit from Figure 32b.

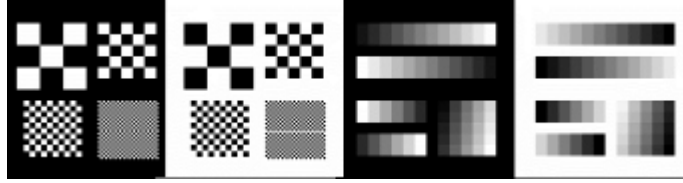


Figure 35: Bmp-file with encoded height for manufacture staircase and chessboard patterns in positive and negative versions

### 4.3.2 Staircase and chessboard pattern

A staircase and chessboard geometry was drawn as CAD geometry. The converted Bmp-file can be found in Figure 35. The negative and the positive version of the structures were written in order to create the same pattern with the positive and the negative resist. The positive resist's development time was  $3 \text{ min}$ . Selected regions of the structures written with the femtosecond laser and the laser diode are compared. Figure 36 shows the staircase structure while Figure 37 shows the chessboard pattern for all four combinations of the two light sources and the two photoresists, spincoated ma-P 1275G and spincoated OrmoComp.

Figure 36 shows SEM and LSM pictures of the staircase structures. The LSM pictures can be used for determining the total height, but show measurement artefacts, so, the SEM pictures are closer to the real structures.

Generally, the reached heights in TPP are smaller than in the OPP case. In OPP, a depth of  $7.1 \mu\text{m}$  was reached in the positive resist case. This is less high than the structure in negative resist which is about  $12.7 \mu\text{m}$  high. In TPP, one can also observe a higher structure when writing into the negative resist ( $9.8 \mu\text{m}$ ) than in the positive resist ( $3.6 \mu\text{m}$ ).

The positive resist shows a good grayscale behaviour in a sense that the resist response is more linear than the negative resist response. However comparing results for the negative resist, TPP shows better grayscale behaviour than OPP.

Further, smaller structures in the negative resists show a relatively low shape fidelity due to very unstable lines. The drawbacks of the negative resist can clearly be seen. The lines written are not totally solidified. They may lay down or bend towards each other, creating stripes instead of plateaus. This effect might be overcome by choosing a smaller line distance.

Figure 37 shows SEM and LSM pictures of chessboard patterns of different sizes. The square side lengths were  $1$ ,  $2.5$ ,  $5$  and  $10 \mu\text{m}$ . This pattern is reasonable when determining the resolution of the processes. The resolution strongly depends on the height difference between neighbour pixels. However, an important measure is to switch from  $0$  to the maximum height since it is the worst resolution  $RMH$  (resolution at maximum height) of the process.

First we will discuss the positive resist behaviour. For TPP, the  $RMH$  is about  $2.5 \mu\text{m}$ . The remaining squares which were not written are smaller but a correction seems possible. On the other hand for OPP, the  $2.5 \mu\text{m}$  squares became significantly blunt due to proximity effects, creating peaks instead of

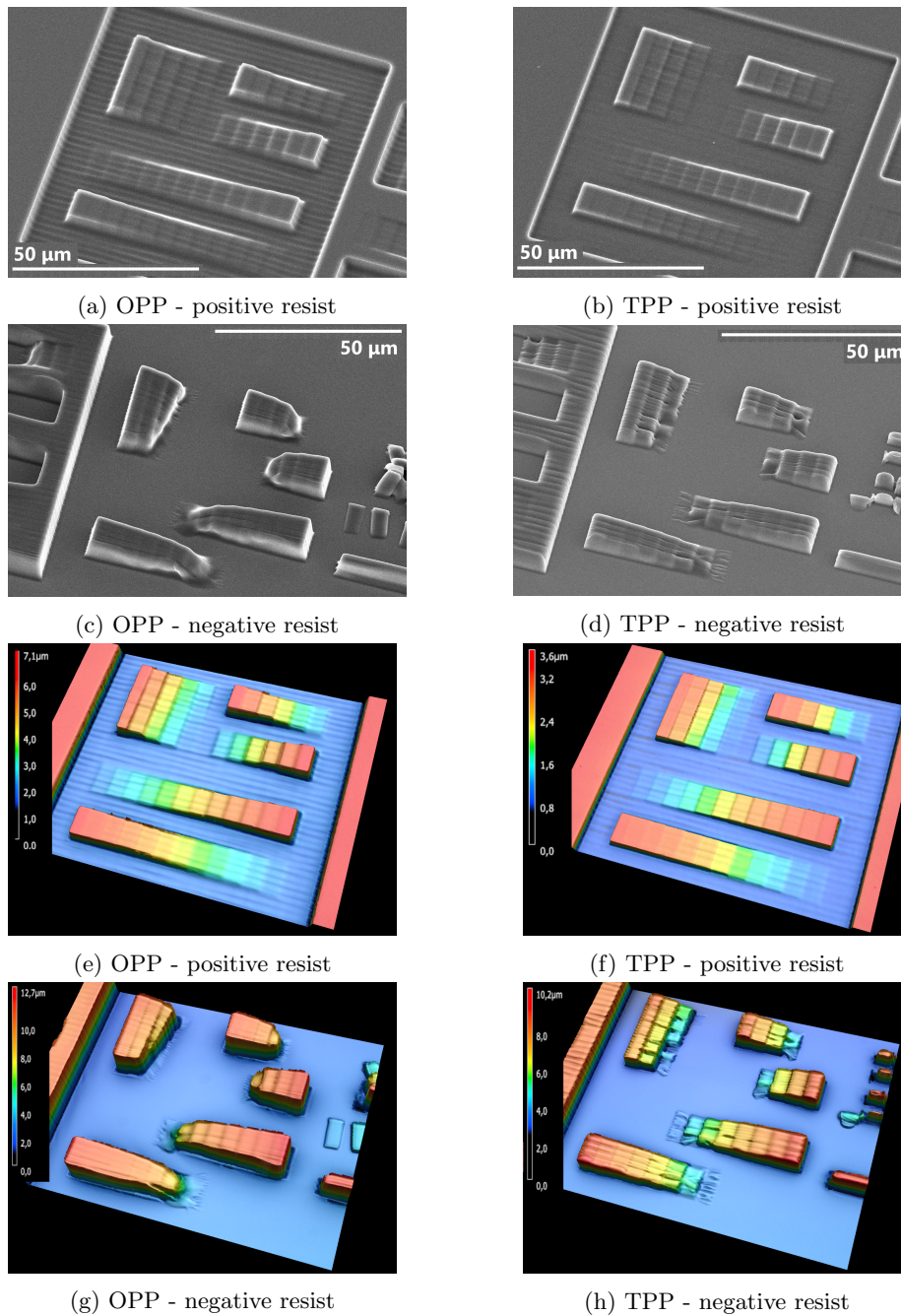
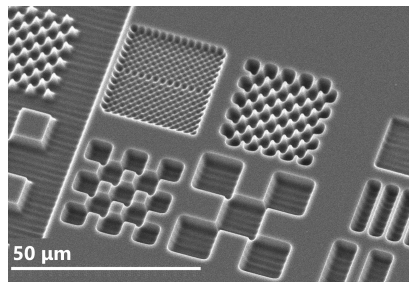
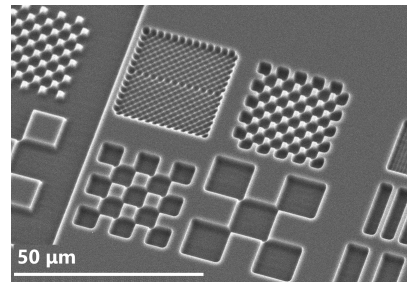


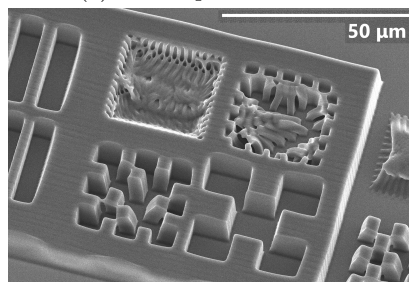
Figure 36: SEM and LSM pictures of staircase structures generated by TPP and OPP. The used resists were the positive resist ma-P 1275G and the negative resist OrmoComp.



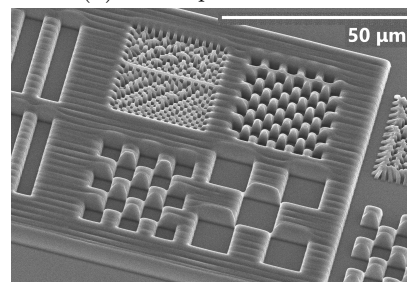
(a) OPP - positive resist



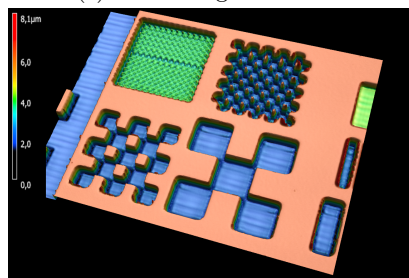
(b) TPP - positive resist



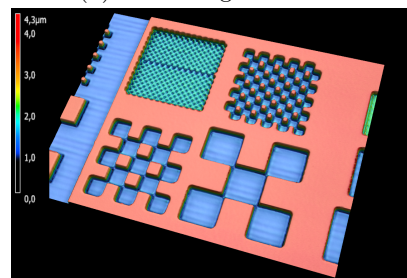
(c) OPP - negative resist



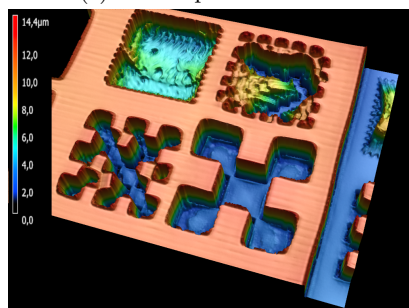
(d) TPP - negative resist



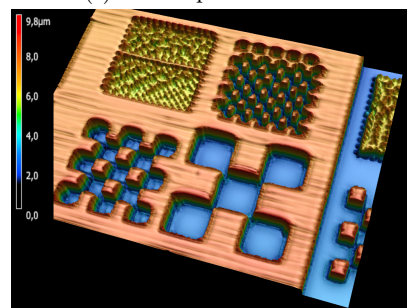
(e) OPP - positive resist



(f) TPP - positive resist



(g) OPP - negative resist



(h) TPP - negative resist

Figure 37: SEM and LSM pictures of chessboard patterns. The structures were written with the femtosecond laser (TPP) and the laser diode (OPP) into the positive resist ma-P 1275G and into the negative resist OrmoComp.



squares which do not maintain the original height of the spincoated layer. The *RMH* for OPP in the positive resist is about  $5 \mu m$ .

The negative resist shows better *RMH* but suffers from the instability of the created structures. The resolution seems to be in both cases between 1 and  $2.5 \mu m$ , with the resolution of the TPP process slightly better than the OPP process. This can be seen in Figure 37d and 37c at the boarder of the  $1 \mu m$ -pattern. However due to the high but thin structures, the pillars created are not stable enough to maintain straight until the feature size of  $10 \mu m$  resp.  $2.5 \mu m$  is reached in the OPP resp. TPP process. The numbers are summarized in Table 6.

| <b>limit</b>      | OPP             | TPP         |
|-------------------|-----------------|-------------|
| $d_{OrmoComp}$    | $14.4 \mu m$    | $9.8 \mu m$ |
| $d_{ma-P1275G}$   | $7.1 \mu m$     | $3.6 \mu m$ |
| $res_{OrmoComp}$  | $2.5 - 5 \mu m$ | $2.5 \mu m$ |
| $res_{ma-P1275G}$ | $5 \mu m$       | $2.5 \mu m$ |

Table 6: Maximum depth (d) and best resolution (res) at maximum depth for the specific OPP and TPP setup. The x20 objective lens was used, both resists were spincoated.

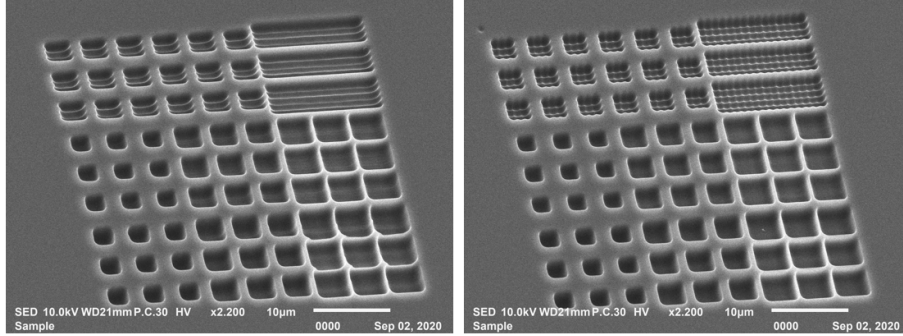


Figure 38: Truncated pyramids written with one x-raster scan (left) and with combined y- and x-raster scan (right). The femtosecond laser, the positive resist and the x20 objective lens was used. The bottom square’s side length is fixed with  $a_{bottom} = 5 \mu m$ . The top square’s side length is varied by  $a_{top} = 2.5, 3$  and  $3.5 \mu m$  (left to right column in each picture). The intermediate line distance is varied from  $d = 1, 0.5$  to  $0.25 \mu m$  (from top to bottom).

### 4.3.3 Pyramids - Manufacturing time

#### Femtosecond laser - positive resist

Here, the setup with the femtosecond laser, the x20 objective lens and the positive resist with spincoated ma-P 1240 G was used. Figure 38 shows truncated pyramids with a bottom square’s side length of  $a_{bottom} = 5 \mu m$  written with different parameters. The intermediate line distance and the top square’s side length were varied. The power was adjusted for each line in order to get approximately the same depth for all pyramids, this is necessary because the depth depends on the intermediate line distances.

The raster scan has an inherent line behaviour since the voxels in the fast scan direction overlap much (voxel distance  $d_v \approx 0.001 \mu m$  for a velocity of  $v = 1 mm/s$  and a repetition rate of  $rep = 1 MHz$ ) whereas the voxels in the other direction have the same distance than the lines ( $d_v \approx 0.5 \mu m$ ). Therefore, one can see a more uniform structure with a better shape fidelity when using x- and y-raster scan. However, it takes twice as long.

The change of the intermediate line distance was already discussed in section 4.1, but here we can see the related resolution. While intuitively one would say that the resolution increases with a smaller raster, the opposite behaviour is observed. On the left upper pyramids one can see a relatively sharp edge with an radius of about  $r = 0.5 \mu m$ . The pyramids written with smaller intermediate line distances have an edge radius of  $r = 0.8 \mu m$  and more. The reason for the loss of resolution is the increasing overlap of the lines. The separated lines can create more distinct structures (compare Figure 40). So, one has to find a trade-off between the resolution of the used pattern and the resolution of the structures produced. The optimal resolution is the point where the two

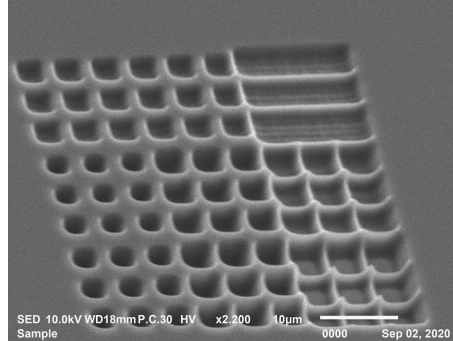


Figure 39: Truncated pyramids written with the combined y- and x-raster scan (right). The laser diode, the positive resist and the x20 objective lens was used. The bottom square’s side length is fixed with  $a_{bottom} = 5 \mu m$ . The top square’s side length is varied by  $a_{top} = 2.5, 3$  and  $3.5 \mu m$  (left to right column in each picture). The intermediate line distance is varied from  $d = 1, 0.5$  to  $0.25 \mu m$  (from top to bottom).

resolutions are equal. For this setting, this optimal resolution is between  $res = 1$  and  $0.5 \mu m$ . However, a intermediate line distance of  $d = 0.5 \mu m$  was widely chosen to keep a grid which is easy to observe because it includes all integer grid points.

Now, we will focus on the parameter of the top square’s side length. While the truncated pyramids are far apart in the  $a_{top} = 2.5 \mu m$ -case, they start to grow towards each other for higher values. One has to take into account that the resulting structure will be strongly influence by the washing-out when writing near the resolution limit. This proximity effect is well known [7]. Figure 40 shows a sketch of profiles of lines. The individual lines are significantly less deep than the resulting structure. One can approximate the resulting shape by adding up the individual line profiles. Another important observation is that the highest slope is limited. A rectangular shape can only be approximated by a trapezoid.

### Diode Laser - positive resist

Like with the femtosecond laser above, the truncated pyramids are here written with the laser diode. This is shown in Figure 39. One can immediately see the worse resolution of the laser diode. Other behaviours like the proximity effect and the dependence between resolution and intermediate line distance are similar. An advantage is the deeper structure. By keeping the development time constant, the laser diode can produce deeper structures than the femtosecond laser. By increasing the intensity, the structure gets destroyed in both cases but in a different way. The effects are now explained and supported by Figure 41. While the femtosecond laser shows evaporation of the resist at high exposure doses, the laser diode exposes big regions. The femtosecond laser burns defined

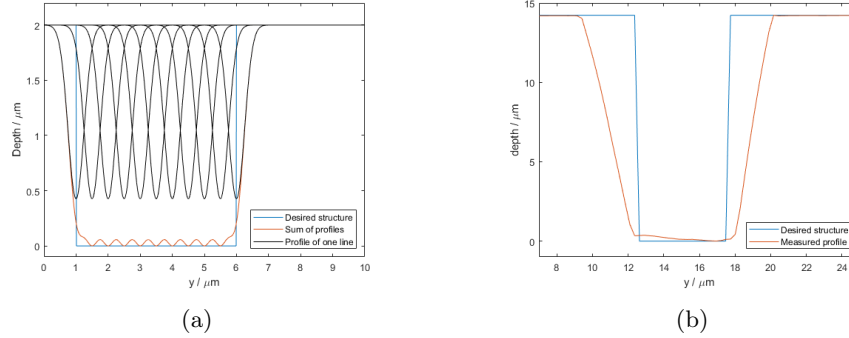


Figure 40: Sketch of the sum and individual profiles of 7 lines written when scanning in x-direction (a). The plane perpendicular to the writing direction is shown. The Gaussian line profiles with half width of  $0.5 \mu\text{m}$  overlap when choosing the intermediate line distance of  $0.5 \mu\text{m}$ . Instead of a rectangular structure, a trapezoidal shape is produced. Measured profile with the LSM (b) of a bar written with 11 lines in x-direction with y-values between 12.5 and 17.5. A similar behaviour than in (a) is seen.

holes in the resist, leaving further away regions insoluble. The impact is a very local one. On the other hand, the blue laser diode increases the influence region significantly if too much light exposes the resist. The propagation radius of the chain reaction is clearly a order of magnitude bigger than the spot size. A high beam intensity will expose a big range, leading to a big hole after developing.

### Best results

For the laser diode, a promising way to produce  $5 \mu\text{m}$ -truncated pyramids with a height of  $4 \mu\text{m}$  was to use spincoated ma-P 1240G with  $4 \mu\text{m}$  thickness. The structure can be seen in Figure 42a and Figure 42b. The line distance was fixed with  $0.5 \mu\text{m}$ . Squares with  $a = 2.5 \mu\text{m}$  were written to achieve maximum slopes. The writing speed was  $v = 8 \text{ mm/s}$ . The total writing time of this  $400 \times 400 \mu\text{m}^2$  structure was about  $7 \text{ min}$ .

For the femtosecond laser, the same pyramids were produced best by the spincoated OrmoComp with  $4 \mu\text{m}$ . A lattice with lattice constant of  $5 \mu\text{m}$  was written and it was modelled in silicon (see Figure 42c and 42d). The writing speed was  $v = 1 \text{ mm/s}$ . Total writing time of the  $4 \times 4 \text{ mm}^2$  structure was about  $135 \text{ min}$ .

### Fast manufacturing

For the laser diode pyramids, we can consider the formula of Malinauskas (equation 14). Since squares with  $a = 2.5 \mu\text{m}$  were written, it results in only writing 5 lines to create the  $5 \mu\text{m}$ -truncated pyramids which saves half of the time than

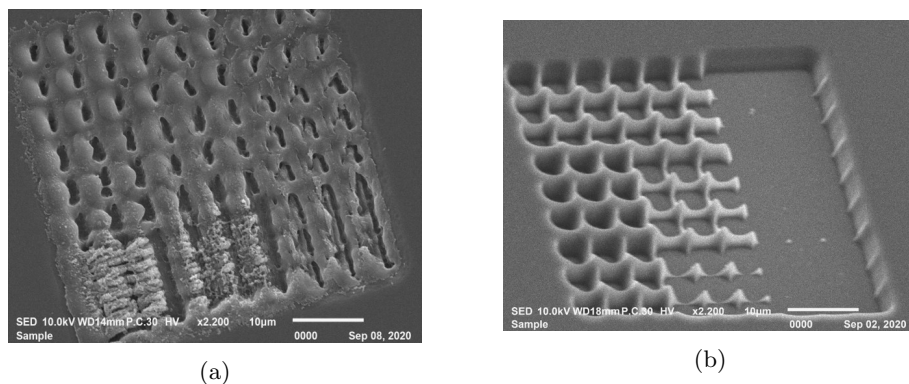


Figure 41: Truncated pyramids written with too high intensities with the femtosecond laser (a) and the laser diode (b). The femtosecond laser starts to evaporate the resist while the laser diode increases the range of the exposed area significantly.

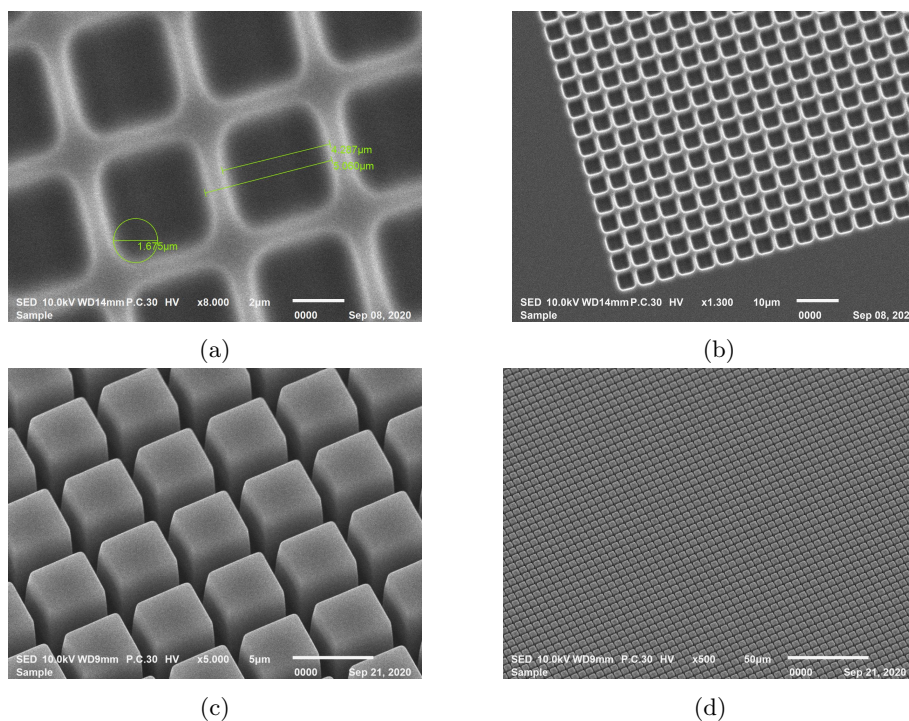


Figure 42:  $5\ \mu\text{m}$ -truncated pyramids with a height of  $4\ \mu\text{m}$  written with the laser diode into spincoated ma-P 1240G. Picture taken with the SEM with magnification  $\times 7000$  (a) and  $\times 1300$  (b). Mold of similar  $5\ \mu\text{m}$ -truncated pyramids written with the femtosecond laser into spincoated OrmoComp. Picture taken with the SEM with magnification  $\times 5000$  (c) and  $\times 500$  (d).

writing arbitrary structures with this resolution (10 lines for the  $5 \mu\text{m}$ ). For the formula, this means a fill factor of 0.5. The formula gives

$$t = \frac{0.4 \text{ mm} \cdot 0.4 \text{ mm} \cdot 0.5}{0.0005 \text{ mm} \cdot 8 \text{ mm/s}} \approx 40 \text{ s}. \quad (16)$$

This is much less than we needed. The reason is the time needed for the 800 acceleration and deceleration processes as well as for the freerun distance. The time needed for the 1600 accelerations with an acceleration of  $a = 100 \text{ mm/s}^2$  are  $t_{acc,dec} = \frac{v}{a} \text{ amount} = 80 \text{ ms} \cdot 1600 = 128 \text{ s}$ . This is now longer than the actual writing time, but it is not for bigger structures close to  $1 \text{ cm}^2$ . The freerun time with the distance of  $d_{free} = 300 \mu\text{m}$  on each side is responsible for the contribution of  $t_{freerun} = \frac{2 d_{free} \text{ amount}}{v} = \frac{2 \cdot 0,3 \cdot 1600}{8} \text{ s} = 120 \text{ s}$ . This gives a total time of  $t_{tot} = t_{struct} + t_{acc,dec} + t_{freerun} = 396 \text{ s}$  which is matching with the 7 minutes we observed. Finally we can conclude, this structure written on  $1 \text{ cm}^2$  will take:

$$\begin{aligned} t_{struct} &= \frac{10 \text{ mm} \cdot 10 \text{ mm} \cdot 0.5}{0.0005 \text{ mm} \cdot 8 \text{ mm/s}} \approx 12500 \text{ s} \\ t_{acc,dec} &= \frac{v}{a} \text{ amount} = 80 \text{ ms} \cdot 20000 = 3200 \text{ s} \\ t_{freerun} &= \frac{2 d_{free} \text{ amount}}{v} = \frac{2 \cdot 0,3 \cdot 20000}{8} \text{ s} = 1500 \text{ s} \end{aligned} \quad (17)$$

Summing up the contributions lead to a total time of

$$t_{tot} = 17200 \text{ s} \approx 4,8 \text{ h}. \quad (18)$$

Similarly, we can calculate the time needed for the femtosecond laser lattice. In this case we will just calculate the total length of the trajectory and add the acceleration processes. For the written structure, it will take  $t_{struct, freerun} = \frac{\text{amount} (s_{online} + 2 s_{freerun})}{v} = \frac{1600 \cdot 4,6 \text{ mm}}{1 \text{ mm/s}} = 7360 \text{ s}$  for the constant velocity parts and  $t_{acc,dec} = \frac{v}{a} \text{ amount} = 10 \text{ ms} \cdot 3200 = 32 \text{ s}$  for acceleration processes. We derive a total time of  $t_{tot} = 7392 \approx 2,1 \text{ h}$ . The result is confirmed by the measured time above. This is very fast but one have to mention that this strategy can only be used for very specific structures. However, here it is possible and different slopes can be tuned by focus offset and power variations. We can now extrapolate to calculate the time for the  $1 \text{ cm}^2$ -structure. We get the time contributions

$$\begin{aligned} t_{struct, freerun} &= \frac{\text{amount} (s_{online} + 2 s_{freerun})}{v} = \\ &= \frac{4000 \cdot 10,6 \text{ mm}}{1 \text{ mm/s}} \approx 42400 \text{ s} \\ t_{acc,dec} &= \frac{v}{a} \text{ amount} = 80 \text{ ms} \cdot 20000 = 80 \text{ s}. \end{aligned} \quad (19)$$

Summing up the contributions for the femtosecond laser pyramids, we derive a doable duration of

$$t_{tot} = 17200 \text{ s} \approx 11,8 \text{ h}. \quad (20)$$

## 5 Conclusion

A self-built system for grayscale two photon polymerisation (TPP) was tested. Programs in Python and LabVIEW were created to write structures while ensuring in-sync power modulation of the femtosecond laser during movement. The polymerization volume of single pulses, so-called voxels, were studied and the physics of the writing process was discussed. Minimal resolutions can be achieved by using a x100 oil immersion objective lens and by applying the drop procedure to the negative-tone photoresist OrmoComp. Smallest voxels had a lateral dimension of  $(200 \pm 50) \text{ nm}$  and an axial dimension of  $(600 \pm 50) \text{ nm}$ .

We compared grayscale one photon polymerization (OPP) with grayscale TPP. Positive and negative photoresists were used for OPP and TPP, to generate lattices, plateaus and truncated pyramids. In contrast to TPP, small intensities are sufficient for OPP. For a speed of  $1 \text{ mm/s}$  and a depth of  $4 \mu\text{m}$  in the ma-P 1240G positive resist, a typical beam intensity of the femtosecond laser was  $1 \text{ mW}$ . The intensity of the blue laser diode was  $70 \mu\text{W}$ .

Reachable resolutions and maximum depths were compared for OPP and TPP when writing in the negative and in the positive resist. TPP allows better resolution but smaller depths. Structures written in the positive resist were less deep but showed a more linear response regarding a linear exposure dose variation. These statements are summarized in Table 7.

In order to produce a large-scale array of  $5 \mu\text{m}$ -truncated pyramids, different strategies were compared. OPP showed good behaviour for the spincoated ma-P 1240G positive resist. While this method can also be used for TPP, spincoated OrmoComp turned out to be best for producing the desired height. In these specialized approaches, an area of  $1 \text{ cm}^2$  can be structured in less than  $12 \text{ h}$ .

In a nutshell, fast manufacturing of microstructures is possible with grayscale OPP and grayscale TPP. The positive resist modified with TPP allows the best resolution and is preferred although higher structures can be created by switching to the negative resist or to OPP.

|                       | OPP | TPP |
|-----------------------|-----|-----|
| $\lambda / \text{nm}$ | 404 | 524 |
| resolution            | -   | +   |
| max. depth            | +   | -   |

(a)

| resist     | neg | pos |
|------------|-----|-----|
| resolution | -   | +   |
| max. depth | +   | -   |

(b)

Table 7: Comparison of OPP vs. TPP (a) written by a light source with a wavelength  $\lambda$ . Advantages of negative (neg) and positive (pos) resists (b).

## 6 Outlook

In order to enhance the process, further improvements might be related to the selection of the resist or to beam engineering.

The results in the ma-P 1240G positive resist were similar for OPP and TPP. It is assumed that this is because the resist is optimized for OPP or being exposed with 404 *nm* wavelength light. By choosing a positive resist which is optimized for TPP, better results might be achieved. PMMA is a good candidate for such a material [17]. It allows high resolution which is shown by experiments done with electron beam lithography. Furthermore, PMMA shows deep-UV absorption, i.e. is suitable for being exposed by a wavelength of 262 *nm* that was used in the TPP process.

The maximum reachable depth of the structures is not satisfactorily deep, but a beam shaping might overcome this problem. All used objective lenses created a Gaussian focus spot. By installing a diffractive optical element in front of the objective lens, it is possible to generate a very long depth of focus [11]. Thus, structures might be build in a significantly larger height range by maintaining the high resolution due to the elongated spot shape.



## 7 Appendix

### 7.1 XPS-D Controller Manual - PVT Trajectories

In this section, an extract from the Newport XPS-D Controller Features Manual can be found [5]. The following pages show the documentation covering the topic of PVT trajectories. The formulas of this section were necessary to understand PVT trajectories for implementing the automatic generation via the Python program.

#### 4.3 PVT Trajectories

##### 4.3.1 Trajectory Terminology

**Trajectory:** continuous, multidimensional motion path. PVT stands for Position, Velocity, and Time. PVT trajectories are defined in an n-dimensional space ( $n = 1$  to 4) and are only available with MultipleAxes groups. A PVT trajectory is generated with continuous movements of the group's positioners over several time periods. For each period, each positioner must complete a defined displacement from its current position and a defined output velocity at the end of the period. By definition, there is no constant vector velocity and no definition for a vector acceleration in contrast to Line-arc trajectories or splines.

**Trajectory element (segment):** An element of a PVT trajectory is defined by a set of all positioner displacements and output velocities and the duration for the segment. In the PVT data file, each element is represented by a line of values:

DT, DP1, VO1, DP2, VO2, ... DPn, VOn

DT: The segment duration in seconds.

DP1, DP2, ..., DPn: Positioners' (#1, #2, ..., #n) displacements during DT.

VO1, VO2, ..., VOn: Positioners' output velocities at the end of DT.

##### 4.3.2 Trajectory Conventions

When defining or executing a PVT trajectory, a number of rules must be followed:

- The motion group must be a MultipleAxes group.
- All trajectories must be stored in the controller's memory. Use the XPS webpage **Files** → **Trajectory files** to edit, upload or download a PVT trajectory file. Once a trajectory is started, it executes in the background allowing other groups to work independently and simultaneously.
- Each trajectory must have a beginning and an end. Endless (infinite) trajectories are not allowed. Although, execution of a trajectory file N-times (N defined by user) is allowed. Since the trajectory is stored in a file, the trajectory's maximum size (maximum elements number) is practically not limited.
- PVT trajectory elements (segments) are 3<sup>rd</sup> order polynomial pieces for each positioner that hit the positions  $P_{i-1}$  (at time  $t_{i-1}$  with a velocity  $v_{i-1}$ ) and positions  $P_i$

(at time  $t_i$  with a velocity  $v_i$ ). There is no direct link between the trajectories of the different positioners in the group.

- PVT trajectories form a continuous path (each segment output position is equal to the next segment input position), and the segment tangential angles at the connection point of any two consecutive segments are continuous including its derivative. It means that the PVT trajectory continuity property is  $R^1$ .
- The input velocity of any element is equal to the output velocity of the previous element. The input velocity for the first element is always zero. The output velocity of the last element must be zero as well.

#### 4.3.3 Geometric Conventions

- The coordinate system can be any convention, it does not need to be an orthogonal system.
- A PVT trajectory can be defined for a MultipleAxes group. The number of positioners in the PVT trajectory must match that of the linked with MultipleAxes group.

#### 4.3.4 PVT Interpolation

For each positioner belonging to the MultipleAxes group, the PVT trajectory calculates a 3<sup>rd</sup> order polynomial curve  $P(u)$  that can be presented by the following equations:

##### Profile coefficient

- Acceleration jerk:

$$\text{Jerk} = \frac{6 \cdot [DT \cdot (V_{in} + V_{out}) - 2 \cdot DX]}{DT^3}$$

- Initial acceleration:

$$G_{in} = \frac{2 \cdot [3 \cdot DX - DT \cdot (2 \cdot V_{in} + V_{out})]}{DT^2}$$

- Final acceleration:

$$G_{out} = \frac{2 \cdot [DT \cdot (V_{in} + 2 \cdot V_{out}) - 3 \cdot DX]}{DT^2}$$

##### Profile equation

- Acceleration:

$$\text{Acc}(t) = G_{in} + \text{Jerk} \cdot t$$

- Velocity:

$$\text{Vel}(t) = V_{in} + G_{in} \cdot t + \frac{\text{Jerk} \cdot t^2}{2}$$

- Position:

$$\text{Pos}(t) = V_{in} \cdot t + \frac{G_{in} \cdot t^2}{2} + \frac{\text{Jerk} \cdot t^3}{6}$$

Here:

DT is the segment duration in seconds

DX is the displacement during DT

$V_{in}$  is the output velocity of the previous segment (which is equal to the input velocity of the current segment)

$V_{out}$  is the output velocity of the current segment.

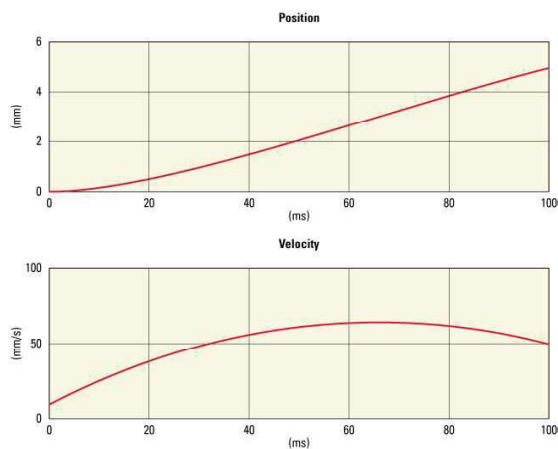
t is the time in seconds starting at 0 (entry of the current element) and ending at DT (end of the segment)

#### 4.3.5 Influence of the Element Output Velocity to the Trajectory

The contour of each PVT trajectory element is influenced not only by the displacement, but also by the input and output velocities. As the user decides on these velocities, attention must be placed on these values to get the desired results.

The effect of the velocity is illustrated in the following example which shows the position and velocity profiles for one segment of a PVT trajectory that has a displacement of 5 mm, a duration of 100 ms, an input velocity of 10 mm/s and an output velocity of either 50 mm/s or 500 mm/s:

- If the output velocity is equal to 50 mm/s.



- If the output velocity is equal to 500 mm/s.

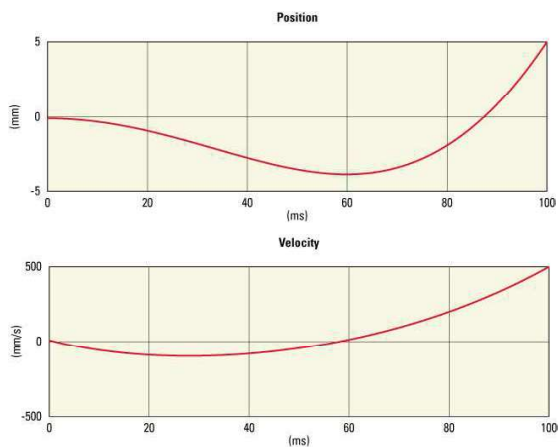


Figure 17: PVT trajectory element in execution: the comparison.

A PVT trajectory must have three parameters: position, velocity and time. With a given target displacement, output velocity and time duration, the PVT trajectory calculates intermediate positions and velocities as a function of time.

With an output velocity of 50 mm/s, the positioner has “enough” time to achieve the displacement within the assigned time (100 ms) in the forward direction. The velocity increases at the beginning and then slows down towards the end. The position always increases up to the target position (5 mm).

On the other hand, when the output velocity is set to 500 mm/s, the positioner does not have enough time to achieve the displacement and speed output required in the forward direction. So, the positioner will first reverse the direction of motion to be able to approach the end position with a speed of 500 mm/s.

#### 4.3.6 Trajectory File Description

The PVT trajectory described must be stored in the controller’s memory. Use the XPS webpage **Files** → **Trajectory files** to edit, upload or download a PVT trajectory file. Each line of this file represents one element of the trajectory.

A line contains several data separated by a comma. The number of data in each line depends on the number of positioners in the group. The first data in each line is the duration of the element. The following data is grouped in pairs of two representing the displacement and the output velocity for each positioner of the group. Comment lines are possible, they must be preceded with a semi-colon (“;”) character.

So, the line format is as follows:

- Data #1: Element duration (seconds).
  - Data #2: 1st positioner’s displacement (units).
  - Data #3: 1st positioner’s output velocity (units/s).
  - Data #4: 2nd positioner’s displacement (units).
  - Data #5: 2nd positioner’s output velocity (units/s).
- (And so on...)

---

#### NOTE

**The first positioner is always the first defined in the system.ini of the MultipleAxes group (see PositionerInUse), the second positioner is always defined as second, and so on...**

---

#### Option to add GPIO outputs

To add either analog or digital outputs during the trajectory the first line of the file should specify the selected outputs and each element should define the GPIO output per plug with the following data:

- Digital Outputs
  - For digital outputs, two values must be specified per element and per selected GPIO plug to define the state of the output at the end of the element, namely Mask and DigitalOutputValue.
- Analog Outputs
  - Analog outputs are handled like position to output a controlled voltage profile. For analog outputs, two values per element and per selected output plug must be specified, the voltage variation (DU) during the element and the rate of change (VU) at the end of the element.

**Example format:**

; Comment: A MultipleAxes group with two positioners, one digital output and two analog outputs.

```
GPIO3.DO, GPIO4.DAC1, GPIO4.DAC2
DT1, DX1, DX2, Mask1, Value1, DU1, VU1, DU2, VU2
DT2, DX1, DX2, Mask1, Value1, DU1, VU1, DU2, VU2
DT3, DX1, DX2, Mask1, Value1, DU1, VU1, DU2, VU2
...
DTm, DX1, DX2, Mask1, Value1, DU1, VU1, DU2, VU2
```

**4.3.7 Trajectory File Example**

Following is an example of a PVT trajectory defined in a MultipleAxes group that contains two positioners. The tabs are added for better readability and are ignored in a line:

|      |          |       |          |      |
|------|----------|-------|----------|------|
| 1.0, | 0.4167,  | 1.25, | 0,       | 0    |
| 1.0, | 2.9167,  | 5,    | 0,       | 0    |
| 1.0, | 7.0833,  | 8.75, | 0,       | 0    |
| 1.0, | 9.5833,  | 10,   | 0,       | 0    |
| 1.0, | 10,      | 10,   | 0.4167,  | 1.25 |
| 1.0, | 10,      | 10,   | 2.9167,  | 5    |
| 1.0, | 10,      | 10,   | 7.0833,  | 8.75 |
| 1.0, | 10,      | 10,   | 9.5833,  | 10   |
| 1.0, | 9.5833,  | 8.75, | 10,      | 10   |
| 1.0, | 7.0833,  | 5,    | 10,      | 10   |
| 1.0, | 2.91667, | 1.25, | 10,      | 10   |
| 1.0, | 0.41667, | 0,    | 10,      | 10   |
| 1.0, | 0,       | 0,    | 9.5833,  | 8.75 |
| 1.0, | 0,       | 0,    | 7.0833,  | 5    |
| 1.0, | 0,       | 0,    | 2.91667, | 1.25 |
| 1.0, | 0,       | 0,    | 0.41667, | 0    |

This file represents the following data:

| Time<br>Period (s) | Axis #1<br>Displacement | Axis #1<br>Velocity Out | Axis #2<br>Displacement | Axis #2<br>Velocity Out |
|--------------------|-------------------------|-------------------------|-------------------------|-------------------------|
| 1.0                | 0.4167                  | 1.25                    | 0                       | 0                       |
| 1.0                | 2.9167                  | 5.0                     | 0                       | 0                       |
| 1.0                | 7.0833                  | 8.75                    | 0                       | 0                       |
| 1.0                | 9.5833                  | 10                      | 0                       | 0                       |
| 1.0                | 10                      | 10                      | 0.4167                  | 1.25                    |
| 1.0                | 10                      | 10                      | 2.9167                  | 5                       |
| 1.0                | 10                      | 10                      | 7.0833                  | 8.75                    |
| 1.0                | 10                      | 10                      | 9.5833                  | 10                      |
| 1.0                | 9.5833                  | 8.75                    | 10                      | 10                      |
| 1.0                | 7.0833                  | 5                       | 10                      | 10                      |
| 1.0                | 2.9167                  | 1.25                    | 10                      | 10                      |
| 1.0                | 0.4167                  | 0                       | 10                      | 10                      |
| 1.0                | 0                       | 0                       | 9.5833                  | 8.75                    |
| 1.0                | 0                       | 0                       | 7.0833                  | 5                       |
| 1.0                | 0                       | 0                       | 2.9167                  | 1.25                    |
| 1.0                | 0                       | 0                       | 0.4167                  | 0                       |

Table 1: The trajectory data file.

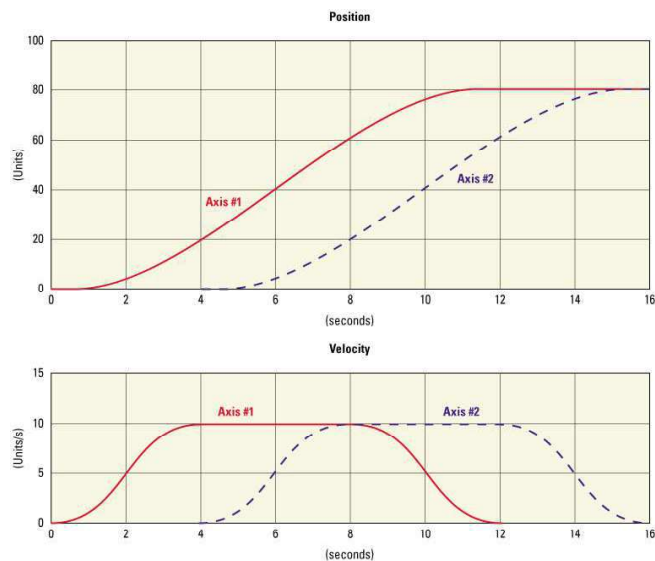


Figure 18: Executing the trajectory data file with the PVT algorithm.

#### 4.3.8 PVT Trajectory Verification and Execution

Here are four functions to verify or execute a PVT trajectory :

- **MultipleAxesPVTVerification():** Verifies a PVT trajectory data file.
- **MultipleAxesPVTVerificationResultGet():** Returns the results of the last trajectory verification call, actuator by actuator. This function works only after a MultipleAxesPVTVerification().
- **MultipleAxesPVTExecution():** Executes a PVT trajectory.
- **MultipleAxesPVTParametersGet():** Returns the trajectory's current execution parameters. This function works only while executing a trajectory.

The function **MultipleAxesPVTVerification()** can be executed at any moment and is independent of the trajectory execution. This function does the following:

- Checks the trajectory file for data and syntax coherence.
- Simulates the trajectory to determine the positioner's travel requirements in negative and positive directions and the maximum allowed speed and acceleration for each positioner. This function determines whether the trajectory is executable.
- If all is OK, it returns an "OK" (value 0). Otherwise it returns a corresponding error. An error for instance is reported if one of the positioner's speed or acceleration reached during the trajectory exceeds the maximum allowed speed or acceleration.

The function **MultipleAxesPVTVerificationResultGet()** can be executed only after a MultipleAxesPVTVerification(). It returns the trajectory limits for each positioner, which are the travel requirements in positive and negative directions, the achieved maximum speed and acceleration.

To execute a PVT trajectory, send the function **MultipleAxesPVTExecution()** while specifying the file name and the number of cycles. This function does not verify the trajectory's coherence or geometric conditions (exceeding any positioner's min. or max. travel, speed or acceleration) before execution, so users must be careful when executing

a trajectory without verifying the trajectory first. In case of an error during execution, because of bad data or because of a following error, the motion group will make an emergency stop and will go to the disabled state.

Finally, the function `MultipleAxesPVTParametersGet()` returns the trajectory name and the number of the trajectory element that is currently being executed. This function returns an error if the trajectory is not executing.

#### 4.3.9 Example with a MultipleAxes Group

##### **MultipleAxesPVTVerification (MyGroup, PVT1.trj)**

*This function returns a 0 if the trajectory is executable.*

##### **MultipleAxesPVTVerificationResultGet (MyGroup.MyPositioner1, \*Name, \*NegTravel, \*PosTravel, \*MaxSpeed, \*MaxAcceleration)**

*This function returns the name of the trajectory verified with the last functions call of `MultipleAxesPVTVerification` to the motion group `MyGroup(PVT1.trj)` and the trajectory limits for the positioner `MyGroup.MyPositioner1`. These trajectory limits are: the negative or left travel requirement, the positive or right travel requirement, the achieved maximum speed and acceleration. Make sure that these trajectory limits (required negative and positive travel, speed and acceleration) are within the soft limits of the stages defined in the `stages.ini` file (section `Travel: MinimumTargetPosition, MaximumTargetPosition` and section `Profiler: MaximumVelocity, MaximumAcceleration`).*

##### **MultipleAxesPVTExecution (MyGroup, PVT1.trj, 5)**

*Executes the trajectory `PVT1.trj` five (5) times.*

##### **MultipleAxesPVTParametersGet (MyGroup, \*FileName, \*ElementNumber)**

*Returns the currently executed trajectory file name (`PVT1.trj`) and the number of the currently executed trajectory element.*

## 4.4 PT Trajectories

### 4.4.1 Trajectory Terminology

Trajectory: continuous, multidimensional motion path. PT stands for Position and Time. PT trajectories are defined in an n-dimensional space ( $n = 1$  to 4) and are available only with `MultipleAxes` groups. A PT trajectory is generated with continuous movements of the group's positioners over several time periods. For each period, each positioner must complete a defined displacement from its current position. By definition, there is no constant vector velocity and no definition for vector acceleration compared to Line-arc trajectories or splines.

Trajectory element (segment): An element of a PT trajectory is defined by a set of all positioner displacements and the duration for the segment. In the PT data file, each element is represented by a line of values:

$$DT, DP1, DP2, \dots, DPn$$

DT: The segment duration in seconds.

DP1, DP2, ..., DPn: Positioners' (#1, #2, ..., #n) displacements during DT.

### 4.4.2 Trajectory Conventions

When defining or executing a PT trajectory, a number of rules must be followed:

- The motion group must be a `MultipleAxes` group.
- All trajectories must be stored in the controller's memory. Use the XPS webpage **Files** → **Trajectory files** to edit, upload or download a PT trajectory file. Once a trajectory is started, it executes in the background allowing other groups to work independently and simultaneously.

## 7.2 Python software - Manual

This chapter includes the manual of the Python program which was created over the course of this master's thesis. The program creates suitable PVT trajectory files for the stage controller. This was necessary since no commercial software fitted the needs of the chosen manufacturing approach.

Handbuch PythonLMS  
Erstellen von PVT Trajektorien

Andreas Ulm

# Handbuch zur PythonLMS Software

## Erstellung von PVT Trajektorien für Graustufen-TPA



## Inhalt

|       |   |    |
|-------|---|----|
| 1     | Starten der GUI.....  | 3  |
| 2     | Fenster.....  | 3  |
| 2.1   | Startfenster.....   | 3  |
| 2.2   | Auswahlfenster.....   | 3  |
| 2.3   | „Create Bitmap-File Pyramids, Rectangle“ - Struktur in Bmp speichern..... | 4  |
| 2.4   | „Create Bitmap-File Grid“ – Gitter-Struktur in Bmp speichern.....         | 5  |
| 2.5   | Create Bmp from Stl“ – Stl Files einlesen.....                            | 6  |
| 2.6   | „CreatePVTfile from Bmp“ – PVT-File aus Bmp erstellen.....                | 7  |
| 2.7   | GUI Fenster – Simulation (Verify PVT Trajectory File).....                | 10 |
| 2.7.1 | Zum Output und zur Analyse.....   | 11 |
| 2.7.2 | Textoutput.....   | 12 |
| 2.7.3 | Scatter Plots.....  | 12 |
| 2.7.4 | Line Plots.....   | 13 |
| 2.8   | GUI Fenster – Simulation Beispiele.....                                   | 15 |
| 2.8.1 | Beispiel 1 – Gutes Ergebnis.....  | 15 |
| 2.8.2 | Beispiel 2 – 0.95 mm/s – schlechtes Ergebnis.....                         | 16 |
| 2.8.3 | Beispiel 3 – 1.25 mm/s – passables Ergebnis.....                          | 19 |
| 2.8.4 | Beispiel 4 – altes PVT File.....  | 21 |
| 3     | Klassen.....  | 23 |
| 3.1   | Klasse graySurface.....   | 23 |
| 3.1.1 | Beispielprogramm.....   | 24 |
| 3.1.2 | Beispielprogramm 2 – PVT Trajektorie.....                                 | 25 |
| 3.2   | Klasse Trajectory (Create).....   | 27 |
| 4     | Diskussion Jerk – Theoretische Betrachtung.....                           | 28 |
| 4.1   | Beschleunigungskurve AccelerationCurveTriangleJerk.....                   | 28 |
| 4.2   | DisplacementKurve DisplacementCurveTriangleJerk.....                      | 28 |
| 4.3   | Zum Klassenaufbau.....  | 29 |
| 4.4   | Beschreibung der Klassenfunktionen.....                                   | 29 |

## 1 Starten der GUI

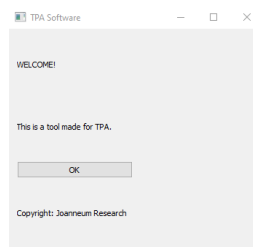
Starten des Programms runGUI.py

Zurzeit müssen noch keine Dateien zwingend von einem Fenster zum nächsten Übergeben. Deshalb können alle Fenster auch individuell gestartet werden. Diese sind im Ordner PythonLMS/Windows zu finden.

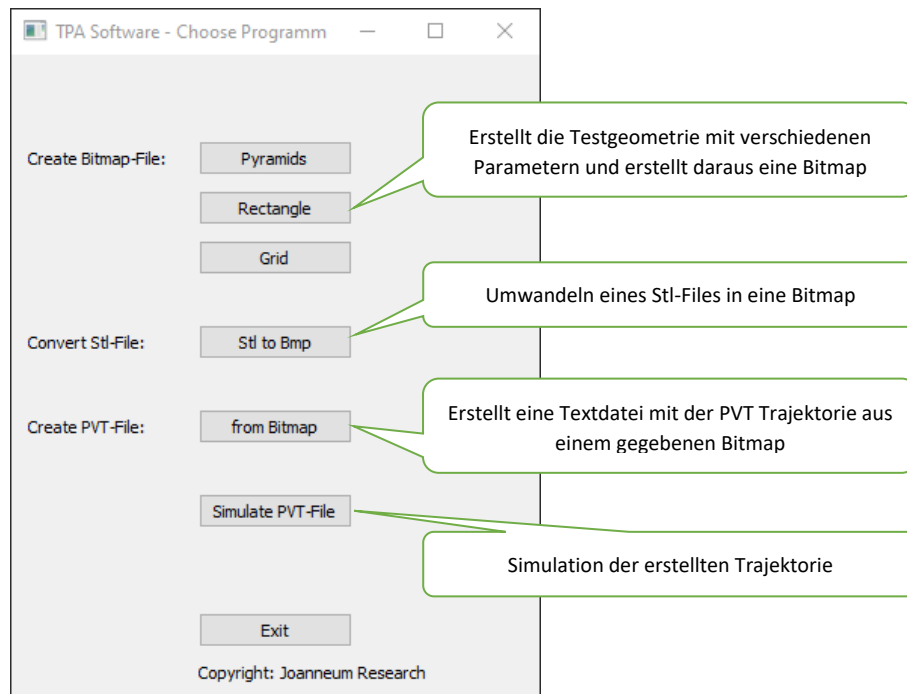
## 2 Fenster

### 2.1 Startfenster

Kurze Begrüßungsnachricht.

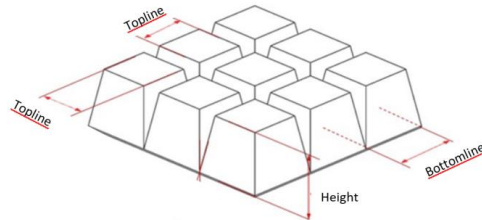


### 2.2 Auswahlfenster

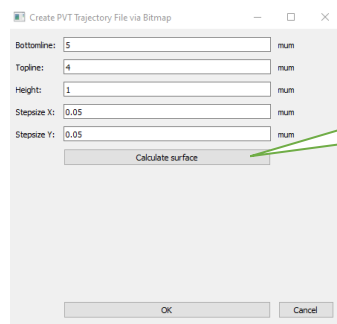


## 2.3 „Create Bitmap-File Pyramids, Rectangle“ - Struktur in Bmp speichern

Dieses Fenster generiert einen Pyramidenstumpf dieser Art (weitere Formen in Zukunft möglich, CAD Geometrie, ...). Die Parameter sind dargestellt. Bei der Funktion Rechteck wird anstelle einer verlaufenden Flanke, ein Quader mit der Grundfläche eines Quadrates (Seitenlänge Topline) in die Mitte des Quadrates (Seitenlänge Bottomline) gesetzt.

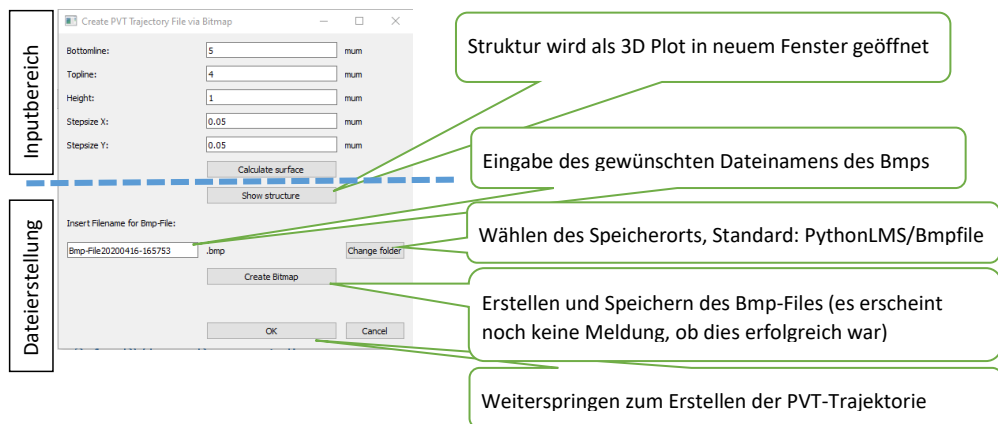


Diese Parameter werden ins Fenster zusammen mit der Grid-Genauigkeit eingegeben.

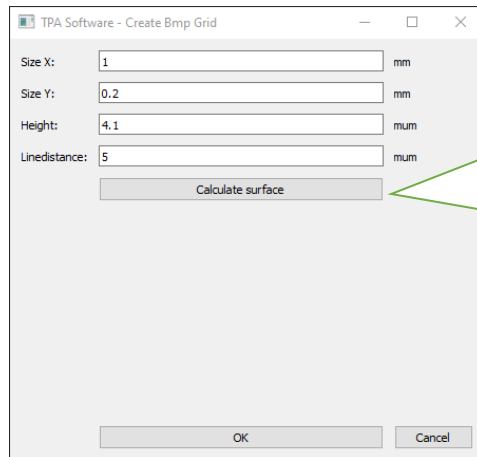


Erstellt ein Objekt GraySurface mit einem Pyramidenstumpf (Vervielfachung später möglich)

Das Fenster wird zu:



## 2.4 „Create Bitmap-File Grid“ – Gitter-Struktur in Bmp speichern



Erstellt ein Objekt GraySurface mit dem gesamten Gitter (Abmessungen Size X, Size Y). Die Bitmap besteht aus lauter weißen Pixel. Wenn dies aber mit Scan „Double“ geschrieben wird, wird somit ein Gitter daraus. Line Distance entspricht dem Pixelabstand in X und Y-Richtung.

Nach Klicken auf „Calculate Surface“ erscheint ein Dateierstellungsbereich wie im letzten Punkt bei den Pyramiden.

## 2.5 Create Bmp from Stl – Stl Files einlesen

The screenshot shows a dialog box titled "TPA Software - Create Bitmap File from Stl File". It contains several input fields and buttons:

- Please select file:** A search bar and a "Show Import" button.
- Number intervals X:** Input field with value "20".
- Number intervals Y:** Input field with value "20".
- Referring to:** Input fields for "x-Pixel:" (0.5) and "y-Pixel:" (0.5), both with "mm" units.
- Insert Filename for BMP-File:** Input field with "empty" and ".bmp" extension, and a "Change folder" button.
- Status:** "Please insert values."
- Buttons:** "Create Bmp", "Cancel", "Show Surface Interpol", "Show Surface", and "Proceed".

Callout boxes provide the following explanations:

- Search bar:** Liest den Pfad des Stl-Files ein.
- Show Import button:** Zeigt den Import mit der Numpy-Stl Erweiterung
- x-Pixel and y-Pixel fields:** Rasterdichte für x- und y-Richtung im Stl-File
- Change folder button:** Rasterdichteäquivalenz für die anschließende TPP-Struktur
- Create Bmp button:** Erstellen der Bitmap. (siehe unten Anmerkung). Kann u. U. lange dauern. Ausgabebereich im Spyder berücksichtigen. (2 Sortiervorgänge und danach einige (je nach Größe) Berechnungen der Teilbilder.)
- Proceed button:** Zeigt die erzeugte Oberfläche
- Status field:** Meldung: Ok oder Fehler
- Filename field:** Filename, wird beim Einlesen automatisch vorgeschlagen
- Dialog box:** Öffnet das Fenster zur PVT-Trajektorienerstellung mit erstellter Bitmap

## Anmerkungen zur Erstellung des Bmp:

Es wird die Minimal- und Maximalschranke des Stl-Files ermittelt. Es wird ein Raster mit gewählter Intervallanzahl (Number intervalls X, Number intervalls Y) über das Stl-File von der Minimal bis zur Maximalschranke gelegt. Danach wird für jeden Punkt des Rasters der z-Wert ermittelt, indem er mit allen vorhandenen Dreiecken geschnitten wird. (Es gibt eine Vorsortierung, die einige Schneidberechnungen überspringt zur Rechenzeiteinsparung). Nach Ermittlung aller Höhenwerte, wird das Raster reskaliert auf den Bereich von 0 bis (Number intervalls X \* xPixel) für die X-Richtung bzw. analog für die Y-Richtung. Die Bitmap wird gespeichert und die Höhen werden reskaliert, um den gesamten Bereich bis zum Weißwert 255 zu überstrecken.

## 2.6 „CreatePVTFile from Bmp“ – PVT-File aus Bmp erstellen

Dieses Fenster wird mit obrigen OK aufgerufen oder gleich bei der Menüauswahl (zweiter Button).

**Strukturparameter**

Suchen eines Bmp-Files, siehe Kommentar unten

Höhe, die dem Schwarzwert 0 bzw. Weißwert 255 entspricht

Reale Abstände zwischen den Pixel

Strukturwiederholungen je Achse

3D Ansicht der replizierten Struktur in Realabständen

**PVT Parameter**

Wahl der Schreibgeschwindigkeit, Maximale Schreibgeschwindigkeit 10 mm/s für xPixel 0.5 µm (Micrometer)

Abstand der nach der Trajektorie in normaler Richtung zur schnellen Scanachse freigelassen wird. (Bei nicht-Auswahl wird die Startposition wieder angefahren.)

**Dateierstellung**

Kommentar Suchen eines Bmp-Files: Wird dieses Fenster vom geometrieerstellenden Fenster übernommen, dann werden die Werte für x-Pixel, y-Pixelabstände und Höhe übernommen. Beim Speichern und späteren Importieren eines Bmp-Files gehen diese Daten verloren. (Könnte noch mit einer zusätzlich abgespeicherten Textdatei verbessert werden.)

**PVT Parameter**

x-Pixels: 0.5    Spacing: 0.5    Unit:  $\mu\text{m}$   
y-Pixels: 0.5    Spacing: 0.5    Unit:  $\mu\text{m}$

Writing-Speed: 1.0    mm/s

Repetitive enable  
Repetitive distance: 0.0025

Scan direction: Double  
Scan Type: Bidirektional

Delay time (Bidirectional offset): 0.00055    s

Voltage/Piezo Trajectory: Voltage  
Piezo writing Voltage: 3.0

Freerun Distance: 0.3    mm

Compress file

**Dateierstellung**

Insert Filename for PVT-File:  
PVT-File20201013-181415 .txt

Status: Done. Textfile created. Total time: 8.5

**Scan direction: „X-Raster“** bedeutet, dass X die schnelle Scan-Richtung ist.  
„Double“scant die Struktur zweimal. Zuerst wird ein Y-Raster Scan ausgeführt, dann ein X-Raster.  
Scan Type: Unidirektional schreibt immer nach positiver Richtung (Leerfahrt auf dem Rückweg).  
„Bidirektional“schreibt in beiden Richtungen (Delay, die das Signal zu langsam ankommen würde, wird mit zusätzlichem Weg ausgeglichen, Controllerproblem)

**Voltage/Piezo Trajectory:**  
„Voltage“ kodiert die höhen in die Spannungsachse, „Piezo“ in die Piezoachse. Bei „Piezo“ wird eine Schreibspannung (Piezo Writing Voltage) zusätzlich benötigt.

**Compress File:**  
Bei Auswahl wird die erstellte Trajektorie nochmals überarbeitet. Aufeinanderfolgende Intervalle mit gleicher Geschwindigkeit und ohne Änderung der Spannung oder Piezoachse, werden kombiniert. So werden Zeilen gespart.

**Freerun:** Weg der zwischen Beschleunigung und Schreiblinie hinzugefügt wird. Während dieser Zeit kann sich der Stage Error minimieren.

**PVT Parameter**

Spacing: x-Pixels: 0.5, y-Pixels: 0.5, Unit: mm, Repetitions: 1

Writing-Speed: 1.0 mm/s

Repetitive enable:

Repetitive distance: 0.0025 mm

**Dateierstellung**

Scan Type: Bidirektional

Delay time: [ ]

Voltage/Power: [ ]

Piezo writing: [ ]

Freerun Distance: [ ]

Compress file:

Insert File Name for PVT-File: PVT-File20201013-181415 .txt

Change folder: [ ]

Create PVT Trajectory, Open file, Simulate, Cancel

Total time: 8.52s

Status: Done, Textfile created, Total time: 8.516224999999

**Textfile wird mit dem Editor geöffnet. (Muss allerdings wieder geschlossen werden, da Python auf das Schließen wartet um weiterzuarbeiten.) Soll das Textfile ungestört geöffnet werden, muss dies weiterhin über den Filemanager extern geschehen.**

**Wählen des Speicherorts, Standard: BitmapFilesOutput**

**Kurze Meldungen zu durchgeführten Berechnungen und Speicherungen**

**Kurze Meldungen zu durchgeführten Berechnungen und Speicherungen**

**Simulation:**

- Die Klasse stageXPSController wird erstellt. Diese liest das Textfile unabhängig vom vorigen Programm ein und interpoliert ein Polynom 3ten Grades zwischen zwei Punkten, wobei Stetigkeit von Weg und Geschwindigkeit gefordert werden (Formeln aus dem XPS Manual)
- neues Fenster (Verify PVT) wird geöffnet.

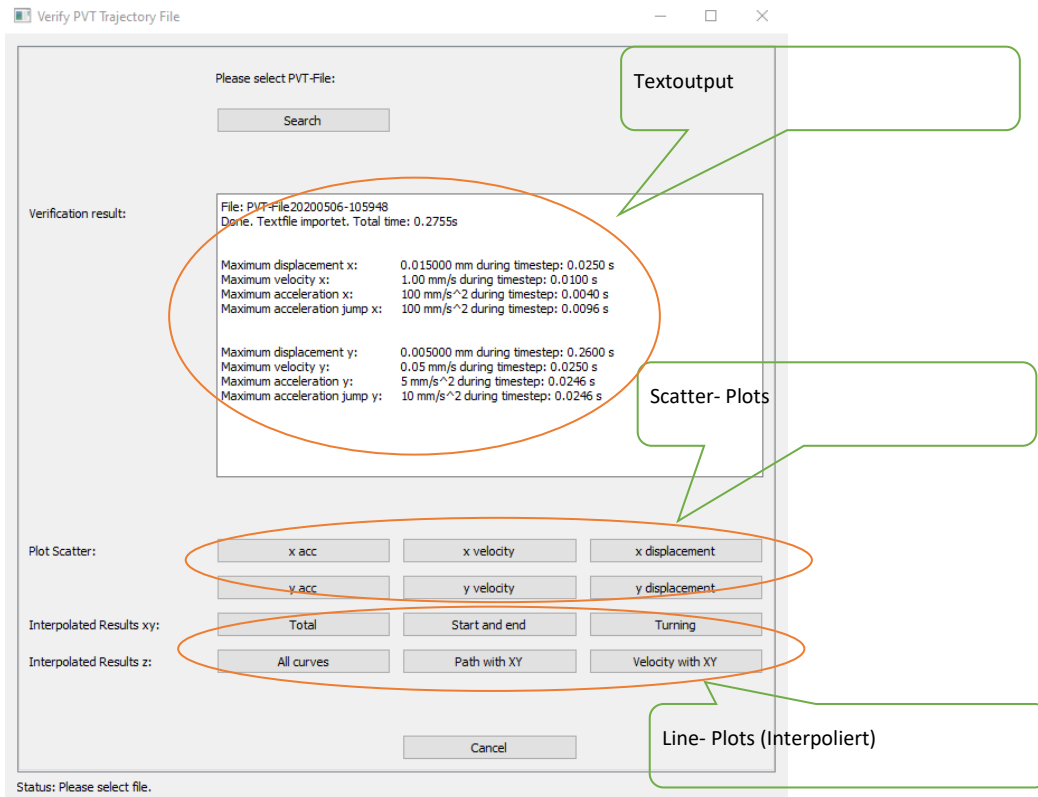
**Erstellt und speichert das PVT-Textfile:**

- Eine neue Klassenvariable Trajectory wird zur GraySurface hinzugefügt, die die konstant-Geschwindigkeitsbereiche mit den dementsprechenden Umkehr- und Beschleunigungskurven zusammenfügt
- Die Punkte der Trajektorie werden in das Textfile geschrieben



### 2.7 GUI Fenster – Simulation (Verify PVT Trajectory File)

Dieses kann direkt aus dem Auswahlfenster aufgerufen werden. Dann muss das PVT-File gewählt werden. Bei Weiterleitung aus dem „Create PVT from Bmp“ -Fenster wird das File automatisch eingelesen und analysiert. Zusätzlich kann danach jederzeit mit dem „Search“-Button ein beliebiges File eingelesen werden.

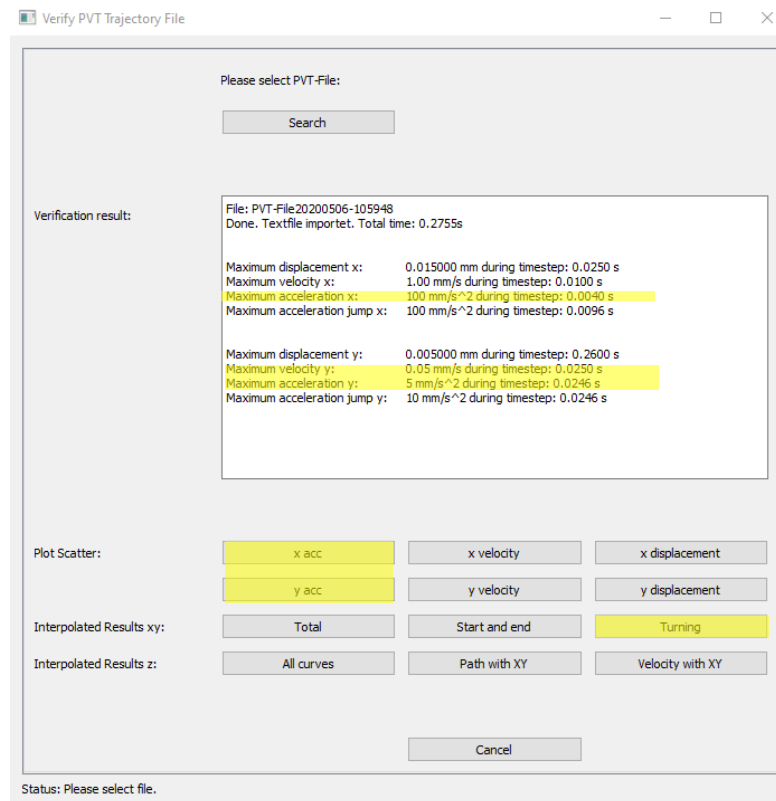


### 2.7.1 Zum Output und zur Analyse

Mehrere Dinge werden hier überprüft, einige Dinge sind wichtiger zu kontrollieren und geben Informationen über die Qualität der Trajektorie.

Es sind hier sehr viel Auswertungen vorhanden. Um den Überblick nicht zu verlieren, habe ich die wichtigsten in **Gelb** markiert.

Untenstehend werden alle Funktionen genauer erklärt.



### 2.7.2 Textoutput

Hier wird in den ersten zwei Zeilen der Filenamen angezeigt und die Gesamtzeit.

Maximum displacement und maximum velocity sollten keine Überraschungen liefern (da diese so im PVT-File direkt stehen) und stehen hier nur nochmal zur kurzen Überprüfung.

```
File: PVT-File20200506-105948
Done. Textfile importet. Total time: 0.2755s

Maximum displacement x: 0.015000 mm during timestep: 0.0250 s
Maximum velocity x: 1.00 mm/s during timestep: 0.0100 s
Maximum acceleration x: 100 mm/s^2 during timestep: 0.0040 s
Maximum acceleration jump x: 100 mm/s^2 during timestep: 0.0096 s

Maximum displacement y: 0.005000 mm during timestep: 0.2600 s
Maximum velocity y: 0.05 mm/s during timestep: 0.0250 s
Maximum acceleration y: 5 mm/s^2 during timestep: 0.0246 s
Maximum acceleration jump y: 10 mm/s^2 during timestep: 0.0246 s
```

Wichtiger zu kontrollieren ist die „Maximum acceleration“: diese sollte unbedingt wie vorher eingestellt sein. Ermittelt wird diese mit dem Maximalwert aller Anfangs- und Endbeschleunigungen wie im XPS-Manuell mit der Formel berechnet.

Der maximum acceleration jump sollte gleich der maximum acceleration sein. Ist dieser doppelt so hoch, ist das noch nicht tragisch. Wichtiger wird der Verlauf der Punkte (siehe nächster Punkt) zu kontrollieren sein.

Für die y-Komponente kann nun die Acceleration und die Geschwindigkeit Y sehr hoch sein, da diese auf Basis der x-Strecke berechnet wird. (Speziell wenn der y-Abstand der Pixel größer als der der x-Pixel ist).

### 2.7.3 Scatter Plots



x,y velocity und displacement (die vier Knöpfe rechts) zeigen so gut wie immer einen sehr glatten Verlauf. Kleine Unebenheiten werden hier nicht sichtbar. Sollte man hier einen Knick erkennen, dann ist schon viel schiefgelaufen.

x acc, y acc berechnen nun die Verläufe von Start- und Endbeschleunigung nach XPS-Manual-Formel.

Genauere Scatterplots sind unten bei den Beispielen zu finden.

## 2.7.4 Line Plots

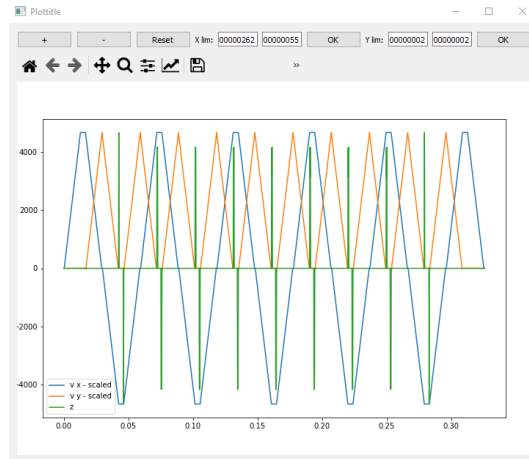


Hier werden die jeweiligen Kurven aus dem File gelesen und mit 10 Zwischenpunkten (nach gegebenen Formeln) interpoliert.

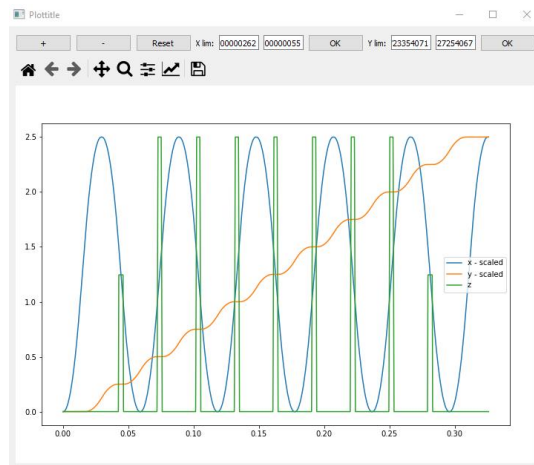
- xy Total
  - Hier zeigt sich Jerk, Acceleration, Geschwindigkeit und Displacement für x und y-Fahrwege.
- xy Start und end
  - Die End- und Beginnstrecke von Total wird versucht herauszuschneiden, um diese zu analysieren. Sollte das schneiden nicht funktionieren muss über „Total“ manuell hingezoomt werden.
- xy Turning
  - der Turningverlauf von Total wird versucht herauszuschneiden, um diesen zu analysieren. Sollte das schneiden nicht funktionieren muss über „Total“ manuell hingezoomt werden.
  - Hier kommt es durch die Verzerrung der Beschleunigungskurve und Rundungen vermehrt zu Oszillationen.
- z all curves
  - Es werden Jerk, Acceleration, Geschwindigkeit und Displacement für den Laser angezeigt, wobei Jerk und Acceleration sehr sprunghaft und hoch sein werden.
- z Path with xy
  - Zeigt, ob das Displacement des Lasers mit dem der Stage zusammenpasst.
- z Velocity with xy
  - Zeigt, ob die Änderungsrate des Lasers mit der Geschwindigkeit der Stage zusammenpasst.

Bei den Beispielen unten wurde immer nur mit den Plots von Scatter (x acc und y acc) sowie xy Interpolated (xy total, turning) gearbeitet, da die anderen Plots immer gut aussehen.

Zur Veranschaulichung hier ein Plot von z Path und z Velocity:



Geschwindigkeitsverlauf. Die Änderungsrate ist nur am Beginn und Ende der Bereiche der x-Konstantgeschwindigkeit ungleich 0.



Displacement. Nur wenn y konstant ist, wird z Angesteuert. x hat in diesen Bereichen konstante Steigung. Die erste Zeile wird mit halber Spannung geschrieben, die weiteren mit maximaler, dies entspricht der Seite bzw. des Plateaus des Pyramidenstumpfes.

## 2.8 GUI Fenster – Simulation Beispiele

Für alle Beispiele wurde das Bmp verwendet, das du mir geschickt hast. Mit Gridsize 0.5 x 0.5 mm. Beschleunigung 100. Geschwindigkeit variierend.

### 2.8.1 Beispiel 1 – Gutes Ergebnis

Geschwindigkeit wurde 1 mm/s gewählt (ergibt 0.5 ms Zeitintervall für die Rasterung), Zeitinkrement für Beschleunigungs- und Turning-Kurve 0.4 ms.

Die Simulation wurde gestartet.

```
File: PVT-File20200506-105948
Done. Textfile importet. Total time: 0.2755s

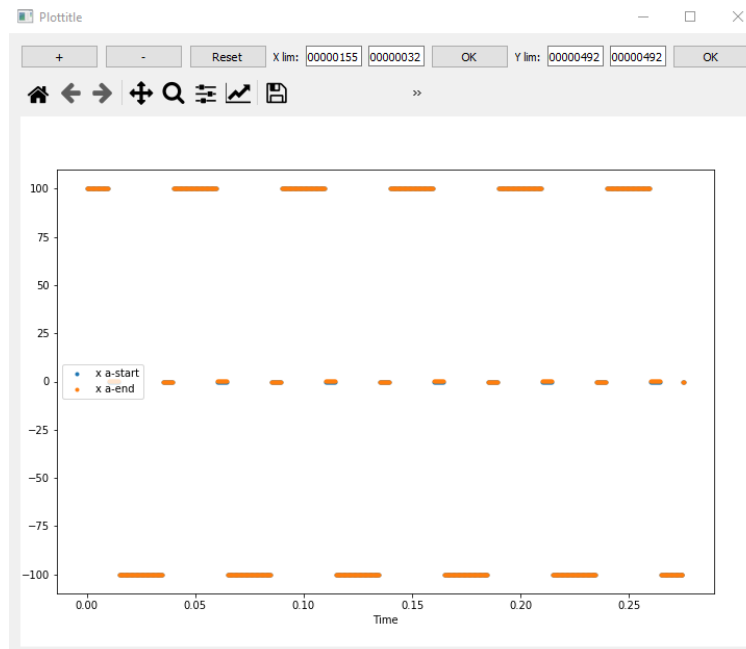
Maximum displacement x: 0.015000 mm during timestep: 0.0250 s
Maximum velocity x: 1.00 mm/s during timestep: 0.0100 s
Maximum acceleration x: 100 mm/s^2 during timestep: 0.0040 s
Maximum acceleration jump x: 100 mm/s^2 during timestep: 0.0096 s

Maximum displacement y: 0.005000 mm during timestep: 0.2600 s
Maximum velocity y: 0.05 mm/s during timestep: 0.0250 s
Maximum acceleration y: 5 mm/s^2 during timestep: 0.0246 s
Maximum acceleration jump y: 10 mm/s^2 during timestep: 0.0246 s
```

Maximum acceleration ist unverändert, sehr gut. Für y Komponente alles sehr niedrige Werte, auch gut.

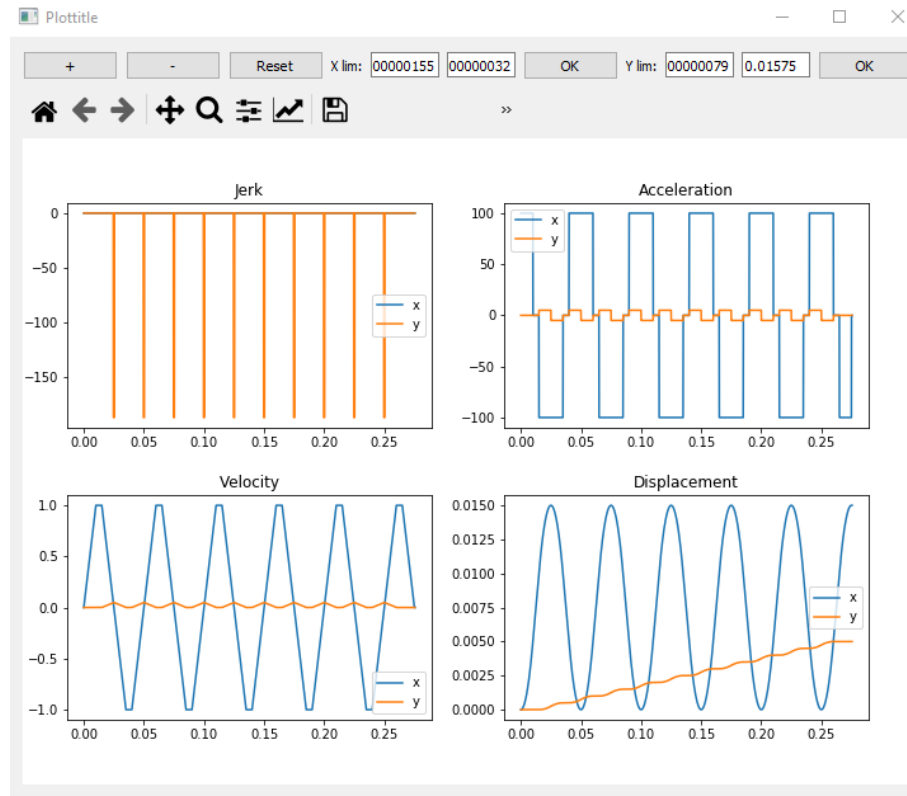
Die Buttons **x acc, y acc** berechnen nun die Verläufe von Start- und Endbeschleunigung nach XPS-Manual-Formel.

Die Scatterplots sollten so aussehen:



Die blauen und orangen Punkte liegen übereinander, das bedeutet, dass die Endbeschleunigung des vorgehenden Zeitintervallstücks, mit der Startbeschleunigung des nachfolgenden übereinstimmt.

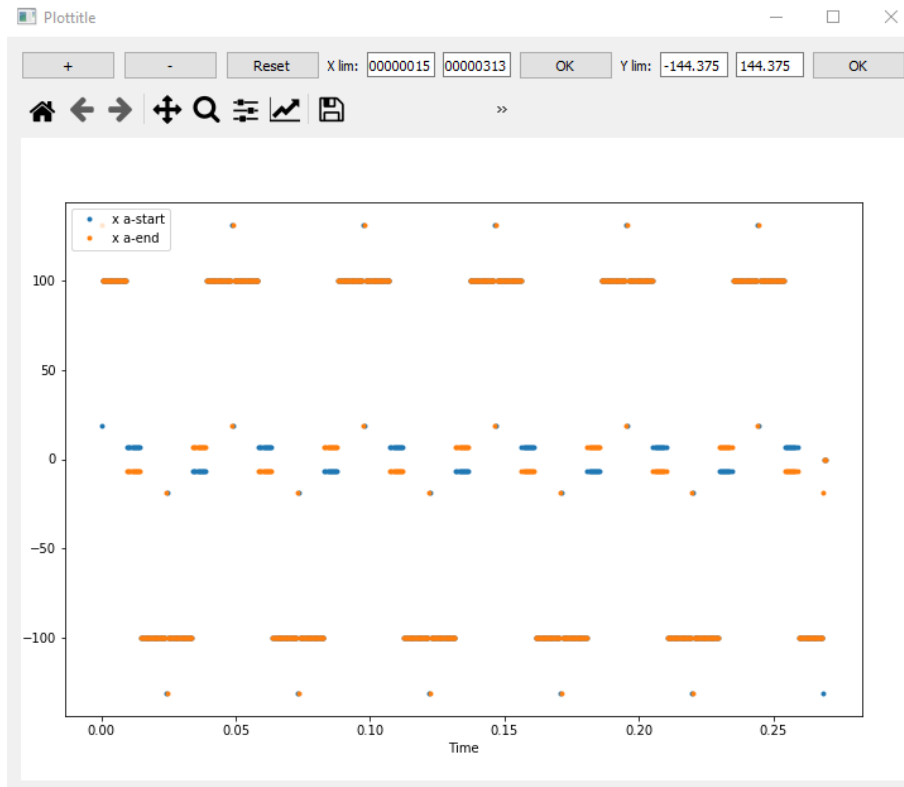
Der Total-Plot Interpolated zeigt folgendes:



Das Displacement zeigt eine hin und herfahrt der x-Achse und ständig wachsende y-Achse. Im Geschwindigkeitsplot sind die konstanten Bereiche der x-Geschwindigkeit und y-Geschwindigkeit = 0 zu sehen. Und die Acceleration zeigt schöne gerade *konstante Abschnitte*, so wie als Inputfunktion definiert. Die x-Acc-Höhe stimmt überein. Die y-Acc-Höhe genau passend für das Fahren in die nächste Reihe, genügend klein und glatt.

### 2.8.2 Beispiel 2 – 0.95 mm/s – schlechtes Ergebnis

Zum Vergleich ist hier die gleiche Simulation mit 0.95 anstatt 1 mm/s Geschwindigkeit zu sehen. Dies ergibt zwar ein nicht passendes Konstantzeitintervall (0.536 ms), es eignet sich aber für die Veranschaulichung möglicher Fehler. Der x acc Scatterplot sieht wie folgt aus:

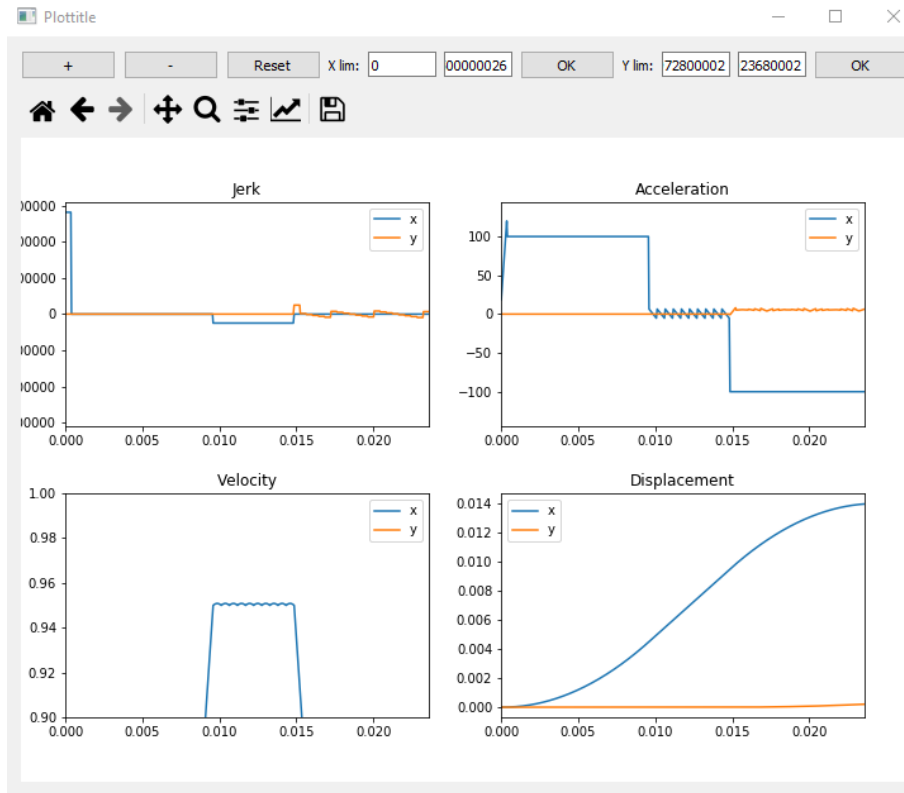


Durch die Verzerrung der Kurve kommt es zu Sprünge, während die maximal angegebene Beschleunigung von 100 überschritten wird, sind diese zumindest ein Oranger und blauer Punkt zusammen, und somit noch vertretbar.

Die Bereiche in der Mitte, wo orange und blaue Punkte getrennt sind, sind allerdings nahe am Unzulässigen. Es bedeutet, das dort wo eigentlich konstante Geschwindigkeit sein sollte, die Geschwindigkeit oszilliert.

Der Plot (interpolated Results xy, total, ein Ausschnitt) sieht wiefolg aus:

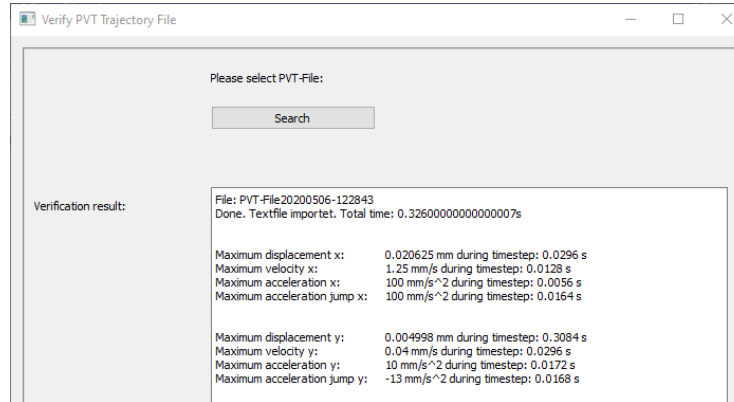




Der Schreibbereich mit konstanter Geschwindigkeit weist Oszillationen auf. (Obwohl konstante Geschwindigkeiten im PVT File stehen). Diese sind nicht groß und im Velocity plot erst nach hineinzoomen sichtbar. Im Acceleration Plot allerdings ist die Auswirkung deutlich größer.

Nichtdestotrotz sind diese noch gering und ich würde ein ausführen der Datei für möglich halten.

## 2.8.3 Beispiel 3 – 1.25 mm/s – passables Ergebnis

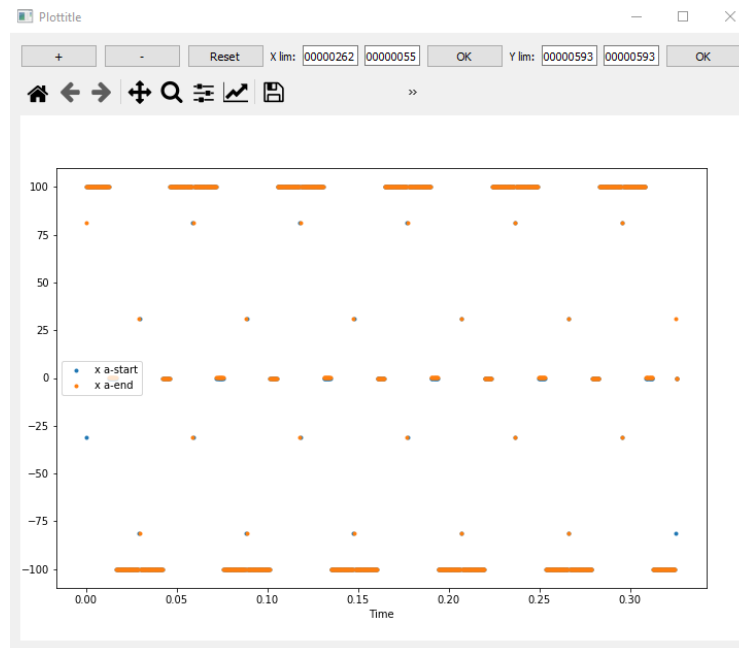


Maximum acceleration x passend.

Maximum acceleration y gut.

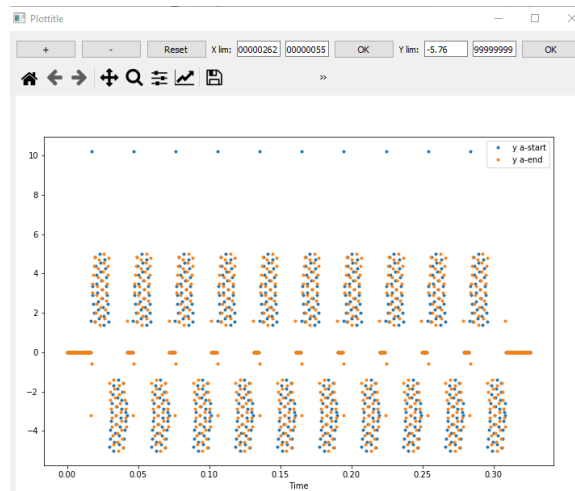
Maximum acceleration jump y > maximum acceleration y weist auf Oszillationen hin.

Der x acc Scatterplot:

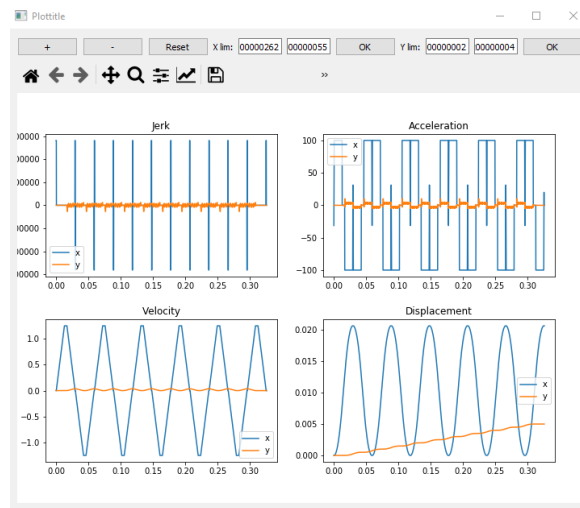


x-Scatters schauen gut aus. Abweichende Punkte vom Maximum treten nur einzeln und immer gemeinsam (orange, blau) auf.

Der y acc – Scatterplot



Y-Scatters schauen eher nicht gut aus. Eine Reihe von blauen Ausreißern oben. Verwaschene Gebiete durch alle Turning-Vorgänge hindurch. Ein Lichtblick ist, dass die Konstantzeitbereiche 0 Beschleunigung haben und die Maximalbeschleunigung doch sehr gering ist.



Weg und Geschwindigkeit sehen sehr gut aus. Acceleration zeigt für x einen Spitz in der Mitte des Turnings. Dies wurde aber bewusst in die Mitte des Turnings gelegt, da es dort fürs Schreiben nicht viel ausmacht.

Acceleration y zeigt leider die Oszillationen wie schon oben analysiert.

Handbuch PythonLMS

Erstellen von PVT Trajektorien

Andreas Ulm

## 2.8.4 Beispiel 4 – altes PVT File

Zum Vergleich die Analyse für das File, das mit der letzten Versions meines Programms generiert wurde (das du getestet hast).

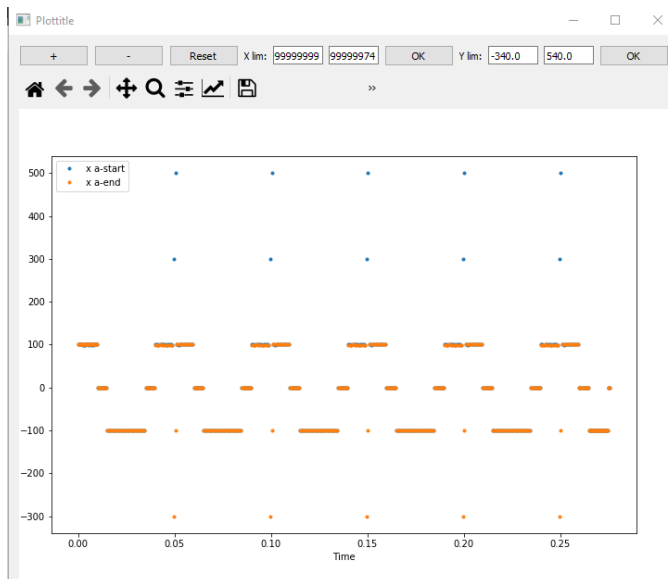
```
File: PVT-File20200428-091033.txt
Done. Textfile importet. Total time: 0.27580000000000005s

Maximum displacement x: 0.015000 mm during timestep: 0.2750 s
Maximum velocity x: 1.00 mm/s during timestep: 0.0100 s
Maximum acceleration x: 500 mm/s^2 during timestep: 0.0504 s
Maximum acceleration jump x: -800 mm/s^2 during timestep: 0.0496 s

Maximum displacement y: 0.005000 mm during timestep: 0.2600 s
Maximum velocity y: 0.05 mm/s during timestep: 0.0246 s
Maximum acceleration y: 7 mm/s^2 during timestep: 0.0246 s
Maximum acceleration jump y: -5 mm/s^2 during timestep: 0.0145 s
```

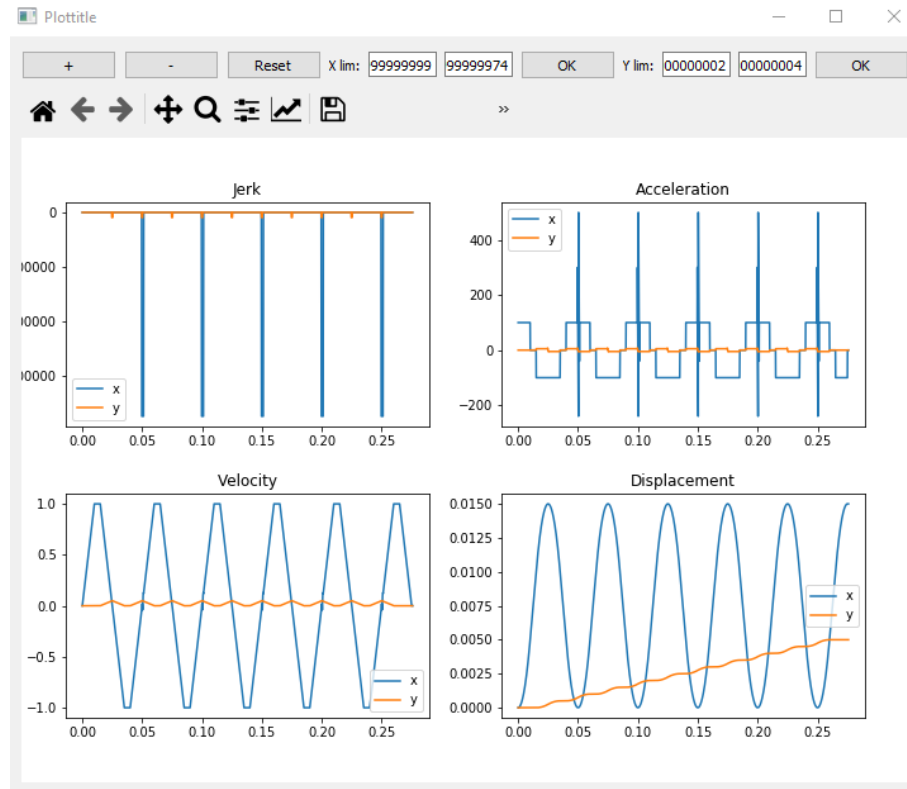
Maximum acceleration x ist um das 5-fache höher als eingestellt. (Sollte aber noch unter der Grenze von 2500 mm/s<sup>2</sup> liegen, also dies bedarf noch Klärung.)

Der x acc Scatterplot:



Der x acc scatter plot zeigt grundsätzlich gute Konstantzeitbereiche, aber gerade die Ausreißer haben einzelne Farbe und sind 5x so hoch wie die eigentlich gewählte Beschleunigung.

Total curves xy:



Genau dort wo die Geschwindigkeit von negativ auf positiv wechselt, gab es ein Problem. Durch die Anzahl der Turning Punkte, die ungerade sein musste um ein gutes Ergebnis zu liefern, war gerade. Dadurch gab es ein Vorzeichenproblem und die Geschwindigkeit wurde für einen Punkt in die falsche Richtung angenommen, deshalb ist die Kurve für die zwei angrenzenden Intervalle entartet.

Der Fehler ist sogar in dem Velocity plot sichtbar. Allerdings sieht dieser noch annehmbar aus, weshalb eine Überprüfung dessen eigentlich keinen Sinn macht.

### 3 Klassen

Im Pogram existieren verschiedene Klassen, die das Programm übersichtlich halten sollen

#### 3.1 Klasse graySurface

Bildet die Oberfläche der zu erzeugenden Struktur nach.

Funktionen:

- `__init__`
  - Der Konstruktor erzeugt ein Grid und initialisiert Z werte null
- `addPyr`
  - Eine Pyramide wird erzeugt. Wo diese höher als die bisherige Oberfläche liegt. Werden die alten Punkte durch diese neuen Punkte ersetzt.
- `plotContour`
  - Konturplot
- `plot3D`
  - 3D Plot
- `saveAsBmt`
  - Bitmap datei wird mit gegebenen Dateinamen erstellt.
- `showBmt`
  - Zuletzt gespeicherte Bitmap datei anzeigen
- `createPVTtrajectorie` nächste zu erstellene Funktion
- verschiedene Funktionen zum Erstellen einer Struktur (z.B.: Pyramide)
- `createPVTconstSpeed(self,filename,speed)`
  - Erstellt PVT Trajektorie für konstante Schreibgeschwindigkeit
  - gegliedert in:
    - Trajektorie erstellen aus vorher definierter Oberfläche (Funktion `createPVTtrajectory` wird aufgerufen)
    - Trajektorie in Datei schreiben
      - Format (passend zu XPS controller), Werte getrennt durch Kommas wie in Outputfile
- `createPVTtrajectory(self,speed)`
  - Trajektorie erstellen aus vorher definierter Oberfläche
  - Neue Klasse `Trajectory` (siehe unten) wird hier erstellt
    - Geschwindigkeit wird der Trajektorie übergeben
  - Schleife über alle Zeilen des Bildes:
    - Übergabe der Punkte einer Zeile an die Trajektorie mit dem Befehl `trajectory.addStraightXLine(xPoints,yCoordinate,colorPoints)`
      - diese werden automatisch an den bisherigen Pfad angefügt
    - Umkehrung/ Kurve (siehe unten) mittels `trajectory.addCurve`
      - am Ende keine Kurve mehr sondern abbremsen
- `printDistanceToAccelerate, printTime`
  - geben entsprechende Werte in der Konsole aus

## 3.1.1 Beispielprogramm

Mit dem Code

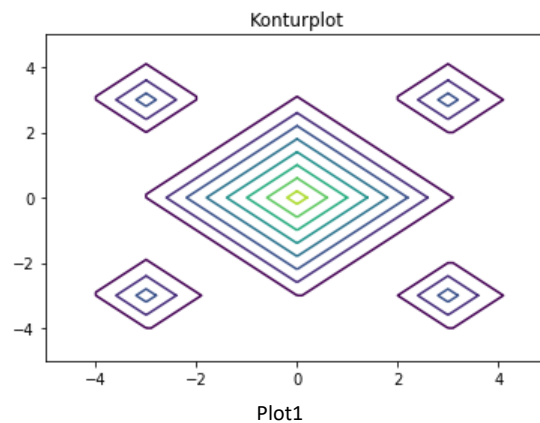
```
from graySurface import graySurface

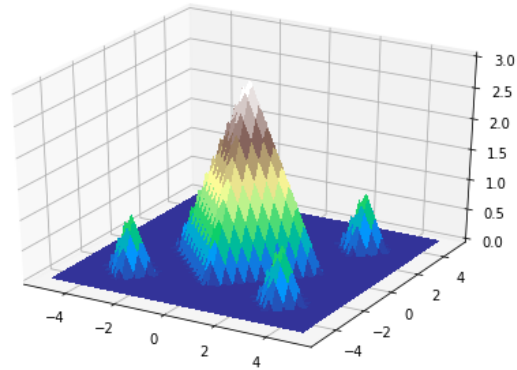
#Klasse erstellen – Ebene / Grid initialisieren
gs = graySurface(-5,5)

#Pyramiden zur Oberfläche hinzufügen (Steigung, Höhe, Mittelpunkt (x), Mittelpunkt (y))
gs.addPyr(1,1,-3,-3)
gs.addPyr(1,1,3,-3)
gs.addPyr(1,1,-3,3)
gs.addPyr(1,1,3,3)
gs.addPyr(1,3,0,0)

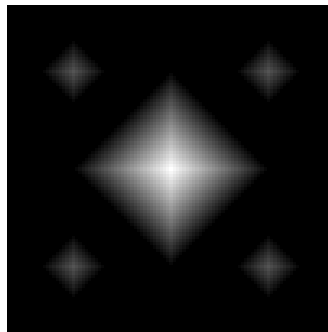
#Plot 1
gs.plotContour()
#Plot 2
gs.plot3D()
#Erstellen Bitmap
gs.saveAsBmt('firstbmt2')
gs.showBmt()
```

wird folgender Output erzeugt:





Plot2



Bitmap

## 3.1.2 Beispielprogramm 2 – PVT Trajektorie

Mit dem Code

```

from graySurface import GraySurface

gs = GraySurface(-10,10) # mum
gs.addPyr(1,10,0,0)

speed = 1000 #mum/s
gs.createPVTconstSpeed("pvt3",speed);

```

```

#Berechne die Beschleunigungsdistanz anzeigen
gs.printDistanceToAccelerate()

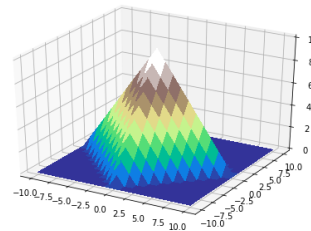
```

```

#Berechnung der Zeit fürs den Laserschreibvorgang in Sekunden
gs.printTime()

```

wird folgender Output erzeugt:





Handbuch PythonLMS

Erstellen von PVT Trajektorien

Andreas Ulm

Distance needed to accelerate : 4.0

Time needed for compeltion : 0.5334142135623733

Textfile pvt3.txt (Ausschnitte):

#Zeit, XPosition, xGeschwindigkeit, yPosition, yGeschwindigkeit, zPosition = 0, zGeschwindigkeit = 0,  
extraAchsePosition, extraAchseGeschwindigkeit

```
0.004000, 4.0, 1000.0, 0.0, 0.0, 0.0, 0.0, 0.0, 0.0 # Beschleunigung von 0,0,0 – Hier ist die
    Beschleunigungszeit und -distanz zum ersten Bildpunkt einzutragen
0.001000, 5.0, 1000.0, 0.0, 0.0, 0.0, 0.0, 0.0, 0.0 # Konstant Geschwindigkeit fürs schreiben – hier
    wird aber noch nichts geschrieben, da Wert der vierten Achse 0 ist
0.001000, 6.0, 1000.0, 0.0, 0.0, 0.0, 0.0, 0.0, 0.0
0.001000, 7.0, 1000.0, 0.0, 0.0, 0.0, 0.0, 0.0, 0.0
0.001000, 8.0, 1000.0, 0.0, 0.0, 0.0, 0.0, 0.0, 0.0
...
0.001000, 22.0, 1000.0, 0.0, 0.0, 0.0, 0.0, 0.0, 0.0
0.001000, 23.0, 1000.0, 0.0, 0.0, 0.0, 0.0, 0.0, 0.0
0.001000, 24.0, 1000.0, 0.0, 0.0, 0.0, 0.0, 0.0, 0.0
0.002586, 27.5, 707.1, 0.0, 0.0, 0.0, 0.0, 0.0, 0.0 # Umkehrung – abbremesen auf
    Umkehrgeschwindigkeit mit benötigter Zeit und Distanz
0.002828, 27.5, -707.1, 1.0, 0.0, 0.0, 0.0, 0.0, 0.0 # Umkehrung abgeschlossen – YKoordinate steigt
    um 1 mum
0.002586, 24.0, -1000.0, 1.0, 0.0, 0.0, 0.0, 0.0, 0.0 # Beschleunigen nach Umkehrung
0.001000, 23.0, -1000.0, 1.0, 0.0, 0.0, 0.0, 0.0, 0.0
0.001000, 22.0, -1000.0, 1.0, 0.0, 0.0, 0.0, 0.0, 0.0
...
0.001000, 18.0, -1000.0, 3.0, 0.0, 0.0, 0.0, 0.0, 0.0
0.001000, 17.0, -1000.0, 3.0, 0.0, 0.0, 0.0, 0.0, 0.0
0.001000, 16.0, -1000.0, 3.0, 0.0, 0.0, 0.0, 1.0, 1.0 # Hier wird der Laser angesteuert. – Umrechnung
    noch erforderlich zwischen Voxelgröße und Spannung
0.001000, 15.0, -1000.0, 3.0, 0.0, 0.0, 0.0, 2.0, 1.0
0.001000, 14.0, -1000.0, 3.0, 0.0, 0.0, 0.0, 3.0, 1.0
0.001000, 13.0, -1000.0, 3.0, 0.0, 0.0, 0.0, 2.0, -1.0
0.001000, 12.0, -1000.0, 3.0, 0.0, 0.0, 0.0, 1.0, -1.0
0.001000, 11.0, -1000.0, 3.0, 0.0, 0.0, 0.0, 0.0, -1.0
0.001000, 10.0, -1000.0, 3.0, 0.0, 0.0, 0.0, 0.0, 0.0
0.001000, 9.0, -1000.0, 3.0, 0.0, 0.0, 0.0, 0.0, 0.0
0.001000, 8.0, -1000.0, 3.0, 0.0, 0.0, 0.0, 0.0, 0.0
...
```

### 3.2 Klasse Trajectory (Create)

Funktionen:

- `__init__(self, numElements, numLines)`
  - Setzt Länge und Initialisiert Matizen
- `setConstantSpeed(self, speed)`
  - `self.maxAccelerationStage = 5000000/10 #mum/s^2`
    - legt die (zurzeit noch maximale lineare) Beschleunigung fest (deshalb wird durch den Sicherheitsfaktor 10 dividiert, da die momentane Beschleunigung höher sein kann (Sicherheitsfaktor 1.5 sollte nach meinen Berechnungen ausreichen, ganz unten im Dokument)
  - Aus der Maximalbeschleunigung und gegebener Geschwindigkeit wird benötigte Beschleunigungszeit und -distanz berechnet.
    - lineare Formeln:  $s = \frac{at^2}{2}$ ,  $s = \frac{v}{t}$
- `firstmove(self, deltaX)`
  - wird vor der ersten Bahn aufgerufen
  - verschiebt das Bild um die Beschleunigungsdistanz in Richtung positive z-Achse, damit vor Schreibbeginn beschleunigt werden kann
  - Errechnet die benötigte Zeit für ein Konstantgeschwindigkeitsintervall in der Mitte einer Bildzeile
- `addStraightXLine(self, xPointsNow, yCoordinate, colorPointsNow):`
  - Setzen der Zeit für den ersten Punkt
    - je ob Anfahrt vom Start oder Beschleunigung nach Kurve
  - Zuweisen der übergebenen Punkte mit Errechnung der anderen Punkte und Geschwindigkeiten
  - Aktualisieren der Laufnummer (`actualStep`) damit ein Anhängen beim nächsten Aufruf möglich ist
- `addEnding`
  - fügt ein lineares Stück am Ende fürs Abbremsen zur Trajektorie hinzu
- `printDistanceToAccelerate, printTime` (Gesamtzeit des Schreibvorgangs)
  - geben entsprechende Werte in der Konsole aus
- `addCurve(self, deltaY)`
  - fügt Kurve hinzu zur Trajektorie – Wichtige Funktion: Beschreibung folgt:

## 4 Diskussion Jerk – Theoretische Betrachtung

Ich habe zwei Kurven unabhängig von den bisherigen Klassen implementiert. Diese können zur gleichmäßigeren Beschleunigung dienen. Da aber der Controller stets mit 0 jerk arbeitet, sieht man in der Simulation Vibrationen. Genauere Untersuchungen wären dazu nötig.

### 4.1 Beschleunigungskurve `AccelerationCurveTriangleJerk`

Die erste Kurve ist eine Beschleunigungskurve, die von einer Startgeschwindigkeit  $v_{in}$  auf eine Endgeschwindigkeit  $v_{out}$  mit minimaler Zeit beschleunigt. Dazu werden auch die Parameter der MaxJerktime und der maximalen Beschleunigung (bzw. der Maximalwert `maxJerk`, der aus der maximalen Beschleunigung berechnet werden kann) übergeben.

Das Profil für den Weg  $s$ , die Geschwindigkeit  $v$ , die Beschleunigung  $a$  und den Jerk sieht wie folgt aus:

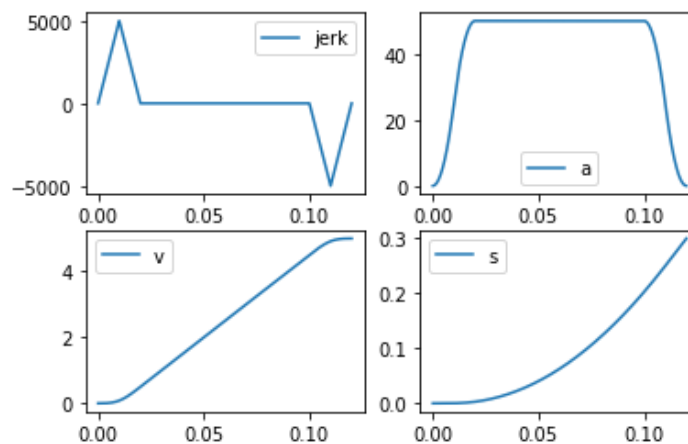


Abbildung 1: Das Dreiecksprofil für den Jerk wird stets erhalten (deshalb auch die Namensgebung). Die Beschleunigung geht auf 0 zurück, die Geschwindigkeit ist also am Ende des Intervalls konstant mit Steigung 0. Der zurückgelegte Weg weist demnach eine konstante Steigung am Ende des Intervalls auf.

Genutzt wird die Klasse später dazu um die Beschleunigungskurven am Start einer Trajektorie und beim Fahren einer Kurve zu erstellen.

Speziell die Funktion `findCurve(maxjerkT, maxjerk, vIn, vOut)` wird dazu aufgerufen. Der Ansatz ist hier für mehrere feste Werte der Beschleunigungszeit die Endgeschwindigkeit zu errechnen. Man erhält also eine Funktion, die Endgeschwindigkeit und Beschleunigungszeit zuordnet. Danach kann für eine gegebene Geschwindigkeit, die Zeit linear interpoliert werden und erhält so eine beliebig genaue Funktion des Wegs, Beschleunigung und Jerks mit gegebenem Profil. (Die Datei `accelerationCurveTriangleJerkFind.py` testet diese Funktion)

### 4.2 DisplacementKurve `DisplacementCurveTriangleJerk`

Diese Kurve arbeitet mit ähnlichem Gedanken als die vorhergehende. Hier wird eine bestimmte Distanz zurückgelegt. Dazu werden ebenfalls die Parameter der MaxJerktime und der maximalen Beschleunigung übergeben. Das Profil für den Weg  $s$ , die Geschwindigkeit  $v$ , die Beschleunigung  $a$  und den Jerk sieht wie folgt aus:

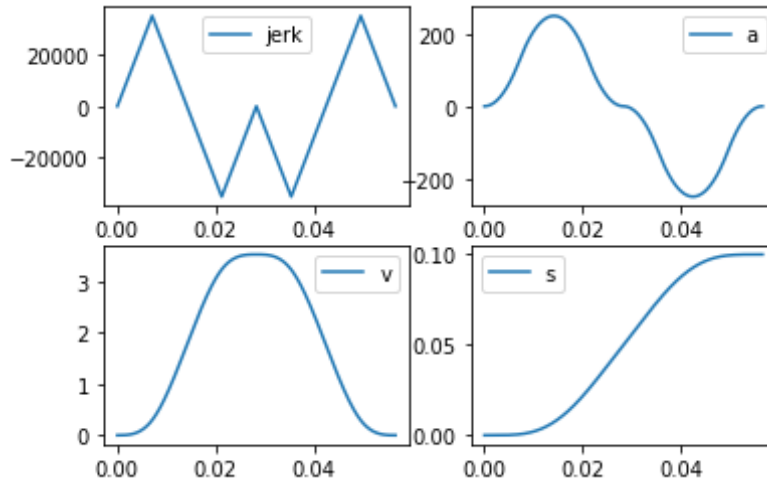


Abbildung 2: Das Dreiecksprofil für den Jerk wird stets erhalten. Die Beschleunigung und auch die Geschwindigkeit gehen am Ende des Intervalls auf 0 zurück. Der zurückgelegte Weg ist die einzige Größe die nicht 0 ist..

Genutzt wird die Klasse später dazu, um die Bewegung der Y-Achse beim Umkehren darzustellen.

Speziell die Funktion `findCurve(maxjerkT, maxjerk, deltaS)` wird dazu aufgerufen. `deltaS` ist hier der Verfahrensweg zwischen den Y-Zeilen. Der Ansatz ist ebenfalls für mehrere feste Werte der Beschleunigungszeit den Endweg zu errechnen. Man erhält also eine Funktion, die Endweg und Beschleunigungszeit zuordnet. Danach kann für gegebenen Endweg, die Zeit linear interpoliert werden und erhält so eine beliebig genaue Funktion der Zwischenpunkte. (Die Datei `displacementCurveTriangleJerkFind.py` testet diese Funktion)

### 4.3 Zum Klassenaufbau

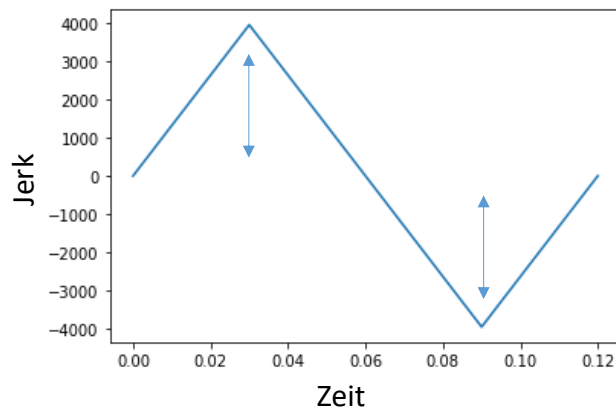
Die Klasse `AccelerationCurve` ist die Mutterklasse für beide obigen Kurven. Sie enthält Funktionen, die von beiden Untergruppen genutzt werden können. Ziel hierbei ist eine sehr flexible Vorgehensweise. Das spezielle an den Kurven ist die Definition der Jerkkurve.

Prinzipiell braucht eine neu erstellte Kurve nur eine Jerkfunktion. Es kann also jede beliebige Jerkfunktion sehr einfach hinzugefügt werden.

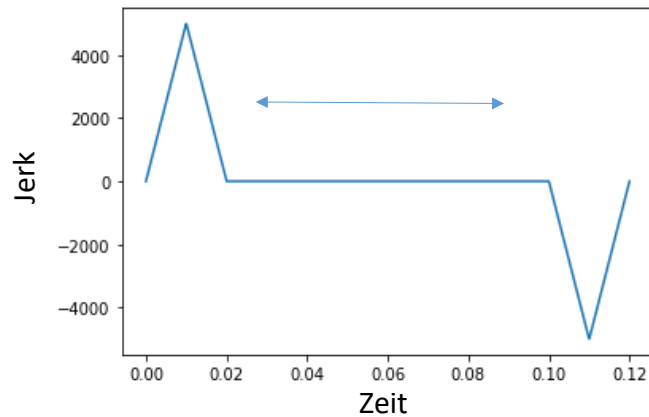
### 4.4 Beschreibung der Klassenfunktionen

- `AccelerationCurve`
  - `__init__(self, tSteps, maxjerkT = 0.02, maxjerk = 500000/10)`  
Speichert die Inputparameter für die maximale Jerkzeit, Maximale Beschleunigung, und die Genauigkeit, gegeben durch Anzahl der Zeitschritte `tSteps`

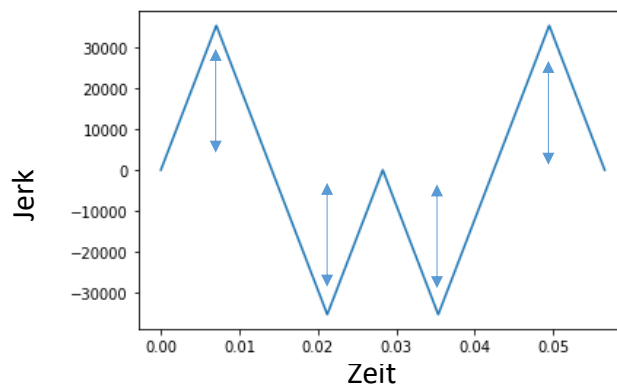
- `calculateCurves(self,deltaT)`  
Berechnet für gegebene Jerkfunktion einer Unterklasse, die Werte für a, v und s per numerischer Integration
  - `calculateJerkfun(self,deltaS)`  
Dies ist eine Dummyklasse die in jeder Unterklasse definiert werden muss.
  - `addLinearVelocity(self,vIn)`  
Ändert die Anfangsgeschwindigkeit (und den daraus resultierenden Weg)
  - `plotCurves(self)`  
Plottet jerk, a, v und s in 4 Quadranten wie in Abbildung 1 und 2
  - `findCurveResult(self)`  
Gibt Endzeit und Geschwindigkeit zurück, plottet die Kurven
  - `getCurves(self, amountPoints = 0)`  
Gibt die Vektoren für jerk, a, v und s zurück mit der Anzahl amountPoints an Zwischenschritten
- `AccelerationCurveTriangleJerk(AccelerationCurve):`
    - `calculateJerkfun(self,deltaS)`  
gibt je nach Zeit die Jerkfunktion aus `getJerkMaxAccelerationReached` oder `getJerkLittleAcceleration` zurück
    - `getJerkLittleAcceleration(self)`  
Die Maximalbeschleunigung wird nicht erreicht. Das Profil sieht wie folgt aus. die Höhe wird variiert, um die Beschleunigung wieder auf 0 zu senken



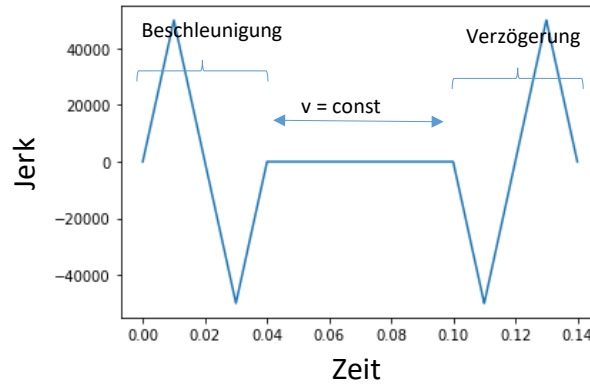
- `getJerkMaxAccelerationReached`  
Die Maximalbeschleunigung wird erreicht. Das Profil sieht wie folgt aus. Sie Zeit konstanter Beschleunigung wird variiert. Danach wird die Beschleunigung wieder 0 durch das untere Dreieck.



- `findCurve(maxjerkT,maxjerk,vIn, vOut)`  
statische Methode, erzeugt eine Instanz der Klasse mit gegebenen Geschwindigkeitsparametern durch eine Schleife (Ausprobieren)
- `DisplacementCurveTriangleJerk`
  - `calculateJerkfun(self,deltaS)`  
gibt je nach Zeit die Jerkfunktion aus `getJerkMaxAccelerationReached` oder `getJerkLittleAcceleration` zurück
  - `getJerkLittleAcceleration(self)`
  - Die Maximalbeschleunigung wird nicht erreicht. Das Profil sieht wie folgt aus. die Höhe wird variiert, um die Beschleunigung wieder auf 0 zu senken.



- `getJerkMaxAccelerationReached(self)`  
Die Maximalbeschleunigung wird erreicht. Das Profil sieht wie folgt aus. Sie Zeit konstanter Geschwindigkeit wird variiert. Danach wird die Geschwindigkeit wieder 0 durch die Verzögerungskurve.



Simulationen zeigen, dass die vorgegebenen Beschleunigungskurven unterschiedlich gut nachgebildet werden können. Wie sehr sich die Abweichungen auf die Vibrationen bei der Herstellung auswirken bleibt zu untersuchen.

## References

- [1] Tommaso Baldacchini. *Three-dimensional microfabrication using two-photon polymerization: fundamentals, technology, and applications*. William Andrew, 2015.
- [2] Wikimedia Commons. File:duty cycle examples.png — wikimedia commons, the free media repository, 2020. [Online; accessed 15-October-2020].
- [3] Keyence corporation. *3D Laser Scanning Microscope VK-X100K User's Manual*. 1-3-14, Higashi-Nakajima, Higashi-Yodogawa-ku, Osaka, 533-8555, Japan, 2012.
- [4] Newport Corporation. Xm series ultra-precision linear motor stages. <https://www.newport.com/f/xm-ultra-precision-linear-motor-stages>. Accessed: 2020-10-16.
- [5] Newport Corporation. *XPS-D Universal High-Performance Motion Controller/Driver Features Manual*. 1791 Deere Ave. Irvine, CA 92606, USA, 2019.
- [6] Sascha Engelhardt, Eva Hoch, Kirsten Borchers, Wolfdietrich Meyer, Hartmut Krüger, Günter EM Tovar, and Arnold Gillner. Fabrication of 2d protein microstructures and 3d polymer–protein hybrid microstructures by two-photon polymerization. *Biofabrication*, 3(2):025003, 2011.
- [7] Heidelberg Instruments. Grayscale lithography. Brochure, 2019.
- [8] Florin Jipa, Marian Zamfirescu, Alin Velea, Mihai Popescu, and Razvan Dabu. Femtosecond laser lithography in organic and non-organic materials. In *Updates in Advanced Lithography*, chapter 3. IntechOpen, Rijeka, 2013.
- [9] Sean Kirkpatrick, JW Baur, CM Clark, LR Denny, DW Tomlin, BR Reinhardt, R Kannan, and MO Stone. Holographic recording using two-photon-induced photopolymerization. *Applied Physics A*, 69(4):461–464, 1999.
- [10] Roland Lachmayer and Rene Bastian Lippert. *Additive Manufacturing Quantifiziert: Visionäre Anwendungen und Stand der Technik*. Springer, 2017.
- [11] HOLO/OR LTD. Elongated focus application notes. <https://www.holoor.co.il/application/diffractive-elongated-focus/>. Accessed: 2020-11-04.
- [12] JEOL Ltd. *JSM-IT100, scanning electron microscope manual*. 1-2, Musashino 3-chome, Akishima, Tokyo 196-8558 Japan, 2015.
- [13] Mangirdas Malinauskas, Maria Farsari, Algis Piskarskas, and Saulius Juodkazis. Ultrafast laser nanostructuring of photopolymers: A decade of advances. *Physics Reports*, 533(1):1 – 31, 2013.



- [14] Shoji Maruo, Osamu Nakamura, and Satoshi Kawata. Three-dimensional microfabrication with two-photon-absorbed photopolymerization. *Opt. Lett.*, 22(2):132–134, Jan 1997.
- [15] Andreas Ostendorf and Boris N Chichkov. Two-photon polymerization: a new approach to micromachining. *Photonics Spectra*, 40(10):72, 2006.
- [16] Julia Purtov, Andreas Verch, Peter Rogin, and René Hensel. Improved development procedure to enhance the stability of microstructures created by two-photon polymerization. *Microelectronic Engineering*, 194:45–50, 2018.
- [17] Faiz Rahman, Daniel J Carbaugh, Jason T Wright, Parthiban Rajan, Sneha G Pandya, and Savas Kaya. A review of polymethyl methacrylate (pmma) as a versatile lithographic resist—with emphasis on uv exposure. *Microelectronic Engineering*, 224:111238, 2020.
- [18] Micro resist technology. *Processing Guidelines – OrmoComp*. Köpenicker Straße 325, 12555 Berlin – Germany, 2019.
- [19] Sofía Rodríguez. Redefining microfabrication of high-precision optics: How two-photon grayscale lithography improves quality and throughput of printing microparts. *Photonics Views*, 17(1):36–39, 2020.
- [20] Jesper Juul Serbin. *Fabrication of photonic structures by two-photon polymerization*. Cuvillier Verlag, 2004.
- [21] Sönke Steenhusen. *Untersuchungen zur Sub-100 nm Strukturierung von Hybridpolymeren mittels Zwei-Photonen Absorption und Anwendungen*. PhD thesis, Friedrich-Schiller-Universität Jena, 2018.
- [22] Shuhui Wu, Jesper Serbin, and Min Gu. Two-photon polymerisation for three-dimensional micro-fabrication. *Journal of Photochemistry and Photobiology A: Chemistry*, 181(1):1 – 11, 2006.
- [23] Jin-Feng Xing, Xian-Zi Dong, Wei-Qiang Chen, Xuan-Ming Duan, Nobuyuki Takeyasu, Takuo Tanaka, and Satoshi Kawata. Improving spatial resolution of two-photon microfabrication by using photoinitiator with high initiating efficiency. *Applied Physics Letters*, 90(13):131106, 2007.

## List of Tables

|   |  |    |
|---|--|----|
| 1 | Abbreviations . . . . .  | II |
| 2 | Objective lenses used with their numerical apertures NA and expected aspect ratios AR for created voxels . . . . .   | 21 |
| 3 | An example PVT trajectory file. The intervals with the time $t$ , their final relative positions $x$ , $y$ and voltage signals $u$ as well as the final absolute velocities $v_x$ , $v_y$ and $v_u$ are listed. The lines where structures are written have a constant velocity of $v = 1 \text{ mm/s}$ (lines 10 - 12 and 31 - 33). . . . . | 26 |

|   |   |    |
|---|---|----|
| 4 | Negative (n) and positive (p) photoresists used with their corresponding developers (D) and aggregate phases (AGG, liquid l or solid s) . . . . .                         | 27 |
| 5 | Measured values of the smallest lateral $d_l$ and axial $d_a$ dimensions with the resulting aspect ratios $ar$ of voxels for the different objective lenses used. . . . . | 39 |
| 6 | Maximum depth (d) and best resolution (res) at maximum depth for the specific OPP and TPP setup. The x20 objective lens was used, both resists were spincoated. . . . .   | 50 |
| 7 | Comparison of OPP vs. TPP (a) written by a light source with a wavelength $\lambda$ . Advantages of negative (neg) and positive (pos) resists (b). . . . .                | 56 |

## List of Figures

|   |  |    |
|---|--|----|
| 1 | Structure of a benzophenone, a photoinitiator (a); Mechanism for radical generation Norrish Type I (b) and Norrish Type II (c) with a coinitiator $HR''$ , chemical structure of acrylate (d), methacrylate (e) and an SU-8 oligomer (f). Reprinted from [1]. . . . .  | 4  |
| 2 | Exposure curve - solubility of the resist as a function as the exposure dose (a): The gray region on the right indicates insolubility, sketch for the threshold dose for insolubility in a lateral intensity profile (b): Feature sizes of the tenth of the wavelength used are possible. Reprinted from [1]. . . . .  | 5  |
| 3 | Sketch of a low-NA objective lens with indicated focal field calculation and used coordinates. Reprinted from [1]. . . . .   | 6  |
| 4 | Elongated focal spot for an objective lens with $NA = 0.1$ , The focal field distributions in the focal plane (a) and normal to the focal plane (b) have different orders of magnitude in length. The horizontal line scans for the figures a and b show the lateral (c) and axial (d) field distributions, respectively. Reprinted from [1]. . . . .                  | 8  |
| 5 | Sketch of the focal field calculation for a high-NA objective lens with the focal length $f$ . The incident wave $u_i$ is mapped onto a spherical reference plane (dashed arched line, $u_0(\Theta, \Psi)$ ). $Q_1(\Theta, \Psi)$ is an point on this reference plane and $Q(r, \phi, z)$ is an observation point within the focal volume. Reprinted from [1]. . . . . | 9  |
| 6 | Focal spot for an objective lens with $NA = 0.95$ , The length scales of the focal field distributions in the focal plane (a) and normal to the focal plane (b) differ in a factor of $\sim 2$ . The horizontal line scans for the figures a and b show the lateral (c) and axial (d) field distributions, respectively. Reprinted from [1]. . . . .                   | 10 |
| 7 | Sketch of a TPP process. The laser focus is moved through the resist and creates a spiral. Reprinted from [8]. . . . .   | 12 |

|    |   |    |
|----|---|----|
| 8  | Process window of TPP. The voxel's dimension scales with the laser intensity between the lower and upper threshold of polymerization. Adapted from [10]. . . . .  | 13 |
| 9  | The volume modified by OPP is shown on the left-hand side. The whole beam reacts with the resist. In TPP (right-hand side), the polymerization only takes place in the focus where the intensity is high enough. Figure modified from [21]. . . . .   | 14 |
| 10 | Resist manipulation by OPP. A sketch of the exposure of the resist (a) is shown. The light is focused through an objective lens O onto the sample consisting of the substrate S with the spincoated resists R. The depth of the structures is proportional to the light intensity (both increasing from left to right). The manipulated resist is indicated in deep red. The left-hand side shows the structure after developing (b). . . . . | 15 |
| 11 | When applying a linear dose variation, the resulting structure will behave non-linear (a). By correcting the dosage distribution, one can achieve linear depth variations (b). Adapted from [7]. . .  | 15 |
| 12 | A mirror galvanometer scanner (a) modifies the beam direction with two movable mirrors. Sketch taken from [15]. A translation stage capable of precise in-plane movement (b). Picture taken from [4]. . . . .   | 18 |
| 13 | Setup - The laser is guided to the objective lens and focused onto the sample. The inline camera allows the observation of the writing process. Adapted from [21]. . . . .  | 21 |
| 14 | Imported Stl-file (a) generated with the 3D Builder and Bmp-file (b) converted with the self-made software for grayscale TPP printing. . . . .  | 24 |
| 15 | Python software user interface: Import of a structure's Stl-file and creation of a Bmp-file with given length and raster parameters   | 24 |
| 16 | Visualization of the example trajectory to write a plateau consisting of two lines. . . . .   | 27 |
| 17 | Python software user interface: Import of a structure's Bmp-file and creation of a PVT trajectory file with writing parameters given. . . . .   | 28 |
| 18 | Drop procedure. The drop of the resist is placed on the substrate and is inserted face down. . . . .  | 30 |
| 19 | Spincoated sample. The resist is placed on the substrate facing up.   | 31 |
| 20 | Pictures of the JOEL scanning electron microscope (a, SEM, Source [12]) and the Keyence laser scanning microscope (b, LSM, Source [3]). . . . .   | 32 |
| 21 | Controlling the output power of the laser diode. The power dependence on the analogue input voltage is shown (a). For the digital input mode, the maximum power is set via the interface and the fraction is controlled by the duty cycle signal (b, taken from [2]) generated by a microcontroller. . . . .  | 34 |

|    |   |    |
|----|---|----|
| 22 | Lines with an intermediate distance of $5\ \mu\text{m}$ (left and detail) and $3\ \mu\text{m}$ (right) written with the x100 objective lens. Fluctuations to a straight line can be seen within the first $300\ \mu\text{m}$ of the $1\ \text{mm}$ -long lines. The scanning speed was $v_{scan} = 1\ \text{mm/s}$ . . . . .  | 35 |
| 23 | Lines with an intermediate distance of $5\ \mu\text{m}$ (left) and $3\ \mu\text{m}$ (right) written with the x100 objective. Fluctuations are not seen in the center of the $1\ \text{mm}$ -long lines. The scanning speed was $v_{scan} = 1\ \text{mm/s}$ . . . . .  | 36 |
| 24 | Ablated holes in a glass substrate written with the femtosecond laser at $2\ \text{mm/s}$ with an pulse picker divider of 1000 and a repetition rate of $1\ \text{MHz}$ . . . . .   | 37 |
| 25 | Voxels written with the x100 objective lens. The voxels were varied in lateral offset from top to bottom ( $\Delta z = 0.1\ \mu\text{m}$ per line) and varied in power from left to right. . . . .  | 38 |
| 26 | Behaviour of the voxel when adapting the focus offset (a) and power (b). The objective lens (O) focuses onto different planes inside the resist (R) or the substrate (S). The focus offset is lowered from a too-high offset (a, situation a-c) to a too-low offset (a, situation e-g). The power is risen from low (b, situation a) to high power (b, situation e). . . . .  | 39 |
| 27 | Voxels written with the x20 objective lens. The distance between two pulses was $\Delta d_{(a)} = 0,7\ \mu\text{m}$ and $\Delta d_{(b)} = 1,25\ \mu\text{m}$ . . . . .  | 40 |
| 28 | SEM (left) and LSM (right) picture of bars written by the laser diode. The distances between lines were $\Delta l = 1, 0.5$ and $0.25\ \mu\text{m}$ for the upper, middle resp. the lower bar. . . . .  | 41 |
| 29 | SEM (left) and LSM (right) picture of bars written by the femtosecond laser. The distances between lines were $\Delta l = 1, 0.5$ and $0.25\ \mu\text{m}$ for the upper, middle resp. the lower bar. . . . .  | 41 |
| 30 | Lattices written with the laser diode (OPP, left column) and the femtosecond laser (TPP, right column), An offset to the glass-resist interface of $-6\ \mu\text{m}$ (a, b), $0\ \mu\text{m}$ (c, d) and $+6\ \mu\text{m}$ (e, f) was chosen. . . . .   | 43 |
| 31 | Exposed volume of the polymerization process shown for different focus offsets with respect to the resist-substrate interface. The objective lens (O) focuses onto different planes inside the resist (R) or the substrate (S). The femtosecond laser (TPP) writes only in the focal region, the diode laser (OPP) writes with the whole beam. The situations where the focus is too high and inside the resist are a-b the situations where the focus is too low and inside the substrate are d-e. . . . . | 44 |
| 32 | Plateaus written with the laser diode for different heights (a). The heights of the structures were measured. A third polynomial dependence was assumed for the dependence between the laser power (voltage) and the height (b). . . . .  | 45 |

|    |  |    |
|----|--|----|
| 33 | Test pattern including plateaus written with the femtosecond laser (a). The heights of the plateaus dependent on the power (voltage) were measured. The reverse function was fitted (b). . . . .   | 46 |
| 34 | A test structure with pyramids (a) with a height of $3\ \mu\text{m}$ and the corrected structure (b) scaled according to the fit from Figure 32b.  | 46 |
| 35 | Bmp-file with encoded height for manufacture staircase and chessboard patterns in positive and negative versions . . . . .   | 47 |
| 36 | SEM and LSM pictures of staircase structures generated by TPP and OPP. The used resists were the positive resist ma-P 1275G and the negative resist OrmoComp. . . . .  | 48 |
| 37 | SEM and LSM pictures of chessboard patterns. The structures were written with the femtosecond laser (TPP) and the laser diode (OPP) into the positive resist ma-P 1275G and into the negative resist OrmoComp. . . . .   | 49 |
| 38 | Truncated pyramids written with one x-raster scan (left) and with combined y- and x-raster scan (right). The femtosecond laser, the positive resist and the x20 objective lens was used. The bottom square's side length is fixed with $a_{\text{bottom}} = 5\ \mu\text{m}$ . The top square's side length is varied by $a_{\text{top}} = 2.5, 3$ and $3.5\ \mu\text{m}$ (left to right column in each picture). The intermediate line distance is varied from $d = 1, 0.5$ to $0.25\ \mu\text{m}$ (from top to bottom). . . . .                   | 51 |
| 39 | Truncated pyramids written with the combined y- and x-raster scan (right). The laser diode, the positive resist and the x20 objective lens was used. The bottom square's side length is fixed with $a_{\text{bottom}} = 5\ \mu\text{m}$ . The top square's side length is varied by $a_{\text{top}} = 2.5, 3$ and $3.5\ \mu\text{m}$ (left to right column in each picture). The intermediate line distance is varied from $d = 1, 0.5$ to $0.25\ \mu\text{m}$ (from top to bottom). . . . .   | 52 |
| 40 | Sketch of the sum and individual profiles of 7 lines written when scanning in x-direction (a). The plane perpendicular to the writing direction is shown. The Gaussian line profiles with half width of $0.5\ \mu\text{m}$ overlap when choosing the intermediate line distance of $0.5\ \mu\text{m}$ . Instead of a rectangular structure, a trapezoidal shape is produced. Measured profile with the LSM (b) of a bar written with 11 lines in x-direction with y-values between 12.5 and 17.5. A similar behaviour than in (a) is seen. . . . . | 53 |
| 41 | Truncated pyramids written with too high intensities with the femtosecond laser (a) and the laser diode (b). The femtosecond laser starts to evaporate the resist while the laser diode increases the range of the exposed area significantly. . . . .   | 54 |
| 42 | $5\ \mu\text{m}$ -truncated pyramids with a height of $4\ \mu\text{m}$ written with the laser diode into spincoated ma-P 1240G. Picture taken with the SEM with magnification x7000 (a) and x1300 (b). Mold of similar $5\ \mu\text{m}$ -truncated pyramids written with the femtosecond laser into spincoated OrmoComp. Picture taken with the SEM with magnification x5000 (c) and x500 (d). . . . .   | 54 |